ELSEVIER

Journal of Geochemical Exploration 74 (2001) 3–55

JOURNAL OF GEOCHEMICAL EXPLORATION

www.elsevier.com/locate/jgeoexp

Element cycling and secondary mineralogy in porphyry copper tailings as a function of climate, primary mineralogy, and mineral processing

Bernhard Dold[a,b,*], Lluis Fontboté[b]

[a]*Department of Earth Sciences, Inst. de Mineralogie, University of Lausanne, UNIL BFSH 2, 1015 Lausanne, Switzerland*
[b]*Department of Earth Sciences, University of Geneva, Rue des Maraîchers 13, 1211 Geneva 4, Switzerland*

Received 27 October 1999; accepted 30 September 2000

Abstract

A comparative geochemical, mineralogical, and microbiological study of three mine tailings impoundments from the La Andina, El Teniente, and El Salvador porphyry copper deposits, Chile is presented. These tailings can be characterized as low-sulfide (1.7, 1.0, and 6.2 wt% pyrite equivalent, respectively) and low-carbonate containing (1.4, 0, and 0 wt% calcite equivalent, respectively). The main focus was on the mineralogical and geochemical changes at the interface between the oxidation zone and the primary zone in the sulfidic flotation tailings. The criteria used for selection of the tailings impoundments included knowledge of climate, flotation process, the absence of anthropogenic alteration (additional water or tailings input) after operations had ceased, and the knowledge that, at each site, all tailings had been derived from only one mine. In this way the influence of climate, flotation process, and ore mineralogy can be qualitatively studied. Two schematic models of element cycling in sulfide mine tailings controlled by climatic conditions are presented.

The secondary minerals jarosite, schwertmannite (for the first time in mine tailings), a vermiculite-type mixed-layer mineral, as well as traces of goethite were determined in the oxidation zones by X-ray diffraction, differential X-ray diffraction, or microscopy. Seven-step sequential extractions and electron-microbeam analyses indicate that schwertmannite and jarosite play an important role in the retention of oxyanions (e.g. $HMoO_4^-$, $H_2AsO_4^-$, and SO_4^{2-}) in the low-pH oxidation zones. The bivalent cations (e.g. Cu^{2+}, Zn^{2+}, and Mn^{2+}) are leached from the oxidation zones in precipitation-dominated climates (e.g. La Andina). Below this zone, increasing pH controls the sorption of bivalent cations through adsorbents as secondary Mn(II) hydroxides, Fe(III) hydroxides, or clay minerals. Below the groundwater table, with increasingly reducing conditions, pH-controlled replacement processes take place, as shown by the alteration of chalcopyrite to covellite, leading to secondary Cu enrichments of potential economic interest.

At El Teniente and El Salvador, in climates where evaporation exceeds precipitation, the water-flow direction changes to upwards migration via capillary forces. As a result mobilized elements are transferred to the top of the tailings under oxidizing conditions. Sulfide replacement processes are less important in arid climates. Supersaturation controls the precipitation of mainly water-soluble secondary sulfates (e.g. bonattite, chalcanthite) and strong enrichment at the top of the tailings. The presence of metals in water-soluble form at the top of the tailings could lead to a low cost recovering technique for low ore-grade material in evaporation-controlled climates. In the low-pH oxidation zone, due to their high ionic activity, certain mobile

* Corresponding author. Address: Earth Sciences Department, Inst. de Mineralogie, University of Lausanne, UNIL BFSH 2, 1015 Lausanne, Switzerland. Fax: +41-24-6924315.
E-mail address: bernhard.dold@terre.unige.ch (B. Dold).

PII: S0375-6742(01)00174-1

elements are found to substitute into secondary minerals. Examples are Al- for Fe substitution in jarosite, and substitution of Cu and Zn for K in biotite, resulting in a vermiculite-type mixed-layer mineral.

At El Salvador the quantities of secondary ferric oxyhydroxide minerals are low in relation to the relatively high pyrite (6.2 wt%) content and the low-pH in the oxidation zone (paste-pH 2). The low oxidation activity obtained during microbiological tests and the presence of higher Mo concentrations (160–1000 ppm) than those of Andina and El Teniente (32–171 ppm), suggest that the sparseness of ferric oxyhydroxides is due, at least in part, to Mo poisoning of sulfide oxidizing bacteria as *Thiobacillus ferrooxidans*. The low-pH (2–3.5) of the El Salvador tailings is attributed to the slow inorganic oxidation of pyrite, the liberation of acidity by supergene jarosite, and the complete absence of carbonate neutralization potential.

Keywords: porphyry copper; low-sulfide tailings; climate; jarosite; schwertmannite; element cycling

1. Introduction

Porphyry deposits are the world's principal source of copper and molybdenum. This deposit type consists of disseminated and stockwork sulfide mineralization emplaced in various host rocks that have been altered by hydrothermal solutions into roughly concentric zonal patterns (Lowell and Guilbert, 1970; Gustafson and Hunt, 1975; Gustafson and Quiroga, 1995). Pyrite, chalcopyrite, bornite, and molybdenite are generally the dominant sulfide minerals. Minor to trace minerals at some locations are magnetite, hematite, ilmenite, rutile, enargite, cassiterite, hübnerite, tennantite–tetrahedrite, cubanite, and gold. Supergene enrichment, which commonly can make these low-grade deposits economically interesting, produces secondary hematite, goethite, jarosite–alunite, chalcocite–digenite, covellite, and native copper. During the flotation process the economically interesting Cu–Mo–sulfides are extracted, whereas pyrite and other gangue minerals are generally depressed from flotation, being exposed to oxidation by deposition at the tailings impoundments. It is generally accepted that sulfide oxidation, and in particular that of pyrite, is the main reason for the formation of acid rock drainage (ARD). These heavy-metal-loaded acid effluents are the principal environmental problem facing the mining industry today.

The aim of this study is to investigate the mineralogical and geochemical changes at the interface between the oxidation zone and the primary (sulfide) zone in sulfidic copper flotation tailings. Three tailings impoundments of the porphyry copper deposits La Andina, El Teniente, and El Salvador in Chile were studied. The criteria used for selection of the impoundments included knowledge of the origin of the tailings (from only one mine at each site), climate, flotation process, and the absence of anthropogenic alteration (additional water or tailings input) after operation had ceased. In this way, we can qualitatively study the influence of parameters such as climate, flotation process, and ore mineralogy. We focus on the effects resulting from sulfide oxidation, especially element mobility and retention by secondary minerals as well as microbial activity.

The three selected tailings impoundments represent different climates and illustrate the influence of this parameter on both, the mobilization direction and the secondary mineralogy. The Piuquenes tailings impoundment at La Andina (alpine climate) is discussed as the prime example and comparisons are made to the tailings of Cauquenes at El Teniente (Mediterranean climate) and El Salvador (hyper-arid).

2. Terminology

For the description of the tailings mineralogy the classification proposed by Jambor (1994) is used: The term 'primary' minerals is used to designate the complete suite of minerals that was initially deposited in the impoundment. The primary suite, therefore, may include both, 'hypogene' and 'supergene' minerals. 'Secondary' minerals are those produced within the tailings impoundment after mining and milling as the result of weathering processes. 'Tertiary' minerals form after the sample has been removed from the tailings environment.

2.1. Description of the studied tailings impoundments

The location of the three studied tailings impoundments is shown in Fig. 1. Piuquenes (La Andina, alpine climate, alkaline flotation circuit), Cauquenes

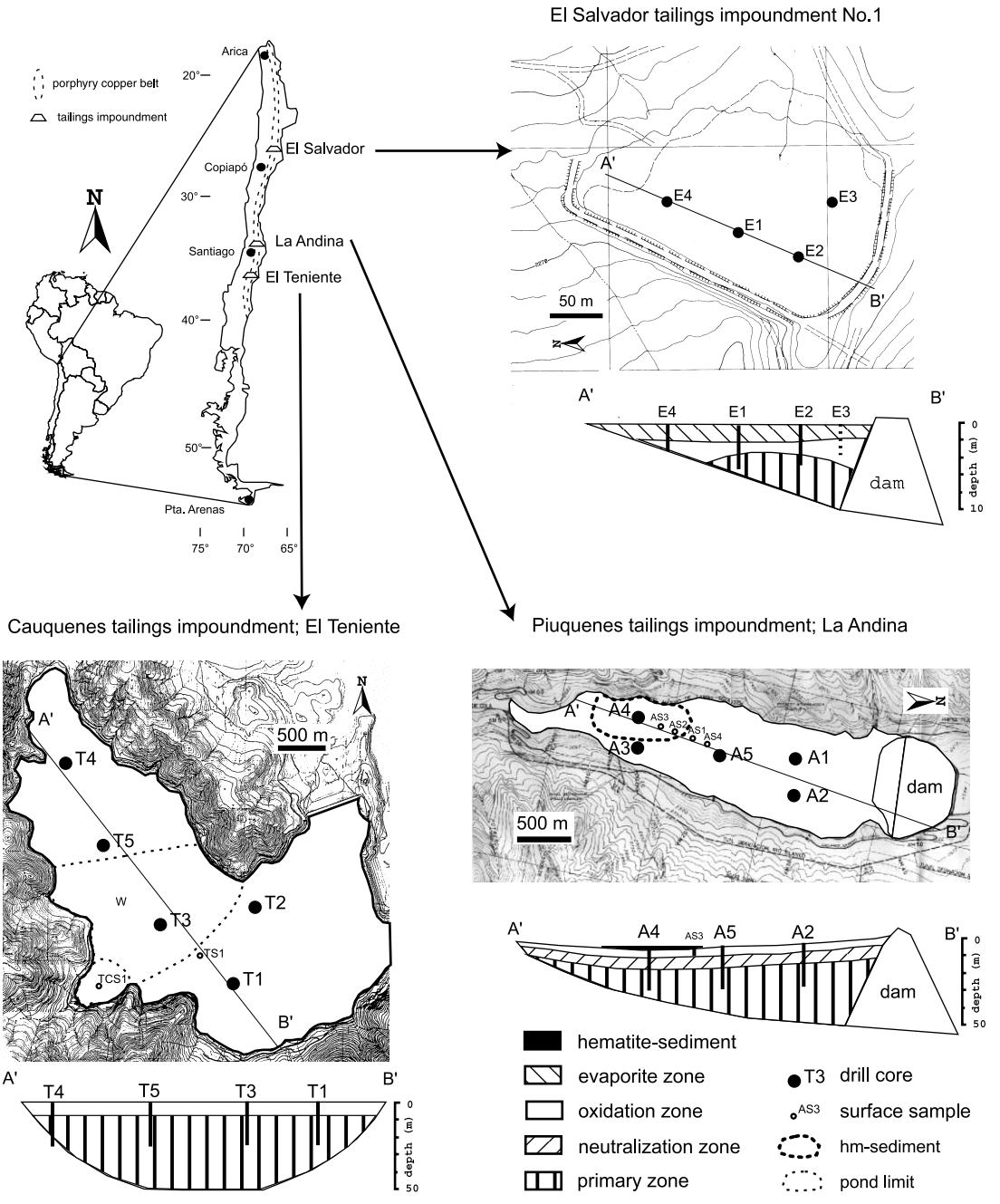

Fig. 1. Overview of the sampled tailings impoundments and their location within the porphyry copper belt in Chile. The climate changes from hyper-arid in the Atacama desert in northern Chile to humid in the South. The studied tailings impoundments Piuquenes (Andina), Cauquenes (El Teniente), and El Salvador No.1 are located in alpine, Mediterranean, and hyper-arid climate, respectively. *Note*: For better visibility of the stratigraphic zonation the cross-sections are vertically exaggerated.

Table 1
Properties of the studied porphyry copper tailings impoundments (abbreviations: al: albite; anhy: anhydrite; ank: ankerite; ap: apatite; bio: biotite; bn: bornite; ca: calcite; cb: cinnabar; cc: chalcocite; cl: chlorite; cp: chalcopyrite; cv: covellite; dg: digenite; ep: epidote; fh: ferrihydrite; gn: galena; gt: goethite; gy: gypsum; hm: hematite; horn: hornblende; ilm: ilmenite; jt: jarosite; kaol: kaolinite; K-feld: K–feldspar; mb: molybdenite; mont: monmorillonite; mt: magnetite; Na-jt: natrojarosite; op: orpiment; py: pyrite; qz: quartz; rut: rutile; ser: sericite; sh: schwertmannite; sid: siderite; sl: sphalerite; stb: stibnite; tour: tourmaline; tn: tennantite; tt: tetrahedrite)

Ore deposit	La Andina	El Teniente	El Salvador
Ore deposit type	Porphyry copper	Porphyry copper	Porphyry copper
Gangue mineralogy	qz, al-K-feld, bio, ank, sid, ca, gy, ser, cl, ep, tour[a]	qz, al-K-feld, bio, ca, anhy, tour, rut, ap, ser, cl, ep, kaol, mont[b]	qz, al-K-feld, bio, anhy, rut, horn, titanite, ca[c]
Hypogene ore mineralogy	py, cp, bn, mb, sl, gn, tn-tt, mt, hm,[a] ilm[d]	py, cp, bn, mb, gn, tn, mt, hm[b]	py, cp, bn, mb, ilm, hm[c]
Supergene mineralogy	cc, cv[a]	cc, cv[b]	cc, cv, jt, hm, gt,[c] Na-jt[d]
Flotation circuit	pH 10.5	pH 4.5	pH 10.5
Tailings impoundment	Piuquenes[e]	Cauquenes[f]	El Salvador No. 1
Pyrite content (wt%)	1.7	1.0	6.2
ABA ($tCaCO_3$/1000t)	−28.3	−18.2; NP ≈ 0	−101.6; NP ≈ 0
Surface	83.7 ha	640 ha	4.2 ha
Volume	24 117 000 m^3	270 000 000 m^3	144 000 m^3
Operation time	1970–1980	1936–1975	1959–1960
Deposition technique	Starter dam, upstream method	Five dams closing a natural depression	Two dams closing natural inclination
Drill cores and samples	A1–A5; 87 samples	T1–T5; 78 samples	E1–E4; 37 samples
Climate	Alpine	Mediterranean	Hyper-arid[g]
Altitude	2150 m	725 m	2270 m
Precipitation	~ 700 mm/a	~ 540 mm/a	~ 20 mm/a
Evaporation	~ 70 mm/a	High in summer	Extremely high all year

[a] Serrano et al. (1996).
[b] Camus (1975).
[c] Gustafson and Hunt (1975).
[d] This study.
[e] Ingeneria y Geotecnia LTDA (1990a).
[f] Ingeneria y Geotecnia LTDA (1990b).
[g] Alpers and Brimhall (1989).

(El Teniente, Mediterranean climate, acid flotation circuit), and El Salvador No.1 (El Salvador, hyper-arid climate, alkaline flotation circuit, strong supergene enriched ore). Table 1 summarizes the main parameters of the tailings impoundments and of the performed sampling.

2.2. Piuquenes tailings impoundment, La Andina porphyry copper deposit, Chile

Regional geology and ore geology. The Río Blanco-Los Bronces ore body is a giant copper–molybdenum porphyry system with $>50 \times 10^6$ tonnes grading 1.0 and 1.5% Cu (Serrano et al., 1996). The deposit is located high on the west flank of the central Chilean Andes, about 50 km northeast of Santiago, at 3500–4200 m altitude (Fig. 1). CODELCO's Andina division owns the main eastern part of the deposit. This deposit is one of three giant late Miocene to early Pliocene copper deposits in the Andes of central Chile, formed as a result of emplacement of both multiple mineralized breccias and porphyry intrusions (quartz diorite, granodiorite, quartz monzonite, and quartz monzodiorite) into early and middle Miocene plutonic rocks and Cenozoic lavas (Serrano et al., 1996). The potassic core, propylitic halo, and superimposed sericitic alteration of the early stage conform to established patterns for porphyry copper deposits (Stambuk et al., 1982). Supergene enrichment is less prominent in the Andina deposit than at other copper deposits in northern and central Chile, but supergene chalcocite and covellite locally double the ore grade. As

the shape and depth of the enrichment zones are spatially associated with the recent groundwater regime, it is believed that leaching and enrichment are still active (Serrano et al., 1996). The mineralization consists mainly of pyrite, chalcopyrite, chalcocite, covellite, molybdenite, sphalerite, galena, tennanite, and tetrahedrite in a gangue of ankerite, siderite, gypsum, quartz, tourmaline, and very minor calcite.

Mining and treatment processes. CODELCO's Andina Division uses both underground and open pit (Sur–Sur) mining. The mineral is conditioned by lime for the flotation process, leading to a pH of 10.5 of the tailings deposited in the impoundment.

History of the tailings impoundment. The Andina division has three tailings impoundments, the currently operating Huechún impoundment, the Los Leones impoundment which was operation from 1980 to 1999, and the Los Piuquenes impoundment which was in operation from 1970 to 1980. Sampling was carried out on Los Piuquenes, which is located at 2150 m altitude in the N–S trending valley of the Río Blanco River (Fig. 1). Los Piuquenes is situated in a valley of glacial origin on fluvial–glacial Quaternary sediments, mainly sandy gravels and clayey sandy gravels. They are underlain by Upper Tertiary volcanic and intrusive rocks (mainly andesites and granodiorites).

The impoundment has a surface area of 83.7 ha, a volume of 24×10^6 m^3, and contains 37×10^6 tonnes of tailings. The maximum height of the impoundment is 57 m and the downstream angle of the dam is 25°. Piuquenes was constructed as a valley dam impoundment with an initial starter dam after the upstream method. The discharge point of the tailings was moved periodically during operation (Ingeneria y Geotecnia LTDA, 1990a). Tailings deposited between 1970 and 1980 average 0.22% Cu.

Climate. Based on data from two meteorological stations in the Andina region the climate of the Piuquenes impoundment, situated at 2150 m altitude, is characterized by an average precipitation of 700 mm/a and evaporation of 70 mm/a. The climate is classified as alpine.

2.3. Cauquenes tailings impoundment, El Teniente porphyry copper deposit, Chile

Regional geology and ore geology. The El Teniente porphyry copper deposit (48×10^6 tonnes of Cu) is located 67 km east of the town of Rancagua, province of O'Higgins, VI Región, Chile (Fig. 1). The mine, owned and operated by CODELCO, is the world's largest underground mine. The two main stratigraphic units in the mine area are the intensely folded Coya-Machalí Formation (Upper Cretaceous), characterized by fine-grained continental sediments interbedded with andesitic flows and pyroclastic deposits, and the unconformably overlying Farallones Formation (Lower Tertiary), consisting of a sequence of continental sediments, andesitic, rhyolitic, and basaltic lava flows with pyroclastic intercalations (Camus, 1975). A quartz–diorite–dacite complex, to which the alteration and mineralization is related, intrudes these two formations. Three main hypogene alteration assemblages and one supergene assemblage have been recognized in the orebody. The hypogene assemblages are potassic (biotite, K–feldspar, anhydrite, quartz, sericite, carbonates, rutile, and apatite), quartz–sericitic (quartz, sericite, pyrite, anhydrite, tourmaline, calcite, pyrophyllite), and propylitic (chlorite, epidote, calcite, magnetite, pyrite, sericite, quartz, and anhydrite). Supergene argillic alteration is recognized by the presence of kaolinite with lesser montmorillonite and alunite. The main sulfide minerals are pyrite, chalcopyrite, molybdenite, sphalerite, galena, and tennantite. The most important secondary mineral present in the orebody is chalcocite, which occurs with minor amounts of covellite (Camus, 1975).

Treatment process. Material rich in supergene argillic alteration with high contents of kaolinite and montmorillonite inhibits flotation in an alkaline circuit. Thus, an acid flotation circuit at pH 4.5 treated the mineral and the tailings were released with this pH to the tailings impoundment.

History of the tailings impoundment. Of the four tailings impoundments that have been built at El Teniente, the Cauquenes impoundment was judged to be the best for sampling because of its favorable age, climate, and the absence of anthropogenic alteration (additional water and tailings input). The tailings impoundment, which operated from 1936 to 1975, is located at 725 m altitude in the central valley of Chile, with a surface of 640 ha, 12 km southeast of Rancagua in a natural depression which is closed by five dams (Fig. 1). It overlies lacustrine sands, silty clays, and

clayey gravels (Ingeneria y Geotecnia LTDA, 1990b). The average Cu content of the tailings deposited between 1971 and 1973 was 0.30%.

Climate. Based on data from the meteorological station Parrón in the neighborhood of the Cauquenes tailings impoundment the climate can be classified as Mediterranean. The average precipitation of 540 mm/a occurs mainly during the winter and high evaporation rates are assumed for the summer period.

2.4. Tailings impoundment no.1, El Salvador porphyry copper deposit, Chile

Regional geology and ore geology. The El Salvador porphyry copper deposit (5.7×10^6 tonnes Cu) is in the Atacama Desert about 100 km northeast of Copiapó (Fig. 1). The mine is owned and operated by CODELCO. Host rocks of the deposit are Cretaceous andesitic flows and sedimentary rocks overlain unconformably by Lower Tertiary volcanics. Early rhyolitic domes, with voluminous rhyolitic and andesitic volcanics, were followed by irregularly shaped subvolcanic intrusions of quartz rhyolitic and quartz porphyry, dated at about 46 Ma (Gustafson and Hunt, 1975). A steep-walled granodioritic porphyry complex and the closely associated main center of mineralization and alteration were dated at 41 Ma. Early mineralization is characterized by distinctive quartz veins and largely disseminated K–silicate assemblages of alkali feldspar–biotite–anhydrite–chalcopyrite–bornite or chalcopyrite–pyrite. Except at the deepest levels exposed in the younger porphyries, incipient K–silicate alteration converted hornblende phenocrysts to biotite–anhydrite–rutile, ilmenite to hematite–rutile, and titanite to rutile–anhydrite. Supergene enrichment formed the commercial ore body. Secondary Cu-sulfides (chalcocite, covellite) extensively replaced chalcopyrite and bornite but coated pyrite with little or no replacement (Gustafson and Hunt, 1975; Gustafson and Quiroga, 1995).

Mining and treatment processes. The El Salvador Division is an underground mining operation. In the flotation the ore is separated from the gangue by a collective Cu–Mo flotation. The mineral is conditioned by lime to a pH of 10.5, which is the deposition pH for the tailings.

History of the tailings impoundment. The Potrerillos-El Salvador mining district sent most of its flotation tailings in suspension through the El Salado River direct to the sea at the Chañaral Bay between 1926 and 1989. Since 1989 the Pampa Austral impoundment has been the active tailings impoundment of the El Salvador mine. The present flotation plant of El Salvador started its activity in 1959. From this time there have been three small tailings impoundments halfway between the plant and El Salvador village. The largest one (tailing No.1, maximum thickness of 8 m and 4.16 ha surface), which went out of operation around 1960, was sampled. The impoundment is situated at 2270 m altitude and was built by using two rectangular dams at the downslope (Fig. 1). The tailings are deposited on continental clastic sediments of the Potrerillos Formation, which mainly consist of Miocene gravels and sands with intercalations of rhyolitic flows.

Climate. The No.1 tailings impoundment is situated in the Andean precordillera at 2270 m altitude. The Atacama Desert is known as the driest desert on Earth and data from precipitation in the El Salvador region from 1962 to 1984 show an average of 20 mm/a as rain or snow and is classified as hyper-arid (Alpers and Brimhall, 1989). No data for evaporation and temperature are available. No vegetation is observed. High evaporation rates must be assumed throughout the whole year.

3. Methodology

3.1. Sampling and field methods

Fourteen holes were drilled, from which 202 samples were obtained from the three impoundments. Percussion drilling equipment was used to reach depths of 10 m ($100 \times 2\ cm^2$ sampling tube) in the first field campaign 1996. Up to five samples of 20 cm length per meter were taken in the oxidation zone and at the interface between the oxidation and primary zone. Three samples per meter were taken in the homogeneous primary zones. Where necessary, smaller sub-samples were taken. In a second field campaign in 1997 detailed surface sampling was undertaken in the transition to a hematite-rich sediment in the Piuquenes tailings (Fig. 1).

The 202 samples were sealed in plastic bags and stored in an ice-packed cooler box after the description

Table 2
Sequential extractions applied in this study (abbreviations as in Table 1)

Leach	Preferentially dissolved minerals	References
(1) Water-soluble fraction 1.0 g sample into 50 ml deionized H_2O shake for 1 h	Water-soluble sulfates, e.g. gy, bonattite, chalcanthite, pickeringite, magnesioaubertite	Dold, 1999; Ribet et al., 1995; Fanfani et al., 1997
(2) Exchangeable fraction 1 M NH_4-acetate pH 4.5 shake for 2 h	ca, vermiculite-type-mixed-layer, exchangeable ions	Dold, 1999; Gatehouse et al., 1977; Sondag, 1981; Cardoso Fonseca and Martin, 1986
(3) Fe(III)oxyhydroxides 0.2 M NH_4-oxalate pH 3.0 shake for 1 h in darkness	sh, 2-line fh, secondary jt, MnO_2	Schwertmann, 1964; Stone, 1987; Dold, 1999
(4) Fe(III) oxides 0.2 M NH_4-oxalate pH 3.0 heat in water bath 80°C for 2 h	gt, jt, Na-jt, hm, mt, higher ordered fh	Dold, 1999
(5) Organics and secondary Cu–sulfides H_2O_2 35% heat in water bath for 1 h	Organics, cv, cc-dg	Sondag, 1981
(6) Primary sulfides Combination of $KClO_3$ and HCl, followed by 4 M HNO_3 boiling	py, cp, cc, bn, sl, gn, tt, cb, op, stb	Chao and Sanzolone, 1977; Hall et al., 1996
(7) Residual HNO_3, HF, $HClO_4$, HCl digestion	Silicates	Hall et al., 1996; Dold et al., 1997

of mineralogical characteristics, color and grain size estimation, and pH measurement were obtained (paste-pH according to MEND, 1991; WTW® pH-meter; in the second field campaign a pH-electrode for measurement in meat was successfully used for in situ pH-measurement in the moist tailings sediment). The samples were transported immediately to local mine laboratories for drying (<35°C) and water-content determination. The dry samples were homogenized and packed into polyethylene (PET) containers for storage at room temperature.

3.2. Physical properties

The wt% of moisture of all tailings samples was measured using sample weight before and after drying to stable weight. The particle-size distribution of selected samples was measured by a Coulter® and a Fritsch Analysette® laser particle-size analyzer. The hydraulic conductivity (K) was calculated after Hazen (1893 in Hölting (1989)) with the d10 concentrations. As the unconformity degree $U = \text{d60/d10}$ was higher than five, the correction after Beyer (1964, in Hölting (1989)) was applied.

3.3. Mineralogical methods

Polished sections and polished thin sections were prepared from bulk samples and undisturbed tailings samples. All samples were analyzed as bulk sample by X-ray diffraction (XRD), using a Philips 3020 diffractometer with monochromated CuKα ($\lambda = 1.54056$ Å) X-radiation. Scan settings were 3–70° 2θ, 0.02° step size, 2 s count time per step. The procedure of identification of clay minerals was as described in Moore and Reynolds (1997), and Brindley and Brown (1980). The <2 μm fraction was separated by centrifugation and oriented samples were prepared on glass slides. The samples were analyzed by XRD before and after glycerol treatment, K- and Mg-saturation, and heat treatment (550°C, 1 h).

The poorly crystalline Fe(III) hydroxides such as ferrihydrite and schwertmannite were detected by differential X-ray diffraction (DXRD) as described by Schulze (1981, 1994). The diffractometer settings were those used by Bigham et al. (1990, 1994, 1996), and Schwertmann et al. (1995), i.e. step scanning with 0.05° 2θ step size and 20 s counting time per step. The samples were treated with 0.2 M ammonium oxalate at pH 3, in darkness, for 15 min, 1 or 2 h. Scans were measured before and after treatment. The treated scans were intensity corrected and then subtracted from the untreated scan. The extraction solutions (leachates) were analyzed for Fe and S by ICP-AES to calculate the Fe/S mole ratios.

3.4. Geochemical methods

3.4.1. Sequential extraction

To study the element speciation in the mine tailings a sequence of seven selective dissolution steps was established (chapter 3 in Dold (1999)) and applied

to 114 samples (Table 2). Iron cycling is the controlling process in sulfidic mine wastes, due to acid production via pyrite oxidation and hydrolysis of Fe(III) to form oxyhydroxides and oxyhydroxide sulfates, and scavenging of mobilized elements via sorption and co-precipitation processes associated by these secondary phases. Because of the importance of the change from sulfide to oxide phases, several sequential extractions were chosen to study this change.

The first four extractions are designed to separate the mobilized elements and the different secondary minerals. Water-soluble secondary and tertiary salts are dissolved in the water extraction. In the second step, acetate, which is a monodentate complex-former, is believed to detach only exchangeable elements that are present as outer-sphere complexes. The third and fourth steps use oxalate, which forms bidentate complexes by dissolving the secondary minerals and by liberating elements, which are fixed as inner-sphere complexes or co-precipitated. The last three extractions (Table 2) try to discriminate the organic compounds from the sulfides and silicates.

The selectivity of sequential extractions by widely used organic acids, such as oxalate, has been criticized by McCarty et al. (1998) on the grounds that various parameters influence the dissolution kinetics of iron minerals as for example acidity, light, temperature, Fe(II) presence, and reducing conditions (Stumm and Sulzberger, 1992). To overcome this problem, dissolution kinetic tests and control of the dissolved phases by XRD and DXRD were used to monitor the selectivity of extractions in representative samples of the tailings (Dold, 1999). Calcite goes into solution in the NH_4-acetate leach. DXRD analyses have shown that the vermiculite-type mixed-layer mineral disappears after the NH_4-acetate leach and a new peak appears at the flank of the 001 illite peak. This is interpreted to result from a detachment of interlayer cations. The dissolution of secondary ferric oxyhydroxides and oxyhydroxide sulfates in NH_4-oxalate is discussed in detail by Dold (1999). The solutions were analyzed by ICP-AES. The sum of all dissolution steps gives the total concentration of an element. To control the accuracy, bulk analysis of a total HNO_3, HF, $HClO_4$, HCl digestion of every sample was done. The sums of the sequential extraction (total) and the bulk analysis show a fair agreement.

Elemental mapping by scanning electron microscope (SEM-EDS) and electron microprobe analysis was used on selected polished sections and polished thin sections to determine the compositional variation of schwertmannite and biotite.

3.4.2. Acid–base accounting

S_{total} was measured using a Leco® furnace, and for measurement of the $S_{sulfate}$ a 0.2 M NH_4-oxalic, hot, 2 h leach (iron oxides, gt, jt, hm, mt; Dold, 1999) was used. This leach has shown to dissolve all sulfate minerals in max. 30 min in all tested samples and does not attack the sulfides (Dold, 1999; Chao and Sanzolone, 1977). Sulfur was determined by ICP-AES. The differences of both results represents the $S_{sulfide}$ content. Total and mineral carbon were analyzed by coulometric titration (Ströhlein CS 702®). The sulfide net neutralization potential (SNNP) was calculated as $t CaCO_3/1000t$.

3.5. Microbiological methods

For the microbiological study, 10 samples were analyzed from three drill cores (T4, A5, and E1). A separate aliquot was taken from each sample in the field and was maintained untreated, at 5°C in ice-packed coolers. The samples were delivered to the laboratory of the biometallurgical group of the Chemical Engineering Department of the University of Chile, Santiago de Chile. The samples were analyzed for total number of cells (direct microscopic counting; Phyroff–Hauser counting chamber), *Thiobacillus ferrooxidans* cultivation (plate counting), and oxidizing activity (Fe(II) oxidation rate).

To determinate the number of bacteria present in the solid, 10 g of the sample were brought into contact with 100 ml of a growth medium, shaken, and centrifuged. The supernatant solution was used for bacterial count (direct and plate) and measurement of pH and Eh. The medium used to grow *T. ferrooxidans* consisted of 0.4 g/l $(NH_4)_2SO_4$, 0.056 g/l $K_2HPO_4.3H_2O$, 0.4 g/l $MgSO_4.7H_2O$, and 33.3 g/l $FeSO_4.7H_2O$ (modified after Tuovinen and Kelley (1973). The pH was adjusted to 1.6 with H_2SO_4.

To determine the oxidation activity of the samples, 3 g/l Fe(II) was added to the sample solutions and shacked at 30°C. Periodically, Fe(II) and Fe_{total} were determined colorimetrically using ferrous-*o*-phenanthroline complex, and pH and Eh were measured.

Bacteria numbers (direct counting and plate counting) were analyzed at the beginning and the end of the experiments.

4. Results and discussion

4.1. Piuquenes tailings impoundment, La Andina

4.1.1. Physical properties and mineralogy

The surface of the Piuquenes (Andina) impoundment was totally dry during the first summer field campaign (1996); the depth to the water-saturated zone was between 2.0 (A4) and 2.6 m (A2). In winter (1997), a pond covered the end of the impoundment (Fig. 1) and the groundwater level was 50 cm below the surface in the proximity of A2. The five drill cores (A1–A5) reveal a very similar stratigraphy of the tailings. The upper part is an *oxidation zone* (Fig. 2B1) with a low pH (2.1–3.5) and that is 0.5–0.8 m thick (A1 = 0.8 m; A2 = 0.5 m; A3 = 0.7 m; A4 = 0.65 m; A5 = 0.5 m). It is underlain by a *neutralization zone* (pH 3.5–5) down to depths of 2.6–4.2 m (A1 = 3.2 m; A2 = 3.3 m; A3 = 4.2 m; A4 = 2.6 m; A5 = 4.3 m). Below, the 'primary zone' was sampled to 10 m depth, wherein paste-pH values increase to as high as 8.4 and is characterized by the presence of the primary sulfide assemblage. However, it will be shown that this primary zone is also affected by secondary products, which result from sulfide oxidation. Fig. 3 shows the stratigraphy, pH, and geochemical data for the representative drill core A2, which is discussed in detail in this section. A *hematite-rich sediment* occurs at the surface in the pond area (Figs. 1, 2 and 9) and will be discussed separately. The geochemical data for the drill core A2 (Fig. 3) are shown in Table A1. Additional geochemical data are contained in Dold (1999).

We will describe first the general mineralogical characteristics of the tailings, before a detailed discussion of the secondary mineralogy of the oxidation zone follows. XRD and microscopic studies show that the primary gangue is dominated by quartz, alkali-feldspar (mainly albite ± anorthoclase), and micas (muscovite and biotite). Illite, chlorite, and kaolinite are the typical minerals in the clay fraction (<2 μm). Calcite and siderite are reported from the ore as minor phases (Serrano et al., 1996), but could not be directly detected in the tailings. Tertiary gypsum is developed in samples close to the groundwater level and, to a lesser extent, from the oxidation zone, where it also may be a secondary mineral. The primary zone is characterized by its dark gray color with some red to dark-brown horizons (indicating the presence of secondary Fe(III) hydroxides, possibly ferrihydrite).

Examination of polished sections show that in the neutralization zone and the primary zone the original sulfide assemblage is dominated by pyrite, which is partly strongly fractured. Chalcopyrite and minor bornite are present as trace minerals and show two types of replacement by chalcocite–digenite and/or covellite. In the primary zone, thick replacement rims mainly composed of chalcocite–digenite with some traces of covellite (Fig. 2E) are observed and interpreted as product of supergene enrichment processes as reported by Serrano et al. (1996). This primary replacement is rare and is only conserved in some grains as complete rims. In contrast, a secondary Cu replacement, found in the neutralization zone directly below the groundwater level, is characterized by complete thin rims dominated by covellite with some chalcocite–digenite that replaced chalcopyrite (Fig. 2F). Most of the chalcopyrite grains show this thin replacement rim, only some chalcopyrite inclusions in silicates have been protected from replacement. Magnetite is generally present as massive grains, partly replaced by hematite at the edges. Traces of enargite, molybdenite, goethite, and hematite were also found in the primary and neutralization zones. Tennantite–tetrahedrite is reported from the ore (Serrano et al., 1996) but could not be detected during the study.

The supergene and hypogene Cu–sulfide have been extensively leached in the oxidation zone, wherein only some residual grains of pyrite and chalcopyrite are observed, and no supergene Cu–sulfides are present. Magnetite with hematite replacement is frequent, and tabular hematite is also present. Pyrite grains do not show Fe(III) hydroxide coatings.

In the oxidation zone, characterized by light gray to yellow–brown colors and alternating fine sandy to clayey-silty ($K = 3.1 \times 10^{-7}$–1.9×10^{-8} m/s) layers, jarosite and a vermiculite-type mixed-layer mineral dominate the XRD detectable secondary mineralogy. This is also the case in the clay fraction (<2 μm),

where additional two small broad peaks at 2.55 and 1.51 Å are visible, which we identify as schwertmannite (see below). No goethite has been recognized.

4.1.2. Identification of schwertmannite

Schwertmannite (ideally between $Fe_8O_8(OH)_6SO_4$ or $Fe_{16}O_{16}(OH)_{10}(SO_4)_3$) was first described by Bigham et al. (1994) as acid mine drainage precipitate (pH 2.8–4.5). It has been since then reported from several locations around the world, mainly as precipitate in heavy metal and sulfate loaded drainage systems (Bigham et al., 1990, 1994, 1996; Schwertmann et al., 1995; Childs et al., 1998; Yu et al., 1998, 1999; Dold, 1999). Jamieson et al. (1995) describe an oxyhydroxysulfate from Geco tailings (Ont., Canada), which on the basis of electron microprobe analysis they reported to be possibly schwertmannite. However, electron microprobe analysis is not sufficient to identify schwertmannite, because SO_4 may be adsorbed as oxyanion at low-pH conditions to Fe(III) hydroxides and mime the stoichiometric composition of schwertmannite. Also Lin (1996) reported the presence of schwertmannite and ferrihydrite in the Rudolfsgruvan mine waste rock dump, central Sweden without offering a clear XRD identification of these minerals. Recently there has been some discussion if the schwertmannite structure is akin to that of akaganéite (Bigham et al., 1990, 1994, 1996; Waychunas, 1995; LRC, 1999). In the present work, we consider schwertmannite to be sufficiently characterized by its XRD pattern, as reported by Bigham et al., in combination with its Fe/S mole ratio and dissolution kinetics. The XRD pattern of schwertmannite is distinct and the principals peaks (peak position Å/intensity; 4.86/37, 3.39/46, 2.55/100, 2.28/23, 1.95/12, 1.66/21, 1.51/24; Bigham et al., 1994) are different from those of goethite (JCPDS card 29-713; 4.18/100; 2.69/35; 2.45/50) making possible the discrimination between these two minerals, even if goethite adsorbs SO_4. Poorly crystalline goethite shows broader peaks and the intensity of the main peak (110) is lower than of the well crystallized mineral (Cornell and Schwertmann, 1996), but the 110 peak still is the second dominant peak and must be present in the XRD patterns for positive goethite detection.

In all known occurrences schwertmannite is a very fine-grained mineral (<1.5 μm) and cannot be separated by physical techniques what makes this mineral extremely difficult to detect, especially in bulk samples. This may be one of the reasons together with its narrow stability field why it has not been detected so far in mine tailings. Goethite and jarosite are the well-crystallized secondary phases in this environment and if present, easily detectable with XRD or microscopy. Thus, the so-called 'X-ray amorphous Fe(III) hydroxides', mainly ferrihydrite and schwertmannite, are mostly not detectable in a bulk XRD of mine tailings, due to their low peak intensities and to be in general a minor phases in relation to the bulk composition of tailings. Differential X-ray diffraction (DXRD, Schulze, 1981, 1994), method commonly used to discriminate ferrihydrite from goethite in soils (Cornell and Schwertmann, 1996), was used to determinate schwertmannite. This technique is based on the dissolution of the searched mineral and the interpretation of the diagram resulting from the difference between the XRD scans obtained before and after dissolution. As no detailed knowledge on the dissolution kinetics of schwertmannite in NH_4-oxalate was available, dissolution kinetic tests with nine

Fig. 2. A, A layer of about 2 cm thick hematite-rich sediment (reddish-brown, pH 7.7) overlying the low-pH (3.1) oxidation zone at the surface sampling point AS3, Piuquenes tailings impoundment, La Andina. B1, Profile of the oxidation zone (yellow to orange–brown; 50 cm thickness) and the underlying dark gray neutralization zone (pH 3–6). The orange–brown ferric oxyhydroxide sulfate determined as schwertmannite by DXRD is enriched in the water-flow paths at grain size boundaries or cracks. B1, Zoom of schwertmannite-rich (sh) streaks and dots in a fine-grained horizon from the low-pH oxidation zone (sample AS3/016). C, Low-pH oxidation zone of the Cauquenes tailings impoundment, El Teniente with surface precipitation of chalcanthite (cha; $CuSO_4{\cdot}5H_2O$), and, at interfaces of layers of different grain size, of schwertmannite. D, Evaporite zone of the El Salvador tailings impoundment No. 1 with a zoom showing secondary efflorescent salts (e.g. chalcanthite and bonattite $CuSO_4{\cdot}3H_2O$). E, Fractured primary (supergene) replacement of chalcopyrite (cp) by chalcocite–digenite on rims, primary zone (sample A2/900), Piuquenes tailings impoundment, La Andina. F, Typical chalcopyrite replacement by secondary covellite (cv) as complete rims, neutralization zone (sample A5/100), Piuquenes tailings impoundment, La Andina. Note that sphalerite (sl) does not show replacement. G, Fractured chalcopyrite grain (cp), showing primary (supergene) replacement by chalcocite–digenite and minor covellite (dark blue) at the borders, primary zone (sample T1/850), Cauquenes tailings impoundment, El Teniente. H, Chalcopyrite replacement by secondary covellite (cv) as thin complete rims, primary zone (sample T1/200), Cauquenes tailings impoundment, El Teniente.

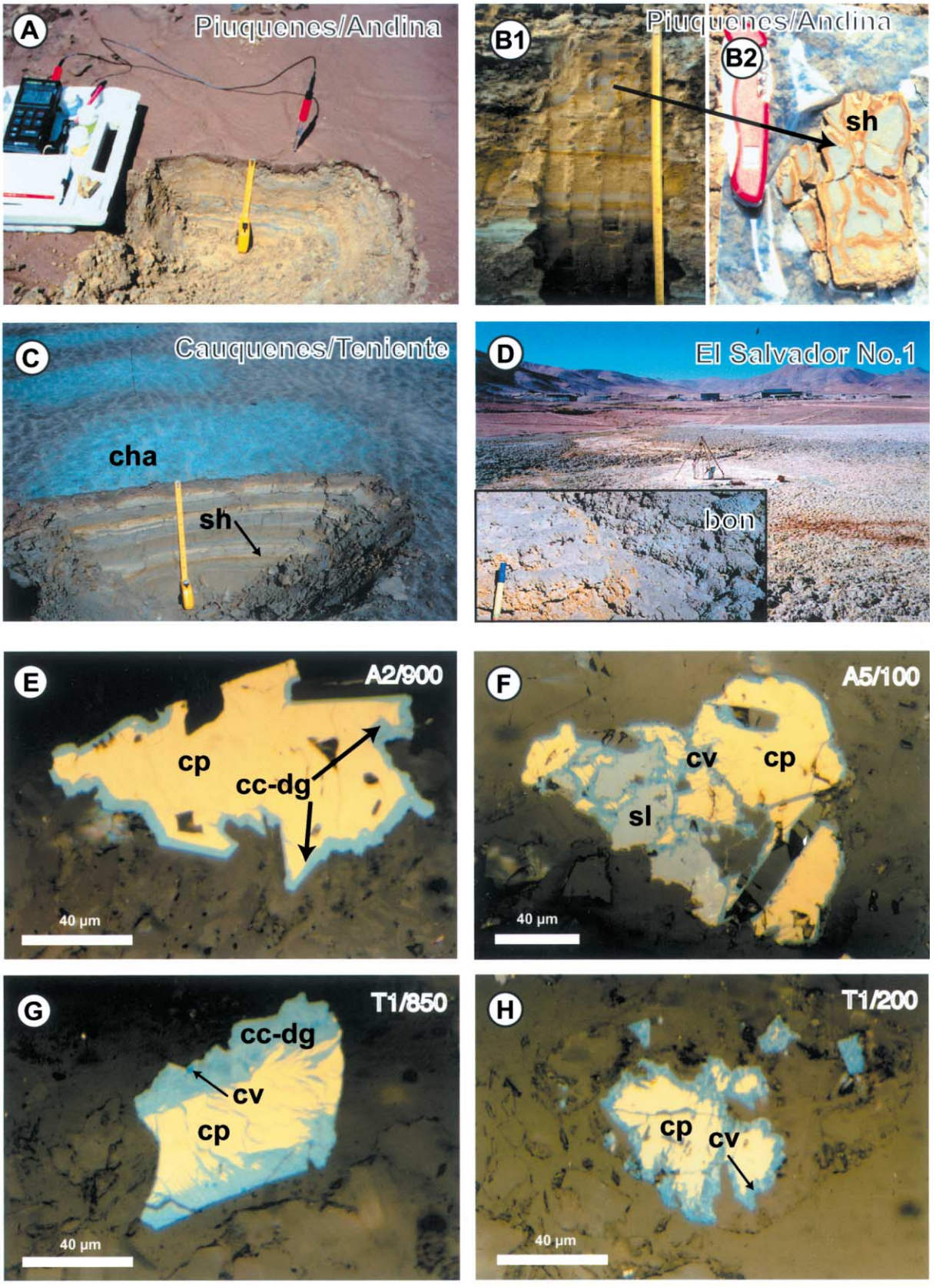
A
Piuquenes/Andina
B1
Piuquenes/Andina
B2
sh
C
Cauquenes/Teniente
cha
sh
D
El Salvador No.1
bon
E
A2/900
cp
cc-dg
40 µm
F
A5/100
cv
cp
sl
40 µm
G
T1/850
cc-dg
cv
cp
40 µm
H
T1/200
cp
cv
40 µm

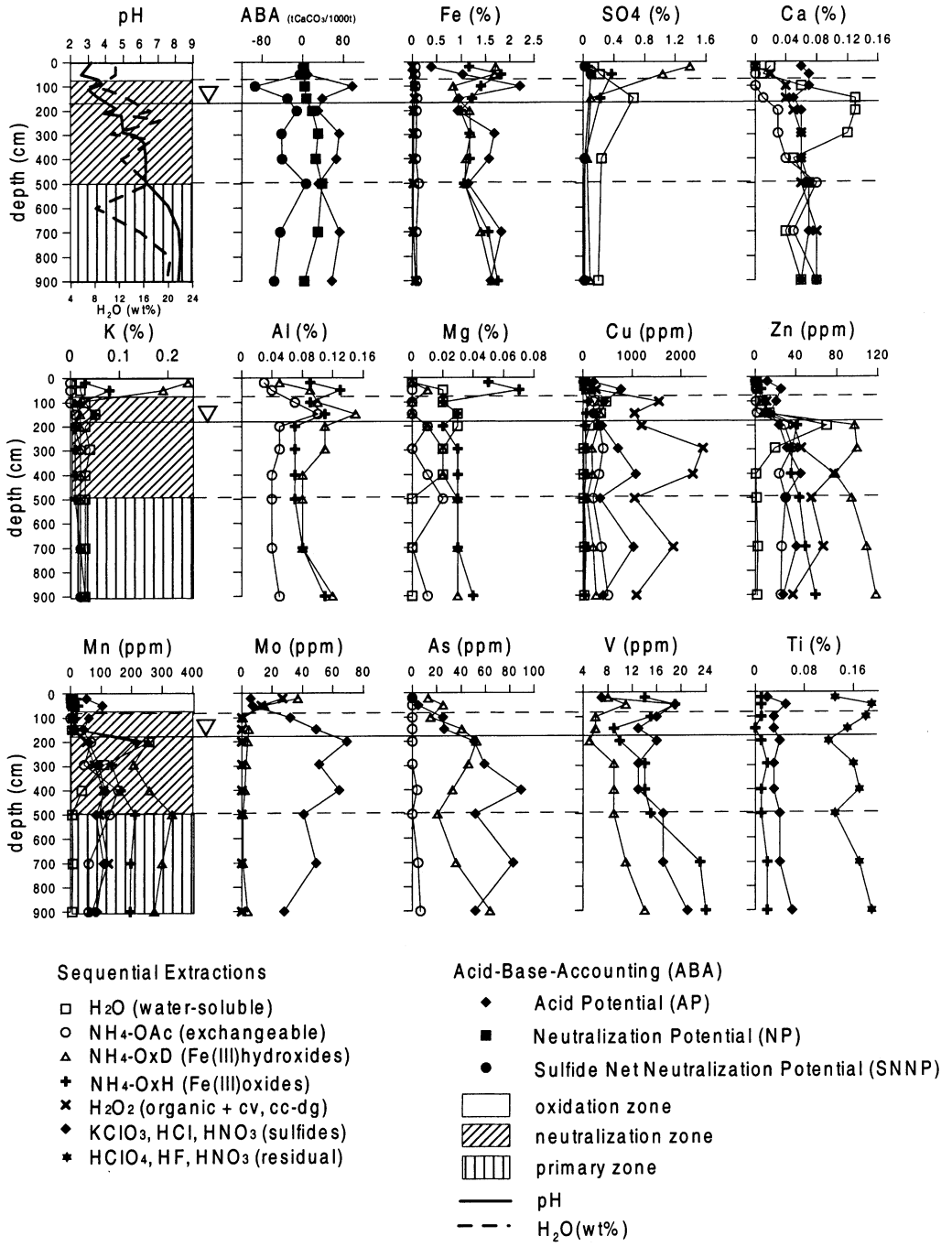

Fig. 3. Results of sequential extractions from the representative drill core A2 from the Piuquenes tailings impoundment, La Andina, Chile. For better visibility of the changes from primary to secondary phases (mainly from sulfides to oxides or sulfates) the concentrations of the residual fraction of some major elements (Fe, K, Al, Mg, Ca) are not shown in this figure and Figs. 10 and 13. Data for the discussed drill cores are in Tables A1–A3. All data (including elements not displayed in the figure) are contained in Dold (1999).

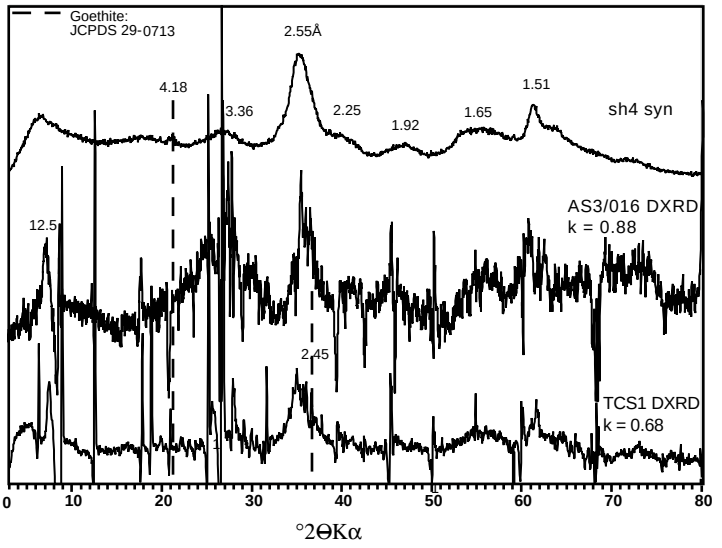

Fig. 4. DXRD of a hand selected schwertmannite-rich samples from the Piuquenes (Andina) tailings (AS3/016) and Cauquenes (El Teniente) tailings (TCS1) after 15 min. treatment with NH_4-oxalate pH 3 under exclusion of light compared to a XRD scan of a synthetic schwertmannite sample (sh4 syn). Due to dissolution of a part of the sample an intensity correction has to be applied denoted by the correction factor $k = 0.88$ for sample AS3/016 and $k = 0.68$ for TCS1. The Fe/S mole ratio in solution is 4.9 and 4.6 and the iron content is 2.6 and 3.6%, respectively. A dissolution test with the schwertmannite containing tailings sample AS3/016 shows fast dissolution of this iron phase (88.4% after 15 min). The peak position of the two main peaks of goethite is shown with the dashed line at 4.18 and 2.45 Å. At 2.45 Å goethite might be in the flank of the main schwertmannite peak, but in this case the main peak at 4.18 should also be present, what is not the case. This indicates that no goethite is dissolved in this leach. The peak at 12.5 Å results from the vermiculite-type mixed-layer mineral and shows that after the treatment an illite-type mineral remains, indicated by the shift to 10 Å. **Note**: This reaction occurs in the exchangeable fraction (2. Step: NH_4-Ac leach) so that in the Fe(III) hydroxides leach (3. Step: NH_4-OxAcD leach) only the secondary ferric oxyhydroxides and oxyhydroxide sulfates are dissolved.

natural and synthetic schwertmannite and ferrihydrite samples with 0.2 M NH_4-oxalate at pH 3.0 under exclusion of light were performed. These tests (described in detail in Dold (1999), chapter 4) show that schwertmannite dissolves very fast (between 15 and 60 min reaction time) under these conditions, behavior which contrasts with that of pedogene goethite, reported not to dissolve (Cornell and Schwertmann, 1996), and with goethite formed in ARD environment which only partially dissolves under the same conditions, as documented by DXRD (Brady et al., 1986; McCarty et al., 1998), and own unpublished results.

In order to ascertain the presence of schwertmannite at Piuquenes (Andina) we performed DXRD analyses and dissolution kinetic tests on a hand selected Fe(III) oxyhydroxide sulfate-rich streak sample (AS3/016, Fig. 5). The resulting DXRD of sample AS3/016 (Fig. 4) shows the typical peak positions (2.54, 2.25, 1.98, 1.65, and 1.52 Å) and peak shapes of schwertmannite. The main peak of goethite (110) at 4.18 Å does not appear in the DXRD. Results show further that after 15 min 88.4% of the fast dissolving ferric mineral is dissolved and the shape of the dissolution curve is similar to that of web-like schwertmannite (Dold, 1999). In the sample AS3/016 also Fe-rich web-like structures could be detected by SEM-EDS. To maximize the selectivity against other possible secondary ferric minerals (e.g. goethite and jarosite), only a dissolution time of 15 min with 0.2 M NH_4-oxalate at pH 3.0 and under exclusion of light was applied. The leach of this sample contains 2.6% Fe and the Fe/S mole ratio is 4.9, value in the typical range of schwertmannite. The DXRD, the extreme fast dissolution kinetics, typical for schwertmannite and faster than of any reported goethite, and the Fe/S mole ratio, typical for schwertmannite, lead us to the interpretation that this Fe(III) oxyhydroxide sulfate mineral is schwertmannite and not a sulfate bearing goethite.

Dissolution kinetic tests and DXRD analyses have

Table 3
Stoichiometric calculation of the sulfate content based on the Fe and K concentrations of the third and fourth leach for jarosite (jt) and schwertmannite (sh; $Fe_{16}O_{16}(OH)_{10}(SO_4)_3$; Fe/S mol ratio ~5). The calculated sulfate concentrations are in agreement with the measured concentrations for the third leach (compare bold columns), indicating that only schwertmannite and jarosite were dissolved Fe(III) minerals in this leach (abbreviations as in Table 2) (calc (%) = calculated; (%) = measured concentrations)

Sample	K third	K fourth	Fe third	Fe fourth	Fe jt third	Fe jt fourth	Fe sh third	Fe ox fourth	sh/jt	sh/sh + jt	jt SO_4 third	sh SO_4 third	SO_4 jt + sh third	SO_4 third	SO_4 jt fourth	SO_4 fourth
	Measured (%)				Calculated (%)				Calc	Calc (%)	Calc (%)	Calc (%)	Calc (%)	(%)	Calc (%)	(%)
A4/035	0.08	0.14	1.08	2.33	0.24	0.59	0.84	1.74	1.02	50.41	0.28	0.29	0.57	0.56	0.69	0.71
A4/065	0.17	0.07	1.42	1.25	0.62	0.30	0.80	0.95	0.88	46.75	0.72	0.28	1.00	1.00	0.35	0.17
A2/020	0.24	0.03	1.71	1.16	0.91	0.13	0.80	1.03	0.76	43.34	1.06	0.28	1.34	1.39	0.15	0.06
A2/050	0.19	0.08	1.68	1.82	0.70	0.34	0.98	1.48	0.94	48.44	0.82	0.34	1.16	1.04	0.39	0.37

also shown, that secondary jarosite dissolves partly when treated with 0.2 M NH_4-oxalate at pH 3 under exclusion of light during 1 h, i.e. the conditions chosen for sequential extractions. The same DXRD analysis did not detect dissolution of goethite. Since with the applied techniques no goethite was found, this mineral, if present, can only be a very minor phase in the oxidation zone of the Piuquenes (Andina) tailings. Additionally, stoichiometric calculations (see Table 3 below, discussion under Section 4.1.5) indicate that effectively only schwertmannite and secondary jarosite (and not goethite), were dissolved in the 0.2 M NH_4-oxalate leach.

In addition, the presence of schwertmannite at the Piuquenes tailings as an important secondary Fe(III) oxyhydroxide sulfate is consistent with typical pH values (2.8–3.5) measured in the oxidation zone and the observed orange–brown color of streaks and dots, where this ferric oxyhydroxide sulfate has been detected (Fig. 2B). The univocal mineral identification of schwertmannite at Piuquenes is the first one for mine tailings.

4.1.3. Significance of the schwertmannite occurrence
Goethite was neither XRD detected in the bulk samples nor in the clay fraction, nor in the DXRD analyses of the different fractions obtained during the dissolution kinetics tests. This contrasts with descriptions of other oxidized sulfide mine tailings where sulfate bearing goethite (adsorbed sulfate), which has a similar ochre color as schwertmannite, is the commonly reported secondary mineral in the oxidation zone together with jarosite (Jambor, 1994; Jambor and Blowes, 1998).

At Piuquenes (Andina) schwertmannite occurs as dots or streaks in the fine grained horizons or as enrichments at the interface with fine to coarse grained horizons (Figs. 2B and 9). This schwertmannite distribution suggests that it is preferentially associated with water flow-paths, whereas jarosite occurs disseminated in the oxidation zone as indicated by SEM-EDS element distribution of K and S (Fig. 5) and microscopical studies, which show this mineral to occur within altered feldspar grains as well as mineral rims and thin coatings. The association of schwertmannite to water paths may be explained by pH-increase through dilution to values in the range of 2.8–3.5 necessary for the schwertmannite formation (Bigham et al., 1996), whereas outside of the water paths the pH values are lower and jarosite forms. This is also supported by the field observation that schwertmannite is more abundant near the pond region. In contrast, jarosite forms possibly as in-situ replacements at lower pH, where the sulfide oxidation and liberation of potassium takes place (feldspar alteration and K liberation from biotite, resulting in the formation of a secondary vermiculite-type mixed-layer mineral, 12.25–12.67 Å). This interpretation is consisting with the findings of Barker et al. (1998), who observed pH values in the range of 3–4 in confined spaces with living microbial colonizing cleavage planes on biotite whereas at the mineral surface the solution pH was near neutral.

The interpretation that jarosite formed first in lower pH microenvironments and schwertmannite formed subsequently in areas of slightly higher pH due to dilution is also supported by the findings of Puura and Neretnieks (2000) who modeled with the

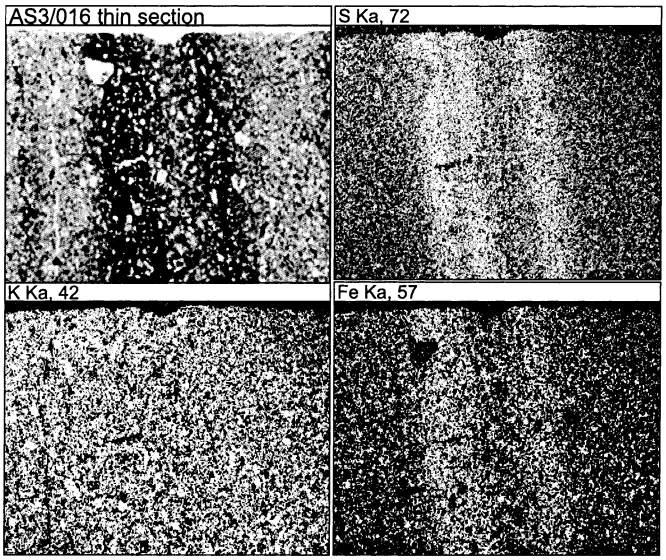

Fig. 5. Undisturbed tailings samples with two schwertmannite-rich streaks from the Piuquenes (Andina) impoundment were impregnated with epoxy resin and a thin section of this sediment was prepared. SEM-EDS element mapping for major elements show that Fe and S, the major elements of schwertmannite, are enriched at the streaks of flow-paths. As indicated by DXRD (Fig. 4) and explained in the text this element distribution responds to the presence of schwertmannite and not to adsorption of sulfur as sulfate to goethite and/or ferrihydrite. Potassium as a tracer for jarosite, shows no relationship to the streak.

computer code PHREEQC (Parkhurst, 1995) the buffering potential of aluminosilicates in a pyritic, low-carbonate waste dump. The results show that at low pH as long as K^+ is available, due to silicate dissolution, K–jarosite is supersaturated. When not any more K^+ is available, schwertmannite becomes the supersaturated phase (goethite formation was not considered in the model). In the jarosite-bearing oxidation zone of the Piuquenes tailings, sequential extractions show that 0.01–0.08% of K is available in the water-soluble fraction (Fig. 3). Samples in which schwertmannite was determined show K concentrations below the detection limit of the water-soluble fraction (e.g. AS3/016, Table 4).

Laboratory work further suggests that also sulfate contents plays a key role in the speciation of the secondary ferric mineralogy. Ferrihydrite transforms at pH 4 preferentially to goethite, whereas at lower as well as at higher pH, with a maximum at pH 7–8, hematite is formed. High sulfate content at low pH seems to favor the goethite formation (Cornell and Schwertmann, 1996).

As mentioned above, goethite is mainly reported from high sulfide mine tailings often as coatings (Jambor, 1994) or as enrichment at cemented layers ('hard pans') formed through neutralization reactions, mainly controlled by carbonate neutralization (Blowes et al., 1991; Jambor, 1994; Dold, 1999, chapter 6). At leached cappings and gossans of porphyry copper systems, increasing amounts of goethite and jarosite correlate with progressively higher ratios of pyrite and chalcocite at depth (Alpers et al., 1994a, b). Thermodynamic data of ferric complex species shows that the solubility of hydroxides is a function of pH and concentrations (Stumm and Morgan, 1996). So, with high Fe(III) concentrations, the stability field of the solid ferric hydroxide increases with low-pH values. This indicates that high iron sulfide contents will favor to the hydrolysis of a ferric phase at low-pH conditions, for example in the microenvironments at the sulfide surface, where oxidation occurs. This might explain that in high sulfide tailings saturation in respect to the ferric phases as goethite and ferrihydrite is reached quickly, leading to the coating of sulfides. High carbonate contents lower additionally the mobility of ferric iron due to pH increase and seem to favor the formation of goethite (Carlson and Schwertmann, 1990).

Table 4
Results from sequential extraction (ICP-AES from Sequence B) from the surface sampling AS3 (Piuquenes tailings, Andina), including the hematite-rich sediment (AS3/002) and the underlying low-pH oxidation zone with schwertmannite-rich horizons (AS3/016) (abbreviations: BDL = below detection limit; – = leach interference, NH_4-OAc = Ammonium acetate leach; NH_4-OxD = Ammonium oxalate 1 h dark; NH_4-OxH = Ammonium oxalate 2 h hot; sulfide = $KClO_3$; HCl, HNO_3 leach; residual = $HClO_4$, HF, HNO_3, HCl leach)

Sample	Depth (cm)	H_2O	NH_4-OAc	NH_4-OxD	NH_4-OxH	H_2O_2	Sulfide	Residual	Total	Bulk
Fe (%)										
AS3/002	2	BDL	0.07	0.56	4.83	0.07	0.93	0.99	7.45	8.07
AS3/010	10	BDL	0.04	1.36	1.47	0.04	0.42	1.09	4.42	5.14
AS3/016	16	BDL	0.12	2.33	1.12	0.02	0.61	1.16	5.36	6.45
Al (%)										
AS3/002	2	BDL	0.07	0.18	0.58	0.3	0.68	7.28	9.09	10.1
AS3/010	10	BDL	BDL	0.04	0.15	0.03	0.26	5.35	5.83	6.43
AS3/016	16	BDL	0.02	0.05	0.18	0.06	0.45	6.22	6.98	7.86
K (%)										
AS3/002	2	0.01	0.02	0.01	0.12	0.1	–	2.75	3.01	3.82
AS3/010	10	BDL	BDL	0.17	0.1	BDL	–	3.17	3.44	4.13
AS3/016	16	BDL	BDL	0.3	0.05	0.01	–	3.55	3.91	4.73
Mg (%)										
AS3/002	2	BDL	0.03	0.03	0.25	0.02	0.42	0.28	1.03	1.09
AS3/010	10	BDL	BDL	BDL	0.07	BDL	0.2	0.29	0.56	0.59
AS3/016	16	BDL	BDL	0.01	0.12	BDL	0.36	0.37	0.86	0.95
Na (%)										
AS3/002	2	BDL	BDL	BDL	BDL	0.01	0.01	1.19	1.21	1.53
AS3/010	10	BDL	BDL	BDL	BDL	BDL	BDL	0.81	0.81	0.94
AS3/016	16	BDL	BDL	BDL	BDL	BDL	BDL	0.76	0.76	0.91
Ca (%)										
AS3/002	2	0.08	0.52	0.02	0.01	BDL	0.45	0.17	1.25	1.31
AS3/010	10	0.02	0.02	0.02	0.01	0.01	0.06	0.11	0.25	0.25
AS3/016	16	0.02	0.02	BDL	0.01	BDL	0.07	0.09	0.21	0.25
Ti (%)										
AS3/002	2	BDL	BDL	BDL	0.05	0.01	0.02	0.44	0.52	0.62
AS3/010	10	BDL	BDL	BDL	0.02	BDL	0.02	0.14	0.18	0.18
AS3/016	16	BDL	BDL	BDL	0.02	BDL	0.02	0.16	0.2	0.25
Ba (ppm)										
AS3/002	2	2	101	106	149	13	81	299	751	853
AS3/010	10	BDL	3	28	47	1	18	460	557	700
AS3/016	16	BDL	BDL	90	39	2	22	464	617	785
Cu (ppm)										
AS3/002	2	9	513	385	322	66	52.8	8	1356	1240
AS3/010	10	9	15	124	35	140	327	14.7	665	676
AS3/016	16	10	14	183	7	34	237	7	493	486
Zn (ppm)										
AS3/002	2	0.8	25.2	26.6	81.9	3.7	60.8	26.4	225.4	219
AS3/010	10	BDL	BDL	3.6	7.4	1.6	13.5	15.3	41.4	44.8
AS3/016	16	BDL	BDL	6.5	9.6	1.2	21.2	16.1	54.6	61.8
Mn (ppm)										
AS3/002	2	12	333	3030	1020	16	408	69	4888	5170
AS3/010	10	BDL	BDL	9	25	3	58	33	128	139
AS3/016	16	2	BDL	17	36	BDL	91	38	184	198

Table 4 (*continued*)

Sample	Depth (cm)	H_2O	NH_4-OAc	NH_4-OxD	NH_4-OxH	H_2O_2	Sulfide	Residual	Total	Bulk
Cr (ppm)										
AS3/002	2	BDL	BDL	1	5	BDL	3	3	12	9
AS3/010	10	BDL	BDL	4	8	BDL	2	4	18	8
AS3/016	16	BDL	BDL	6	5	BDL	4	4	19	11
Pb (ppm)										
AS3/002	2	BDL	BDL	7	25	BDL	15	BDL	47	48
AS3/010	10	BDL	BDL	9	5	BDL	4	BDL	18	27
AS3/016	16	BDL	BDL	12	6	BDL	9	BDL	27	35
Mo (ppm)										
AS3/002	2	BDL	BDL	2	4	7	BDL	BDL	13	7
AS3/010	10	BDL	BDL	29	4	39	4	2	78	70
AS3/016	16	BDL	BDL	58	5	6	5	BDL	74	76
V (ppm)										
AS3/002	2	BDL	BDL	6	51	6	13	82	158	174
AS3/010	10	BDL	BDL	8	19	BDL	6	48	81	87
AS3/016	16	BDL	BDL	13	16	BDL	12	61	102	116
As (ppm)										
AS3/002	2	BDL	BDL	21	43	BDL	BDL	BDL	64	78
AS3/010	10	BDL	BDL	17	BDL	BDL	BDL	BDL	17	28
AS3/016	16	BDL	BDL	29	BDL	BDL	BDL	BDL	29	61

The here presented porphyry copper tailings of Piuquenes (Andina) and Cauquenes (El Teniente), as well as those of El Salvador No.1 which will be described in the next section are characterized by low-sulfide contents (1.66, 1.0, and 6.19 wt% pyrite, respectively) and extreme low-carbonate content (1.42, 0, and 0 wt% calcite equivalent, respectively) leading to low Fe(III) concentrations and pH, and ensuring therefore a high mobility of ferric iron.

Shaw et al. (1998) and Jambor et al. (1999) report from low-sulfide tailings (mainly pyrrhotite) lysimeters tests (0.4, 1.0, and 2.3 wt% S) where oxidation of pyrrhotite results in pseudomorphic replacement by goethite, lepidocrocite, native sulfur, and an iron sulfate after 2.5 years of oxidation. After this time frame only in the higher sulfide tailings (2.3 wt% S) a vermiculite-type mineral occurs, indicating biotite alteration. After 4.5 years all three tailings show the presence of the biotite alteration in form of the vermiculite-type mineral and subsequently the formation of jarosite. This suggest, that in a first phase, pyrrhotite oxidation (which provides maximum 0.25 mole H^+ per mole pyrrhotite oxidized; Nicholson and Scharer, 1994) is faster than the K release by biotite alteration, so that goethite can form directly as in situ replacement of pyrrhotite given that no K is still available for jarosite formation. In a second phase, hydrolysis of goethite and lepidocrocite is nearly the only source of acidity during pyrrhotite oxidation, as the maximum 0.25 moles of protons produced during oxidation of this mineral are consumed during oxidation of ferrous iron and the formation of elemental sulfur (Ahonen and Tuovinen, 1994). When oxidation progresses and pH decreases, due to goethite and lepidocrocite hydrolysis, more aluminosilicate alteration liberates the K necessary for the jarosite formation and the subsequent formation of the vermiculite-type mineral (in the case reported by Shaw et al. (1998), and Jambor et al. (1999), after 4.5 years). In other words, in the case described by these authors, goethite is formed as in the initial step of pyrrhotite oxidation when moderate acidity prevents Fe^{3+} mobilization and K liberation. In contrast, in the studied porphyry copper systems, where potassic alteration ensures the availability of K^+, and very low neutralization potential low pH, already in the early oxidation steps monovalent cations (e.g. K^+, Na^+, H_3O^+) are available and jarosite can form suppressing goethite

formation. Additionally, Cu^{2+} and Zn^{2+} seem to increase the kinetics of K^+ release from biotite (Farquhar et al., 1997). Subsequently, if K^+ availability is limited and the pH can increase slightly to values around 3, schwertmannite may form under strongly oxidizing conditions.

The question may be also rosen why, after schwertmannite formation this mineral has not transformed to goethite in the Piuquenes tailings, as schwertmannite is reported to be meta-stable with respect to goethite. The knowledge of the transformation kinetics of schwertmannite to goethite are based on three laboratory experiments (Bigham et al., 1990, 1996; Murad et al., 1994) which show that the release of sulfate under slightly reducing conditions (aqueous solution) leads to the transformation towards goethite in 77–543 days, depending on the reagents forcing the sulfate release. None of these laboratory studies reflect the conditions of the studied tailings in which schwertmannite is formed characterized by strongly oxidizing, unsaturated conditions during the whole year and high sulfate activity. The pe–pH diagram presented by Bigham et al. (1996), shows that schwertmannite is stable at strongly oxidizing conditions whereas goethite is stable at more reducing conditions. Thus, it can be suggested that in the Piuquenes (Andina) tailings the prevailing high oxygen fugacity and sulfate activity slow down a schwertmannite to goethite transformation. The only field hint of the transformation kinetics from schwertmannite to goethite is given by Childs et al. (1998). They concluded that the transformation of schwertmannite to goethite (as acid mine drainage precipitates in aqueous solution) at Lake Matsuo-Goshikinuma, Japan, was incomplete even in samples ~30 years in age. The oxidation zone of Piuquenes has a maximum age of 17 years.

4.1.4. Acid–base accounting

The oxidation stratification is also confirmed by the results of acid–base accounting (Fig. 3, ABA). In the primary zone the average $S_{sulfide}$ content is 0.95 wt% and the C_{tot} is 0.17 wt%, thus giving a sulfide net neutralization potential (SNNP) of -45.35 $t CaCO_3$/1000t. The tailings therefore have a low acid potential (AP). Nevertheless, a well-developed oxidation-neutralization stratigraphy is observed in the tailings. In the oxidation zone the SNNP is near zero, indicating that the AP and the neutralization potential (NP) have been consumed (Fig. 3). If all S_{sulfur} is assumed to be present as pyrite, the average pyrite content in the primary and neutralization zones is 1.77 wt%. Correction using the Cu concentrations in the sulfide fractions of sequential extractions leads to an average pyrite content of 1.66 wt%.

4.1.5. Sequential extractions

The element distribution is discussed considering first its relation to the formation of detectable secondary minerals (major elements) and then the behavior of the trace elements. Data from one representative drill core (A2) are shown in Fig. 3 and in Table A1. The other drill cores show similar behavior (Dold, 1999).

Fe. Pyrite is the main source for iron and sulfur. Iron values in the sulfide fraction are depleted from 1.5 in the primary zone to 0.5% in the oxidation zone in the four analyzed drill cores (A2–A5). The residual 0.5% Fe is not necessarily from pyrite dissolution. Chao and Sanzolone (1977) reported that the $KClO_3$, HCl, HNO_3 leach may also attack the edges of silicates, thus liberating additional Fe. The presence of schwertmannite and jarosite as significant secondary minerals in the oxidation zone is reflected in an increase of the Fe concentrations in the Fe(III) oxyhydroxide (from 0.5 to 1.5%) and Fe(III) oxide leach (from 1 to 2.3%) in the analyzed drill cores (Fig. 3). The sulfur concentrations in these fractions parallel these increases. The iron content of the Fe(III) oxides leach in the primary zone represents the primary iron oxides (hematite, magnetite, ilmenite, goethite), as well as a part of the higher ordered secondary ferrihydrite. In the oxidation zone, Fe from secondary jarosite is superimposed on this primary Fe content. The iron concentrations in the water-soluble and exchangeable fractions are negligible. The increased potassium concentrations of the Fe(III) oxyhydroxide (from 0.02 in the primary zone to 0.24% in the oxidation zone) and Fe(III) oxide leach (from 0.01 to 0.08%) in the oxidation zone confirms the dissolution kinetics and DXRD data indicating that part of jarosite is dissolved in the Fe(III) oxyhydroxides fraction. Assuming that the potassium concentrations in the Fe(III) oxyhydroxide (third leach) and Fe(III) oxide (fourth leach) leachates correspond to jarosite dissolution, the total Fe content

associated to jarosite can be calculated (Table 3). The Fe contents associated to schwertmannite are calculated from the measured Fe_{total} in the Fe(III) oxyhydroxide leach minus the calculated Fe contents associated to jarosite in this extraction. Comparison of the sum of calculated sulfate concentrations related to schwertmannite and jarosite with the measured sulfate concentrations in the Fe(III) oxyhydroxide leach show a good agreement (Table 3), indicating that essentially schwertmannite and jarosite were the main dissolved Fe(III) minerals in this leach. The difference of Fe_{total} minus the calculated Fe contents related to jarosite in the Fe(III) oxide leach represents the primary iron oxide content of hematite, magnetite, and goethite content, as well a part of secondary higher ordered ferrihydrite. Results show that the schwertmannite/(schwertmannite + jarosite) ratio increases from 45.9% (A2) in the dam area to 52.5% (A4) in the pond area. This corresponds with the field observation that in the pond area more schwertmannite exists and supports the interpretation that schwertmannite precipitation is associated with dilution via water flow, as discussed before.

The iron concentrations in the two fractions which represent the secondary Fe(III) oxyhydroxides and their sulfates (i.e. third and fourth leach), decrease towards the oxidation front and in the neutralization zone, whereas in the primary zone the concentrations increase to levels similar to those seen in the oxidation zone (1.5–1.7%). This increase is interpreted to be the result of ferrihydrite hydrolysis. DXRD results suggest the presence of higher ordered ferrihydrite and goethite. The interpretation is also supported by the Fe/S mole ratios, which range from values of 2.1–6.2 in the oxidation zone up to values of 14.6–1001 in the zones below. The ferrihydrite is believed to be a secondary mineral and not a tertiary product, due to the observation in the field of brown to red–brown horizons in the primary zone. A tertiary ferrihydrite should also show lower ordering (e.g. two-line), due to faster hydrolysis (Schwertmann et al., 1999).

As already discussed above, this distribution of the secondary ferric minerals is different to most reported tailings, probably due to the low-sulfide, extreme low-carbonate contents, and high availability of K^+ of the primary porphyry copper mineralogy. Thus, the low NP is not able to produce a sharp pH gradient, which could limit the mobility of the ferric iron produced in the oxidation zone. Additionally, the low-pyrite content delivers not enough Fe to form a cemented layer or coating. As a result, and due to the slow pH increase, the supernatant ferric iron, which is not fixed as secondary ferric mineral in the oxidation zone, can migrate downwards and hydrolyze slowly to higher ordered ferric polymers (e.g. ferrihydrite). This pH-controlled mineralogical and geochemical distribution of Fe is consistent with the observations of Schwertmann et al. (1995) in a natural occurrence of jarosite, schwertmannite, ferrihydrite and goethite in the Austrian Alps. In the Rötlbach, jarosite forms at the strongly acid (pH 2.3) stream source, followed by schwertmannite (pH 3–4), and ferrihydrite and goethite downstream as the pH rose to pH 5–7 because of dilution with fresh water tributaries.

Ca. The distribution of Ca (Fig. 3) is an important indicator of neutralization reactions related to carbonates. Concentrations of Ca in the water-soluble fraction reflect the distribution of gypsum, confirmed by XRD data. In some areas, an increase of what might be secondary gypsum is observed in the oxidation zone, whereas the increase in concentrations of tertiary gypsum is associated with the phreatic level, as in the drill core A2 (Fig. 3). This also correlates with the sulfate concentrations found in the water-soluble fraction, in which gypsum dissolves. The Ca concentrations in the exchangeable fraction (NH_4-acetate leach) is interpreted as the calcite content ± adsorbed Ca, based on XRD control of dissolved phases (Dold, 1999). The Ca concentrations in the oxidation and neutralization zone are below the detection limit, increasing in the primary zone to average concentrations of 0.1% (average of all tailings samples, data not shown), corresponding to an equivalent calcite content of 0.17 wt%. This is much less than the calculation of the calcite equivalent by using the average of 0.17 wt% total carbon of all samples in the primary zone, which would lead to a content of 1.42 wt% calcite equivalent. As the Ca concentrations show that only 0.17 wt% can be associated with calcite, it is assumed that the rest of the carbon is present as 1.44 wt% of siderite ($FeCO_3$), as this carbonate is also reported from the mine. This correlates with the pH distribution. Near neutral pH values are found in the primary zone where calcite is apparently still present. Above, in the lower neutralization zone the pH seems to be buffered by siderite at values

around 5–6. In the upper neutralization zone, where all carbonates have been consumed, possibly gibbsite ($Al(OH)_3$) dissolution buffers the pH around 4–5, whereas in the oxidation zone, with pH < 3.5 (Fig. 3) the pH seems to be controlled by dissolution of Fe(III) hydroxides. This carbonate-mineralogy suggests that the effective NP is lower than the calculated NP with the assumption that all carbon is present as calcite as siderite dissolution combined with hydrolysis of Fe^{3+} might produce acidity.

Ti. Titanium is generally considered to be an immobile element. It has low concentrations (0.01–0.03%) in the Fe(III) oxide fraction, indicating that in this leach minor ilmenite or some Ti containing iron oxides were dissolved. Low concentrations in the sulfide leach (0.02–0.05%) may be an indicator of the partial dissolution of rutile and/or Ti bearing silicates.

Al. The trivalent aluminum has as its source mainly in the weathering of aluminosilicates. It shows slightly increased concentrations in the oxidation zone of the Fe(III) oxides fractions (0.09–0.13%), possible due to co-precipitation or substitution with the secondary ferric phases. A slight increase in the upper neutralization zone in the exchangeable (0.1%) and Fe(III) oxyhydroxide fraction (0.15%) is noted, possibly due to gibbsite ($Al(OH)_3$) hydrolysis, which could not be detected by XRD due to the low Al concentrations.

Cu. The average Cu content of the tailings deposited in the Piuquenes (Andina) impoundment is 0.22%. Our geochemical results reflect a continuous decrease of the average Cu content in the primary zone from the dam to the pond (A2 $Cu_{primary}$ $\emptyset$ = 0.25%; A5 $Cu_{primary}$ $\emptyset$ = 0.22%; A3 $Cu_{primary}$ $\emptyset$ = 0.17%; A4 $Cu_{primary}$ $\emptyset$ = 0.15%). This results from gravitational separation of the heavier sulfide minerals near the discharge point in the dam area. Cu shows in all drill cores a strong total enrichment below the groundwater level (0.37–0.60%) mainly in the H_2O_2-leach (0.2–0.27%) which mainly dissolves the secondary (and/or primary = supergene) Cu–sulfides such as covellite and chalcocite–digenite. A slight Cu increase near the groundwater level is also recognized in the water-soluble fraction. The enriched Cu zone extends to depths of 3–4 m, where upon the pH reaches values of 6, the sulfide enrichment stops, and the Cu in the exchangeable fraction increases slightly. As stated above, this zone of secondary Cu enrichment is correlated to thin covellite and chalcocite–digenite rims formed exclusively on chalcopyrite and bornite (Fig. 2E and F). Jang and Wadsworth (1994) have shown in a laboratory study at hydrothermal conditions (170–200°C), that chalcopyrite replacement starts with covellite and changes to digenite replacement. They postulate that even at low temperatures chalcopyrite will undergo enrichment to more readily leachable secondary Copper-sulfides. Alpers and Brimhall (1989) reported this Cu-sulfide sequence from supergene enrichment at La Escondida, northern Chile. In other tailings impoundments, where no primary supergene enrichment exist in the primary ore, the presence of secondary covellite enrichment is reported (Boorman and Watson, 1976; Blowes and Jambor, 1990; Lin and Qvarfort, 1996; Holmström et al., 1999). Supergene replacement is recognized in the primary zone of the Piuquenes tailings. It occurs only occasionally as complete rims, as most of grains were broken during milling. The supergene (primary) replacement rims are thicker ($>5 \times 10^{-3}$ mm) than the very thin secondary rims ($<3 \times 10^{-3}$ mm). This primary Cu enrichment mainly consists of chalcocite–digenite, whereas the secondary replacement consists mainly of covellite, which is in agreement with the findings of Jang and Wadsworth (1994) and Alpers and Brimhall (1989) that covellite is the first stage in replacement. The texture and mineralogy of secondary replacement and the association with the saturated neutralization zone, where more reducing conditions dominate, strongly suggest that this copper enrichment is a secondary process taking place in-situ in the tailings impoundment. In the Piuquenes (Andina) tailings, this process shows a strong association with pH. Webster et al. (1998) showed that Cu adsorption at natural acid mine drainage precipitates starts at lower pH (adsorption begins at pH 4 and 6 80–100% of the Cu is adsorbed) than for synthetic schwertmannite and ferrihydrite. In Piuquenes, Cu adsorption seems to compete with Cu replacement in Cu-sulfides. In pH ranges where Cu^{2+} is mobile (<pH 5), replacement of chalcopyrite by covellite dominates, whereas with increasing pH, adsorption immobilizes Cu^{2+} and replacement decreases. The concentrations of Cu and Zn in the exchangeable fraction (adsorbed) are clearly pH dependent (Fig. 6). Cu adsorption begins at pH 3.5, and with increasing pH the Cu concentration on solids

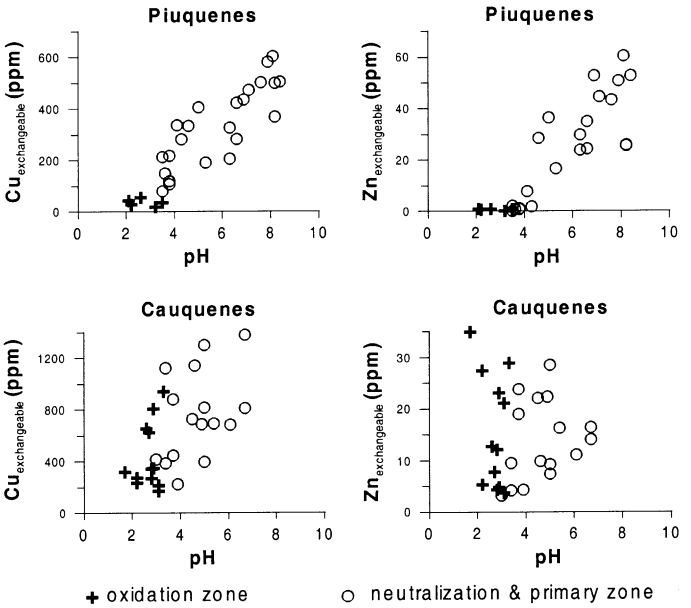

Fig. 6. Cu and Zn concentration of the exchangeable fraction (NH_4-acetate) versus the paste pH values from the Piuquenes (Andina) and Cauquenes (El Teniente) tailings. Data are from three drill cores in each tailings impoundment. For detailed discussion see text.

increases. Zn adsorption starts at a slightly higher pH than Cu (pH 4), thus confirming the results of the laboratory adsorption study by Webster et al. (1998).

Other bivalent cations. The other bivalent cations Mg, Mn, Zn, Ba, Pb, and Sr behave in a similar way. An enrichment of these elements in the water-soluble fraction is associated with the phreatic level. The exchangeable fraction, together with the reducible fractions, show nearly complete leaching in the oxidation zone and increasing concentrations downwards to the primary zone. This reflects their pH dependence with adsorption to clay minerals and secondary phases as $Fe(OH)_3$, $Al(OH)_3$, and $Mn(OH)_2$ and the diffusion into the crystalline systems and the co-precipitation with these secondary minerals. The sulfide fraction is generally depleted in the oxidation zone.

Mo. In contrast to bivalent cations, which are mobile under acid conditions, oxyanions as Mo(V, VI), As(V), and V(III, IV) show increasing adsorption to Fe(III) oxyhydroxides with decreasing pH (Dzombak and Morel, 1990). Chao and Sanzolone (1977) reported the partial dissolution of molybdenite in a H_2O_2-ascorbic acid leach. In our H_2O_2-leach the Mo concentrations were below the detection limit in the primary zone, indicating that no molybdenite was dissolved in this leach. In the Piuquenes (Andina) tailings, Mo is depleted in the sulfide fraction (molybdenite) from an average of 48 ppm in the primary zone to 7 ppm in the oxidation zone, due to molybdenite oxidation. The liberated Mo is stable as molybdate under acid oxidizing conditions and is mainly (37 ppm) associated with the Fe(III) oxyhydroxides fraction (schwertmannite) in the oxidation zone (Fig. 3). A semi-quantitative electron microprobe traverse of a schwertmannite streak (sample AS3/016) from the oxidation zone (Fig. 7) shows that Mo is slightly enriched in the matrix, confirming the preferentially adsorption by schwertmannite under acid conditions. As schwertmannite is associated with water flow paths, the enrichment of Mo in the schwertmannite streaks indicates certain mobility under acid conditions, possibly transported as molybdate adsorbed on ferric polymers. All drill cores show increased concentrations of Mo in the sulfide fraction in the neutralization zone (values up to 104 ppm Mo in the neutralization zone, whereas the Mo values in the primary zone range between 28 and 49 ppm). When the molybdate reaches reducing conditions (below the water table), this oxyanion is transformed to insoluble lower valence compounds.

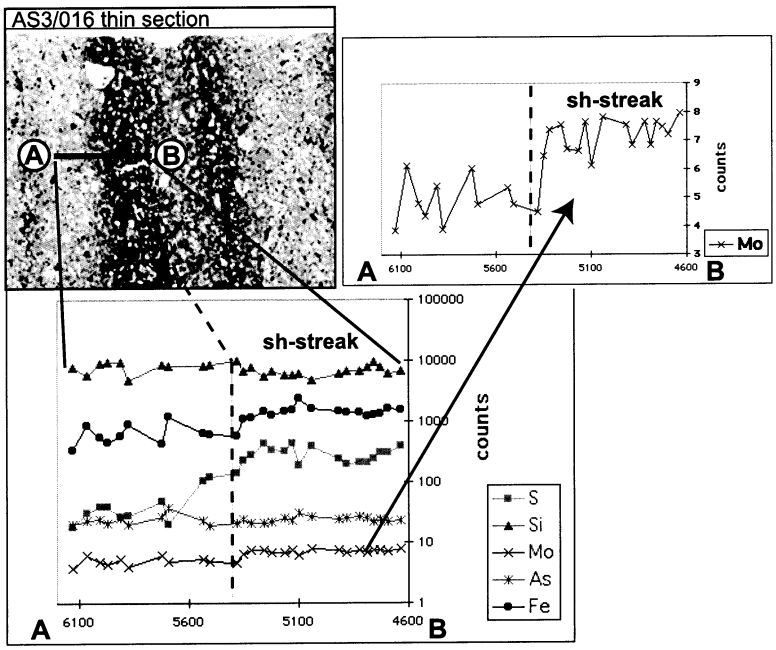

Fig. 7. Semi-quantitative microprobe analysis in the matrix of the schwertmannite-streaks (sh-streak) of sample AS3/016 (Piuquenes, Andina) showing increasing concentrations of Fe, S, and Mo. The higher concentrations of Mo in the sh-streak suggest the adsorption of molybdate at sh under low pH (2.5–3.5). The slight enrichment of Mo in the sh-streak indicates a certain mobility of this element, possibly transported as adsorbed oxyanion at ferric polymers. Arsenic does not show increased values in the sh-streak.

Thus, Mo may be incorporated into the cryptocrystalline variety of molybdenite called jordisite (Brookins, 1988). As the enrichment of Mo occurs in the same conditions in which secondary Cu replacement takes place, there is the possibility of secondary Mo enrichment by secondary sulfide precipitation or replacement. However, the Mo concentrations are too low (<160 ppm) to detect a mineral phase to explain this apparent enrichment.

A further specific feature of Mo in the oxidation zone is that it is enriched in the organic fraction (27 ppm). This may be from Mo fixation in dead cell material of sulfide oxidizing bacteria (e.g. *T. ferrooxidans*). *T. ferrooxidans* is known to oxidize molybdenite but is poisoned by the resultant molybdate unless this is fixed, e.g. by ferric iron (Tuovinen et al., 1971; Ehrlich, 1996).

As. Arsenic is depleted in the sulfide fraction of the oxidation zone, possibly due to oxidation of traces of tennantite. It is fixed in the Fe(III) hydroxide fraction, with a minimum (15 ppm) at the oxidation front (pH < 3) and a slight increase towards the oxidation (25 ppm) as well to the primary zone (64 ppm). The As concentrations in the exchangeable fraction are below the detection limit in the oxidation zone and increase slightly to the primary zone (7 ppm). Arsenopyrite is reported to be oxidized by *T. ferrooxidans* under the production of arsenate and arsenite and enargite with the release of cupric copper and arsenate (Ehrlich, 1996). Due to slow redox transformations, both arsenite and arsenate are often found in both redox environment together, either oxidizing or reducing (Raven et al., 1998; Stichbury et al., 2000). Arsenate is strongly adsorbed by hydrous ferric oxides (HFO) under acid conditions (Dzombak and Morel, 1990) in the tailings, this relationship is reflected by the increased As concentrations in the Fe(III) oxyhydroxides fraction in the oxidation zone. In-situ measurement of As by electron microprobe at a schwertmannite streak did not show any enrichment so that As replaces possibly in solid solution in jarosite. Substitution of arsenate and phosphate for sulfate in jarosite as a solid solution is known (Alpers et al., 1989), but due to the low concentration of As

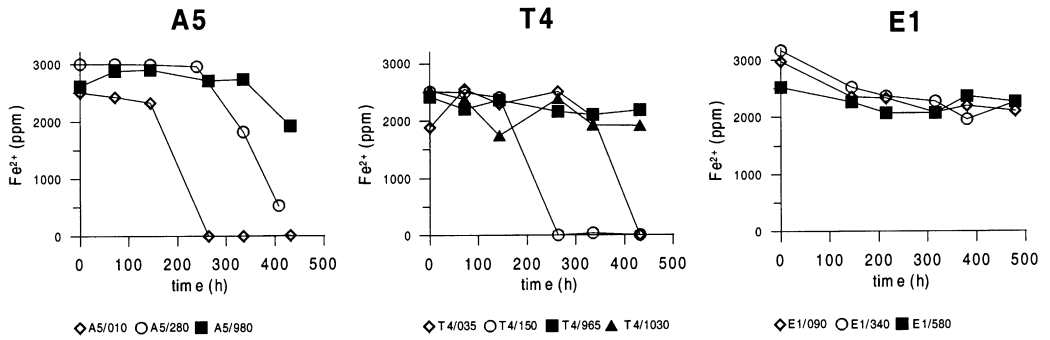

Fig. 8. Microbial iron (Fe^{2+}) oxidation activity of representative samples from the three studied tailings. The drill core A5 is from Piuquenes (Andina), T4 from Cauquenes (Teniente), and E1 from El Salvador No. 1. Filled dots are samples from the primary zone and unfilled dots are from the oxidation or neutralization zone. As expected, samples from the oxidation zone from Piuquenes and Cauquenes start to oxidize. In contrast, none of the samples from the oxidation zone of El Salvador show important oxidation. This is interpreted as an effect of higher molybdenite contents in the Salvador tailings, metal lethal to oxidizing bacteria (see text).

(<150 ppm) in the Fe(III) oxides leachates (Step 3 and 4) no mineralogical determination by XRD of possible members of the beudantite and crandallite groups was possible. Arsenite is relatively mobile at pH values below 4 and its adsorption increases with increasing pH up to concentrations of pH 8, before adsorption decreases again with increasing pH (Dzombak and Morel, 1990). Downwards mobilized arsenite may be an explanation for the increased As concentrations associated to the Fe(III) oxyhydroxides fraction in the primary zone.

V. Vanadium and As show similar distributions. In the sulfide fraction the V concentrations decrease in the oxidation zone (7 ppm), whereas they increase in the two reducible fractions towards the oxidation and primary zone (maximum 24 ppm) displaying the lowest concentrations at the oxidation front (6 and 9 ppm).

4.1.6. Microbial activity

Three representative samples from the oxidation, neutralization, and primary zones were tested for bacterial counts and oxidation activity. In all samples, high bacteria concentrations were observed by direct counting (2.6×10^7–3.4×10^8 bact/ml). *T. ferrooxidans* was cultivated (3.2×10^3 bact/ml) in the sample from the neutralization zone. Oxidizing activity tests show that the sample from the oxidation zone first starts to oxidize Fe^{2+} to Fe^{3+} after an initial or lag phase of 144 h. The lag phase is characterized by cell growth, and by the absence of cell division (Fig. 8). This good oxidation activity may indicate the presence of *Leptospirillum ferrooxidans* in the oxidation zone, as *T. ferrooxidans* plate counting yielded no result. Oxidation activity in the sample from the neutralization zone began after 240 h growth time. Once oxidation started, the oxidation velocity (growth rate) was similar to that of the sample from the oxidation zone. The sample from the primary zone showed slow oxidation starting after 336 h (Fig. 8), indicating relatively low microbial oxidizing activity in the primary zone.

4.1.7. Hematite-rich sediment of the pond area

The maximum extension of the pond in winter is associated with the presence of a clay-size ($K = 8.47 \times 10^{-9}$ m/s), intense red–brown laminated sediment with a maximum thickness of 15 cm at the center of the pond, which had a pH of 7.6 during sampling. The sediment, which has a paste-pH between 7.6 and 8.4, overlies the low-pH (paste-pH 2.1–3.5) oxidation zone, separated by a well-defined contact (Figs. 2A and 9). The lateral transition zone of this sediment to the underlying low-pH oxidation zone was sampled in detail in a second field campaign 1997 (Fig. 1, AS1–AS4).

Polished thin sections, as well as XRD and DXRD show that the red sediment is enriched in oriented tabular hematite and a higher ordered ferrihydrite (5–6 line). The high crystallinity (results of Mössbauer spectroscopy, Friedl, 1997, personal communication) of the hematite in relation to

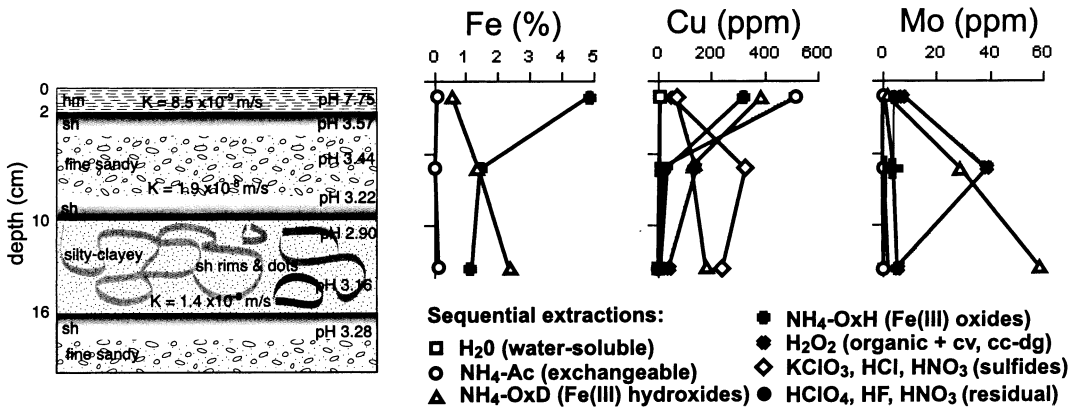

Fig. 9. Zoom of the first 20 cm of the pond surface at Piuquenes (Andina) with the hematite-rich sediment and the underlying schwertmannite-rich oxidation zone (sampling campaign 1997, AS3). Geochemical results from sequential extractions of Fe, Cu, and Mo from the three upper horizons are presented. The Cu distribution is representative for the behavior of bivalent cations and Mo is representative for oxyanions in the oxidation zone. *K* values (hydraulic conductivity) were calculated from laser-particle-size analyses. For detailed discussions see text.

pedogene hematite and the fact that this type of tabular hematite is also found in the primary zone of the tailings, suggest a hypogene origin. The fine layering, the location at the lowest elevation of the impoundment, and the sharp contact with the low-pH oxidation zone indicate that the hematite-rich sediment is a product of 'alluvial' enrichment taking place on the tailings surface. The results of sequential extraction confirm this interpretation, showing strong enrichment of bivalent cations mainly in the exchangeable and Fe(III) oxyhydroxides fractions of the hematite-rich sediment, whereas the underlying oxidation zone is leached out with respect to these elements (Fig. 9). In contrast, Mo is not enriched in the hematite-rich sediment, due to the low mobility of molybdate under the acid conditions prevailing in the oxidation zone, which surrounds and underlies the pond.

At the geochemical interface between the hematite-rich sediment and the oxidation zone the different geochemical behavior of oxyanions and bivalent cations is documented by the sequential extraction results (Fig. 9, Table 4). Mo is enriched in the organic fraction (H_2O_2-leach) of the oxidation zone below the hematite-rich sediment in a coarser horizon. This may indicate that in coarser material the microbial activity is higher due to better O_2 transport, resulting in higher molybdenite oxidation and increased poisoning of sulfide oxidizing bacteria as *T. ferrooxidans*, as discussed above.

The following genetic model for this hematite-sediment is proposed: Rainfall (pH 5.5) causes dilution of the acid in the oxidation zone, subsequently the pH increases, and Fe, Al, or Mn hydrolyze to polymers. The polymers, together with fine-grained material as clay minerals and fine tabular hematite are transported following the hydraulic surface gradient to the pond and enriched in its depression, where the particles settle. In winter, the low permeability ($K = 8.5 \times 10^{-9}$ m/s) of the hematite-rich sediment forms a barrier to the underlying low-pH oxidation zone and the phreatic level. Bivalent cations are still mobile during the transport on the top of the low-pH oxidation zone. But when they reach the pond with pH 7.6 they are adsorbed and ferrihydrite forms. In summer, cracking of the fine sediments permits oxygen and water flux into the underlying oxidation zone, reflected by increased concentrations of bivalent cations in the first centimeters below the hematite-sediment. The fact that the pond and the sediment have neutral pH cannot only be explained by dilution with rainwater (pH 5.5). Ligand exchange of adsorbed elements with functional OH^--groups of the Fe(III) hydroxides can lead to an additional increase of the pH, due to strong adsorption processes in the hematite-rich sediment. In the pond water bicarbonate is also slightly enriched to 44 mg/l possibly due to eolic input, as the surrounding oxidation zone cannot be the source.

4.2. Cauquenes tailings impoundment, El Teniente

4.2.1. Physical properties and mineralogy

The surface of the Cauquenes (El Teniente) impoundment was totally dry during the first summer field campaign (1996) with groundwater levels between 2.4 and 3.7 m below surface. In winter an extended pond covers the center of the impoundment (Fig. 1). A general trend with coarser grain size at the edges (T4 $ØK = 2.3 \times 10^{-7}$ m/s) and finer grain size at the center (T2 $ØK = 2.8 \times 10^{-8}$ m/s) of the impoundment can be observed. In the center area spots of XRD determined blue chalcanthite ($CuSO_4 \cdot 5H_2O$) occur as secondary surface precipitates (Fig. 2C). The five drill cores (T1–T5) show a very similar stratigraphy of the tailings (Fig. 1). The stratigraphy, pH distribution and geochemical data from the representative drill core T1 are presented in Fig. 10 and Table A2. All geochemical data are contained in Dold (1999). The *oxidation zone* at the top reaches 1.05–1.65 m depth (T1 = 1.05 m; T2 = 1.65 m; T3 = 1.50 m; T4 = 1.53 m; T5 = 1.40 m), with paste-pH values of 1.72–4.12. The color is yellow with orange–brown horizons, streaks, and dots (Fig. 2C). The grain size is generally smaller than in the primary zone, due to breakdown to clay minerals. Fine sandy and silty–clayey horizons alternate. The oxidation zone is sharply separated from the dark gray to brown–gray colored primary zone, which as in Piuquenes (Andina) is defined by the stability of the primary sulfide assemblage, but is affected by secondary products of sulfide oxidation. No neutralization zone as that observed at Piuquenes is developed, possibly due to the total lack of carbonate neutralization potential (see ABA). Some brown horizons in the primary zone indicate the precipitation of secondary Fe(III) oxyhydroxides. The pH increase in the primary zone is generally up to maximum of 5, and only in drill core T3 neutral values are reached.

Quartz, albite, and micas (mainly biotite, as well as muscovite) dominate the gangue mineralogy, as shown by XRD. Illite, chlorite and kaolinite are the typical minerals in the clay fraction. In the oxidation zone the secondary mineralogy is dominated by disseminated jarosite and a vermiculite-type mixed-layer mineral (11.7–11.9 Å) as well by minor schwertmannite. The latter is associated with dots or streaks as well as horizon interfaces of different grain size (Fig. 2C). The presence of schwertmannite was proved by DXRD of a hand selected Fe(III) oxyhydroxide sulfate-rich streak by application of 15 min 0.2 M NH_4-oxalate at pH 3.0 under exclusion of light (sample TCS1 from the pond area, Fig. 1). Peak position and peak shape are typical for schwertmannite (Fig. 4; 2.56, 1.66, and 1.51 Å). The leach of this sample contains 3.6% Fe and the Fe/S mole ratio is 4.6, value in the typical range of schwertmannite. Gypsum is present as traces and mainly associated with samples from the phreatic level and is interpreted as a tertiary mineral. The traces of gypsum found in the oxidation zone may be secondary.

The study of polished sections show that sulfide oxidation is nearly complete in the oxidation zone. Only some small residual grains of pyrite or chalcopyrite could be observed. One pyrite grain was found to be coated by ferric hydroxides (goethite) and thus protected from further oxidation; in general pyrite does not show this coating. Magnetite is also present with hematite replacement.

The primary zone is dominated by pyrite, which shows strong fracturing. Chalcopyrite is present as traces and sometimes intergrown with bornite. Both hypogene sulfides commonly show partial replacement by chalcocite–digenite, and covellite. As in the Piuquenes (Andina) impoundment, two different generations of replacement can be differentiated. Camus (1975) reported that the most important supergene sulfide mineral present in the ore is chalcocite, with minor proportions of covellite. Hence, the stronger chalcocite–digenite with traces of covellite replacement in the tailings is interpreted to be primary supergene enrichment, consistent with its occurrence as fractured incomplete thick rims (Fig. 2G). The secondary replacement is characterized by thin, complete rims of mainly covellite with traces of digenite also associated exclusively with chalcopyrite (Fig. 2H). This secondary replacement is mainly found within a 2–4 m thick zone below the water-level. Most of the magnetite occurs as massive grains partly altered to hematite. Traces of sphalerite, molybdenite, rutile, goethite, hematite, and galena were observed.

4.2.2. Acid–base accounting

C_{tot} is below the detection limit in the Cauquenes (El Teniente) tailings and the $S_{sulfide}$ content in the

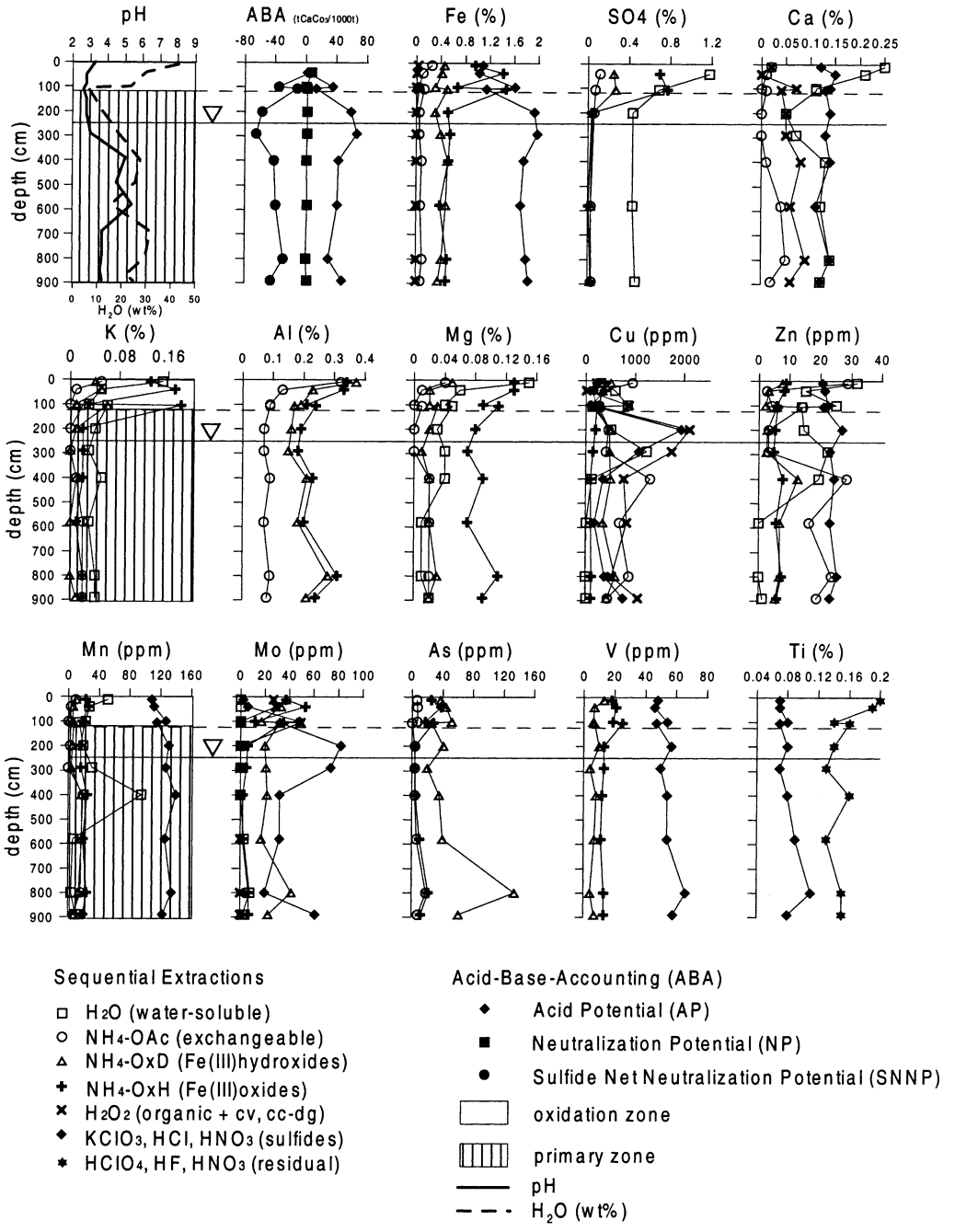

Fig. 10. Results of sequential extractions from the representative drill core T1 form the Cauquenes tailings impoundment, El Teniente, Chile.

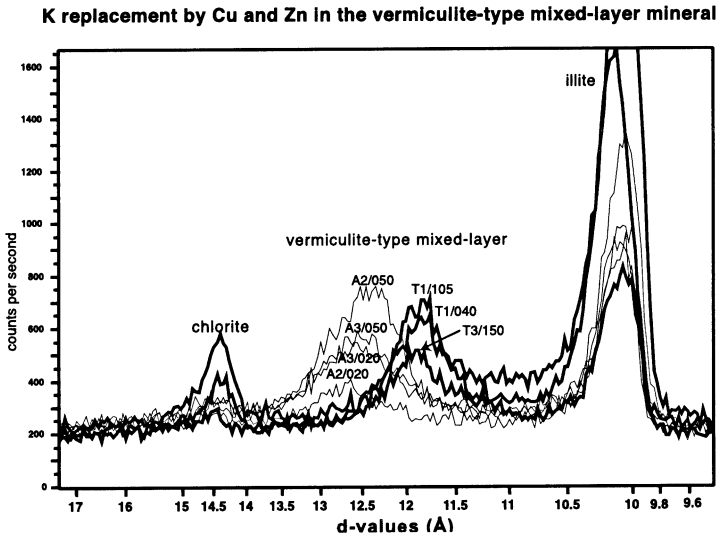

Fig. 11. Peak position (XRD results) of the vermiculite-type mixed-layer mineral in samples from the oxidation zones of the Piuquenes (Andina) tailings impoundment (A2/020, A2/050, A3/020, A3/050) and the Cauquenes (El Salvador) tailings impoundment (T1/040, T1/105, T3/150). The shift to lower *d*-values in the samples from Cauquenes is interpreted as replacement of K by Cu and Zn, due to higher activity during capillary controlled upwards migration during summer. This interpretation is supported by geochemical and microprobe analyses. For details see text.

primary zone averages 0.59 wt%, thus giving as ABA results an average sulfide net neutralization potential (SNNP) of −34.55 tCaCO$_3$/1000t (Fig. 10). If all $S_{sulfide}$ was in the form of pyrite, this would correspond to an average of 1.09 wt% pyrite in the primary zone. A correction with the Cu concentrations in the sulfide fractions of sequential extractions leads to an average pyrite content of 0.99 wt%.

The acid flotation circuit has a pH of 4.5, which explains the absence of a carbonate NP. The acid circuit is possibly also the reason for the low-pyrite content, as under acid conditions, and in contrast to alkaline circuits, a relatively high percentage of pyrite floats and end up in the concentrate. Low carbonate NP (0.12 and 0.16 wt% C_{tot}) was found in two samples of the T3 drill core what is consistent with pH locally approaching neutral values in this drill core. It might be that in this area material was deposited before the change from an alkaline to an acid circuit.

4.2.3. Sequential extractions

In the Cauquenes (El Teniente) drill core T4 (data in Dold (1999)) the element distribution is very similar to that of the Piuquenes (Andina) tailings. T4 is situated at the edge of the tailings impoundment (Fig. 1) and has permeability values one order of magnitude higher than in the tailings center (e.g. T1 and T2). Bivalent cations, e.g. Cu and Zn, are nearly completely leached out of the oxidation zone, whereas oxyanions such as Mo and As show low mobility through adsorption to Fe(III) oxyhydroxide sulfates. Data from a representative drill core in the center of the impoundment (T1; Fig. 10; Table A2), where the grain size is generally finer, show that cations Ca, K, Mg, Cu, Zn, Mn, as well as sulfate concentrations increase in the water soluble-fraction to the top of the tailings. In contrast to the exchangeable fraction of the oxidation zone of the Piuquenes tailings, the oxidation zone of the Cauquenes tailings (T1, T2, and T3) has elevated Cu and Zn concentrations in the oxidation zone (Fig. 6). Electron microprobe analysis of biotite from the oxidation zone shows that Mg and K decrease to the grain edges and Cu and Zn increase. The peak position of the vermiculite-type mixed-layer mineral is at lower *d*-values (11.7–11.9 Å) than at Piuquenes (Fig. 11, 12.25–12.67 Å). DXRD of the dissolved phases has shown that in the exchangeable fraction (NH_4-acetate) the vermiculite-type mixed-layer mineral is not present and that a new peak with lower *d*-values appears at the flank of the 001

illite peak. As discussed above, high activity of Cu and Zn favor the release of K from biotite and Cu and Zn can be fixed in the interlayer of the resulting vermiculite-type mixed-layer mineral, leading to the lower *d*-values (Fig. 11). This mineral is affected by the NH_4-acetate leach possibly due to detachment of the interlayer cations, and the peak shift to the lower *d*-values indicates that the mineral is not completely dissolved and an illite-type mixed-layer mineral remains.

Fe and Al are at or below their detection limits (0.01%) in the water-soluble fraction but show increasing concentrations (up to 1.46 and 0.37%, respectively) in the exchangeable, Fe(III) oxyhydroxide and Fe(III) oxide leaches of the oxidation zone (Fig. 10). K is available up to 0.15% in the water-soluble fraction of the oxidation zone. This high K content is also reflected by the high K concentrations in the Fe(III) oxide leaches of the oxidation zone, in which mainly jarosite dissolves as seen by high Fe concentrations. These data support the hypothesis discussed above that if K is present at low-pH jarosite will form and suppress the goethite formation. In the oxidation zone Mo is associated with the Fe(III) oxyhydroxide and Fe(III) oxide fractions possibly because it is adsorbed to schwertmannite and jarosite. As in Cauquenes (El Teniente), jarosite is the dominant secondary ferric phase (sh/jt ratio is below 0.5), and it seems to play a more important role in Mo retention as in Piuquenes (Andina), where this ratio reaches values >1. Mo is depleted in the sulfide fraction of the oxidation zone, but near the water table the Mo concentrations in the sulfide fraction double those of the primary zone. This may indicate that sulfide precipitation or replacement processes enrich Mo also, similarly as Cu.

The total As contents (between 25 and 202 ppm) are distributed in the exchangeable and reducible fractions, no As is detectable in the sulfide fractions, possibly also a result of low-pH conditions in the Cauquenes tailings. V does not display significant mobilization.

Water content and geochemical data from drill cores from the center of the impoundment (T1; Fig. 10) indicate that in the upper 100 cm a significant upwards mobilization of SO_4, Ca, K, Mg, Cu, Zn, and Mn takes place during the dry season. Fine grain size increases the water retention capacity and the capillary force, resulting in higher water content at the surface and an enrichment of bivalent cations in the form of water-soluble phases (Fig. 10), mainly as sulfates (e.g. gypsum, chalcanthite). This upwards migration is subsequently superimposed on the general trend of downwards mobilization during the rainy season. The downwards mobilization is reflected in the leached oxidation zone in T4 (coarse grain size) and the secondary replacement of chalcopyrite by covellite below the ground water table.

Stoichiometric calculation of the jarosite content leads to an overestimation of the sulfate content. Substitution of Al^{3+} for Fe^{3+} at the B site of jarosite ($AB_3(SO_4)_2(OH)_6$) or the presence of alunite could be the source for the excess in calculated SO_4 contents. This is supported by increasing concentrations of Al in the Fe(III) oxyhydroxide and Fe(III) oxide leach in the oxidation zone. Detailed XRD studies of the jarosites from the Piuquenes tailings and the jarosites from the T4 core (Cauquenes), which do not show increased concentrations of Al in this leach, show peak position near those of synthetic K–jarosite (Fig. 12). In contrast, jarosites from T1 show a peak shift to lower *d*-values, suggesting the substitution of Fe^{3+} (ion radius 0.65 Å) by the smaller Al^{3+} (0.53 Å). This is supported by an increase of Al content in the Fe(III) oxide leach (dissolution of jarosite) in samples from the oxidation zone. Correction with the Al content increases the accuracy of the stoichiometric calculation and suggests that up to 20% of the B site of the jarosite is substituted by Al^{3+}. These findings show that the evaporation controlled upwards mobilization of elements has direct influence on the composition of the secondary minerals.

As mentioned, Cu shows in Cauquenes (El Teniente) enrichment below the water table similarly as in Piuquenes (Andina) by replacement of chalcopyrite by covellite. Due to the lack of carbonate NP the neutralization sequence is not as well developed as in the Piuquenes tailings and the secondary Cu enrichment along the stratigraphy not so well defined. Ti concentrations are below the detection limit in the Fe(III) oxides leach indicating that no significant ilmenite is present in the Cauquenes tailings.

4.2.4. Microbiology

Four representative samples from the oxidation zone and primary zone of the Cauquenes (El Teniente) tailings were submitted to bacterial count and iron

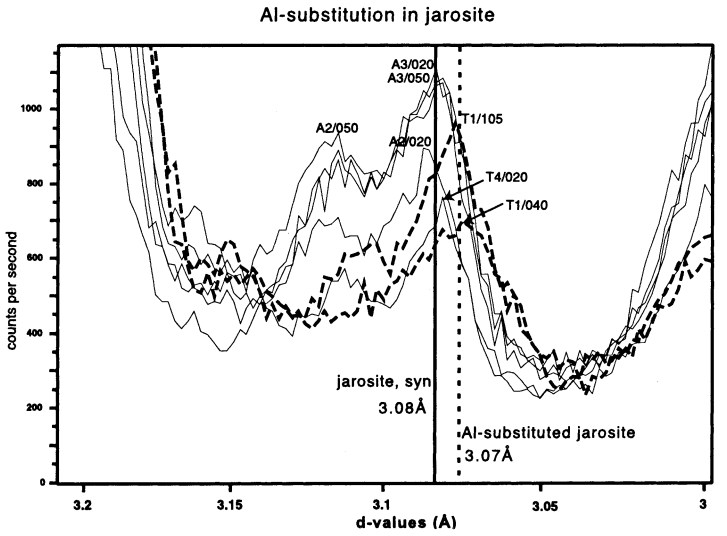

Fig. 12. Peak position (XRD results) of jarosites in samples from the oxidation zone of Piuquenes (Andina) and Cauquenes (El Salvador) tailings impoundments, indicating Al-substitution, resulting in a peak shift to lower *d*-values in sample T1/040 and T1/105. This interpretation is supported by geochemical results. For details see text.

oxidation activity tests (Fig. 8). In all samples high bacteria numbers by direct counting were observed (3.0×10^8–5.0×10^8 bact/ml). *T. ferrooxidans* could only be cultivated (1.4×10^5 bact/ml) in the sample from the oxidation front (T4/150). Oxidizing activity tests show that the sample from the oxidation front started first to oxidize Fe^{2+} to Fe^{3+} after an initial or lag phase of 144 h. This is consistent with the findings of Davis (1997) showing the highest population of *Thiobacillus ferrooxidans* at the oxidation front, whereas the population of *Acidiphilium* spp. increased to the top of the oxidation zone. The sample from the upper part of the oxidation zone started the oxidation activity after 336 h growth time, indicating a low population of active iron-oxidizing bacteria. Once oxidation started, the oxidation velocity (growth rate) was similar. The sample from the primary zone did not start significant oxidation in the time range (432 h) of the experiment (Fig. 8).

4.3. El Salvador No.1 tailings impoundment, Chile

4.3.1. Mineralogy

The four drill cores in the El Salvador No.1 tailings show at the top a 0.3–1.5 m (E1 = 0.3 m; E2 = 0.35 m; E3 = 1.5 m; E4 = 0.35 m) thick *evaporite zone* (Fig. 2D) with extensive blue, yellow, white and brown efflorescent salts formation (paste-pH 2.00–3.53). Below, an *oxidation zone* with orange–brown horizons and paste-pH values from 1.88 to 2.80 is observed. The primary zone (paste-pH 2.50–3.50), which was defined visually by its dark gray color but that, as discussed below, is significantly affected by oxidation, was intersected by two drill cores at depths of 1.7 m (E1) and 4.7 m (E2). It displays some dots and streaks of orange–brown Fe(III) hydroxides. Geochemical data for the representative drill core E2 are presented in Fig. 13. The moisture content in the evaporation zone was 0–8 wt% and increased downwards to constant 20 wt%. This relative high moisture content is surprising in view of the extremely low precipitation rates (20 mm/a), the high evaporation and the age of the tailings (36 years). It should be noted, however, that similarly old tailings in hyperarid climate (P. Cerda; Dold, 1999) also show moisture contents within this range.

In the *evaporite zone* at the top of the tailings a wide range of water-soluble secondary efflorescent salts were identified by XRD including bonattite ($CuSO_4 \cdot 3H_2O$), chalcanthite ($CuSO_4 \cdot 5H_2O$), pickeringite ($MgAl_2(SO_4)_4 \cdot 22H_2O$), and magnesioaubertite ($(Mg,Cu)Al(SO_4)_2Cl \cdot 14H_2O$). Hand picked specimens could be identified as chalcanthite, halotrichite ($FeAl_2(SO_4)4 \cdot 22H_2O$), and hexahydrite ($MgSO_4 \cdot 6H_2O$).

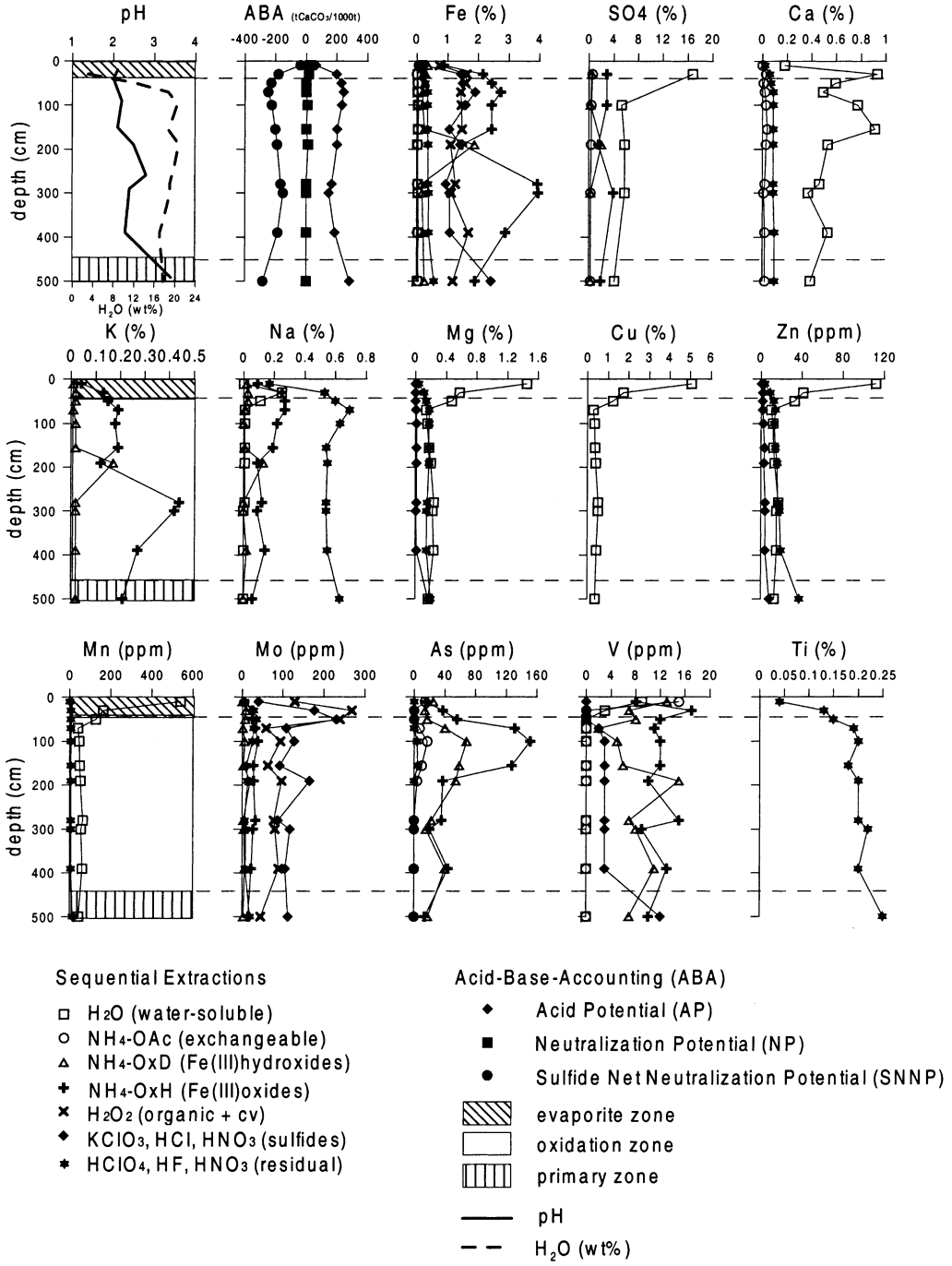

Fig. 13. Results of sequential extractions of the representative drill core E2 from the tailings impoundment No. 1, El Salvador, Chile. Note: Results of Na are shown instead of Al. Al has the same distribution as Mg, Cu, Zn, and Mn.

In the underlying *oxidation zone*, orange–brown ferric oxyhydroxides with the same appearance as in the Piuquenes (Andina) and Cauquenes (El Teniente) tailings, possibly schwertmannite, are enriched in some layers, but detection by DXRD failed, due to low Fe concentrations (1.59 and 1.88% Fe in the NH_4-OxD leach). A vermiculite-type mixed-layer mineral was detected in the oxidation zone in some samples by DXRD. The jarosite detected in low quantities in the clay fraction (<2 μm) is identified by XRD as hydronian and was only detected in samples from the oxidation zone and is interpreted as secondary. The presence of hydronian jarosite in these tailings could be explained by the low availability of K and Na (mainly at or below the detection limit in the water-soluble fraction of the oxidation zone, Fig. 13, Table A3) in the arid environment. However, as hydronian jarosite is thermodynamically less favored than K or Na–jarosite, it is more likely that this secondary jarosite is a solid solution of K and Na–jarosite resulting in a similar X-ray pattern than hydronian jarosite as pointed out by Dutrizac and Jambor (2000).

XRD studies show that quartz, alkali-feldspar (mainly albite ± anorthoclase), biotite ± muscovite, jarosite and natrojarosite dominate the primary zone mineralogy. Kaolinite and illite are the typical clay minerals. The study of polished sections shows that pyrite is abundant (about 6.2 wt%, see below) in all zones and generally is still relatively fresh and even in the oxidation zone it does not show Fe(III) oxyhydroxides rims or coatings. Minor traces of covellite ± chalcocite are only observed in the primary zone of samples E1/350 and E1/580. XRD data indicate that natrojarosite occurs in similar amounts in the primary and in the oxidation zones. In addition, in the clay fraction of the primary zone no 'hydronian jarosite' is detected. This suggests that natrojarosite and jarosite of the primary zone are primary i.e. supergene. The geochemical results discussed below support this hypothesis.

The low quantities of secondary ferric minerals in the El Salvador No.1 tailings are explained by the high preservation degree of pyrite, both in the primary and in the oxidation zone. In spite of the low degree of sulfide oxidation at El Salvador No.1 tailings, the pH is very acidic (1.88–3.53). This may be a result from acidity liberated by primary jarosite in combination with zero carbonate neutralization potential and hyper-arid conditions, and from the relative high pyrite content of the El Salvador No. 1 tailings. The reason of the low pyrite oxidation rate will be discussed together with the microbiological results.

4.3.2. Acid–base accounting

ABA reflects the relative high pyrite content of the El Salvador No.1 impoundment (Fig. 13). The average $S_{sulfide}$ content is 3.3%, which corresponds to an average pyrite content of 6.2%, as pyrite is nearly the only sulfide. The carbonate NP is generally at the detection limit so that the SNNP is strongly negative with an average from -183 $t CaCO_3/1000t$ (Fig. 13). A decrease of the AP at the top of the tailings impoundment is normally interpreted as a result of oxidation of sulfides, mainly pyrite (compare Fig. 3 and Fig. 10). In the case of El Salvador No. 1 the decrease of the AP in the evaporite zone is more likely an effect of upwards mass-transfer resulting from the extreme aridity. This is supported by low concentrations of the immobile element Ti in the evaporite zone (0.04%), compared to the original Ti average content of 0.2% in the underlying tailings. Additionally, the concentrations of Fe, K, and Na are also lower in the evaporite zone, likely reflecting a dilution of the primary jarosite and natrojarosite content and not an effect of pyrite oxidation.

4.3.3. Sequential extractions

The sequential extractions trace strong enrichments of SO_4, Al, Mg, Na, Cu, Zn, and Mn in the water-soluble fraction of the evaporite zone at the top of the tailings (Fig. 13; Table A3). This is consistent with the abundance of the water-soluble salts described before. The concentrations of Cu and Zn in the sulfide fraction are generally very low throughout the whole tailings stratigraphy (below 100 and 10 ppm, respectively), indicating that nearly all mobile elements are mobilized upwards and that the primary zone, which is defined by its dark color, has been in fact significantly affected by leaching resulting from low-pH conditions.

Fe shows at El Salvador constant and comparable concentrations around 1.5% in the weakly oxidizing H_2O_2-leach (suggesting that pyrite is not very resistant to oxidation, possibly due to surficial alteration) and in the strong oxidizing $KClO_3$–HCl–HNO_3 leach

throughout the tailings stratigraphy (Fig. 13, Table A3). This Fe distribution is different to that of the tailings at Piuquenes (Andina) and Cauquenes (El Teniente) where Fe concentrations in the H_2O_2-leach are near or below the detection limit (maximum 0.24 and 0.03%, respectively) and those in the sulfide leach are higher in the primary (about 1.5 and 1.8%, respectively) than in the overlying oxidation zones (about 0.5 and 1.3%, respectively, Figs. 3 and 10, Tables A1 and A2).

As noted above, XRD data suggest that at El Salvador possibly primary natrojarosite occurs in similar amounts in the primary and oxidation zone. The coupled behavior of the elements Fe, K, Na, and SO_4 at El Salvador and dissolution kinetics has been used to support the discrimination between primary and secondary jarosite. Fe, K, Na, and SO_4 show a similar distribution in the Fe(III) oxyhydroxide and in the Fe(III) oxide fractions (Fig. 13). These elements show a peak in the Fe(III) oxyhydroxide fraction of the orange–brown horizons from the oxidation zone, where possibly secondary schwertmannite and jarosite have formed. According to stoichiometric calculations based on K, Na, Fe, and SO_4 values the amount of schwertmannite is subordinated compared to those of jarosite and natrojarosite. However, it has to be taken into account that non-stoichiometric Fe:S ratios of the alunite–jarosite group are frequently observed (Alpers et al., 1989) and may range from 3:2 to 2.3:2. The jarosite found in the El Salvador No. 1 tailings displays a K/Na ratio in the Fe(III) oxide leach of 1.8 suggesting that K–jarosite is the dominant species but that natrojarosite also occurs. This contrasts with the studied tailings at Piuquenes (Andina) and Cauquenes (El Teniente) where natrojarosite is not recognized. In addition, the jarosite solubility at El Salvador (less than 10% the Fe(III) oxyhydroxide leach with exception of the schwertmannite/jarosite horizon where it is >50%) is lower than at the Cauquenes and Piuquenes tailings (>50% in the Fe(III) oxyhydroxide leach together with schwertmannite) where no secondary natrojarosite is recognized although albite is potential Na source. This may be explained by the dissolution kinetics of albite, which is much lower than that of biotite (Jambor and Blowes, 1998), resulting in a preferential formation of secondary (K-rich) jarosite instead of natrojarosite. All this supports the primary (supergene) character of the natrojarosite at El Salvador compared to the secondary K-rich jarosite found at Piuquenes and Cauquenes.

It remains the question if significant amounts of secondary jarosite are formed during weathering of the El Salvador No. 1 tailings. Biotite alteration may produce a vermiculite or a vermiculite-type mixed-layer mineral (Acker and Bricker, 1992; Jambor, 1994; Malmström and Banwart, 1997; Farquhar et al., 1997). Per mole of biotite, 2 moles of K^+ are liberated, available for the formation of 2 moles of jarosite (Eq. (10), below). Biotite is the main source for K^+ and Mg^{2+}, and also a source for Fe^{2+}, as K–feldspar as muscovite have an about 40 times slower reactivity than biotite (Jambor and Blowes, 1998). If jarosite was an important secondary mineral at El Salvador No. 1 tailings, it should be found in the clay fraction as shown by Stoffregen and Alpers (1992) for secondary alunite, and as it has been recognized at Piuquenes (Andina) and Cauquenes (El Teniente). Also abundant vermiculite or vermiculite-type mixed-layer minerals should be detected by XRD, as in the Piuquenes and Cauquenes tailings. However, in the El Salvador tailings this mineral could only be identified by DXRD as a very minor secondary phase. Only small amounts of jarosite (XRD patterns of hydronian jarosite) could be detected in the clay fraction. The peak position of the hydronian jarosite may also result from a solid solution between K and Na–jarosite (Dutrizac and Jambor, 2000). In Piuquenes and Cauquenes, a strong release of K^+ from biotite, and hence available for jarosite formation, is documented in the water-soluble fraction. At El Salvador the values of this fraction for K^+ and Na^+ are in most samples from the oxidation zone below detection limit. In summary, the data strongly suggest that at El Salvador natrojarosite and jarosite are primary (i.e. supergene) and only low quantities of secondary hydronian jarosite were formed in the tailings.

The oxyanions show a specific behavior. Mo concentrations (160–1000 ppm) are clearly higher than in the other two tailings (32–171 ppm). Mo is slightly enriched in the Fe(III) oxyhydroxide fraction of the Fe(III)oxyhydroxide-rich layers. The concentrations in the Fe(III) oxide fraction are constant throughout the tailings stratigraphy and may represent the Mo adsorbed through primary jarosites.

Arsenic is enriched in the exchangeable, Fe(III) oxyhydroxide, and Fe(III) oxide fractions of the upper part of the oxidation zone (17, 68, and 251 ppm, respectively), but is not mobile enough to be enriched in the evaporite zone. This can be explained by the fact that arsenate adsorbs preferentially to Fe(III) hydroxides and that these secondary iron phases are scarce in the evaporite zone. V shows more mobility than Mo and As, resulting in an enrichment in the evaporite zone in the water-soluble, exchangeable and Fe(III) oxyhydroxide fractions. Nevertheless, the main part of V is associated with the Fe(III) oxyhydroxide and Fe(III) oxide leach.

4.3.4. Microbial activity

The results of bacterial count and oxidation activity tests show in all samples (evaporite, oxidation, and primary zone) high bacteria numbers by direct counting (2.0×10^7–1.8×10^8 bact/ml). *Thiobacillus ferrooxidans* could not be cultivated in any of the El Salvador tailings samples. The oxidizing activity tests show that all three samples started a slow oxidation and reached a plateau after 150 h at around 2000 ppm Fe^{2+} (Fig. 8). The very low or non-existent bacterial oxidation activity at the El Salvador No.1 contrasts with the higher oxidation activities detected in similar microbiologic tests carried out on tailings from Piuquenes and Cauquenes (Fig. 8). This may be due to the high molybdenum contents of the El Salvador tailings (160–1000 ppm) which are higher than in Piuquenes and Cauquenes (32–171 ppm). As stated before, molybdate poisons *T. ferrooxidans* during oxidation (Tuovinen et al., 1971).

4.3.5. Slow pyrite oxidation and acid availability

The very low or non-existent microbial oxidation, possibly due to molybdate poisoning, at the El Salvador No.1 tailings constitutes the best explanation for the above mentioned high preservation degree of pyrite in the 'primary' and oxidation zones, as non-bacterial oxidation is much less efficient. Singer and Stumm (1970) have shown that microbial mediation of sulfide oxidation may accelerate the oxidation rates by a factor larger than 10^6. The low quantities of secondary ferric minerals compared to the relative high pyrite content at El Salvador No. 1 tailings are interpreted to be the result of slow inorganic pyrite oxidation. The possibility that a lack of oxygen or water is responsible for the slow pyrite oxidation is less probable, as cracking assures availability of oxygen even in the deeper part of the tailings and the 20 wt% of moisture content is in the range of those of Piuquenes and Cauquenes (Figs. 3 and 10).

5. Conclusions

5.1. Mineralogy and geochemistry

In this study, the geochemical behavior of three inactive flotation tailings from the porphyry copper deposits La Andina, El Teniente, and El Salvador, Chile is compared. The climate is characterized as alpine, Mediterranean, and hyper-arid, respectively. Sulfide assemblages of these three deposits are comparable and are dominated by pyrite, chalcopyrite, minor bornite and molybdenite, and traces of magnetite and hematite. The gangue mineralogy is in all three deposits dominated by quartz, alkali-felspars (albite to K–feldspar), and micas (biotite, muscovite). El Salvador contains additionally supergene jarosite, Na–jarosite, goethite, and hematite. The average pyrite contents of the tailings impoundments Piuquenes (Andina), Cauquenes (Teniente), and El Salvador No. 1 are 1.7, 1.0, and 6.2 wt%, respectively. Carbonate contents are in all tailings low (1.4, 0, and 0 wt% calcite equivalent, respectively). The zero carbonate NP of the Cauquenes tailings may results from the application of an acid flotation circuit (pH 4.5) and in case of El Salvador possibly is a result of strong supergene enrichment.

The developed seven-step sequential extraction method for copper sulfide mine tailings (Dold, 1999) has shown to be a useful tool for the study of the effects of sulfide oxidation and neutralization processes to element mobility. However, it is crucial, due to the wide range of possible secondary phases in these systems, to investigate the primary and secondary mineralogy of the tailings through careful mineralogical studies and dissolution kinetic tests. These mineralogical data have to be coupled with the geochemical data.

The secondary mineralogy of the Piuquenes (Andina) and Cauquenes (El Teniente) tailings is dominated in the oxidation zone by jarosite, schwertmannite, and a vermiculite-type mixed-layer

mineral. Jarosite is disseminated and mainly associated to feldspar alteration and mineral rims. Schwertmannite could be mineralogically detected by DXRD in the Piuquenes and Cauquenes tailings, what is the first detection in mine tailings. Its presence is additionally supported by dissolution kinetic tests (88.4% dissolved in 15 min in 0.2 M NH_4-oxalate, pH 3.0, under exclusion of light), Fe/S mole ratios in the leachates, SEM-EDS element mapping, electron microbeam analyses, and stoichiometric calculations. Schwertmannite is associated to water-flow paths and its geometrical distribution suggests that it forms after jarosite, possibly due to pH increase by dilution during rainfall. Goethite could only be detected as very minor secondary phase in Cauquenes and as primary mineral in El Salvador. This low goethite content is believed to have its origin in the primary mineralogy of the porphyry copper deposits. The low pyrite content in combination with the low neutralization potential of these tailings and the high availability of K for the formation of jarosite, due to the potassic alteration, are seen, together with extreme oxidizing conditions, as reason for the suppression of the goethite formation at low pH.

In addition, the fact that schwertmannite, which is meta-stable (Bigham et al., 1990, 1996) has not been transformed to goethite suggests that the kinetics of this transformation is lower in the oxidizing high-sulfate conditions prevailing in the oxidation zones studied in this work, or in the AMD precipitates reported by Childs et al. (1998), than the kinetic values obtained in laboratory studies under more reducing conditions (Bigham et al., 1990, 1996; Murad et al., 1994).

The presence of schwertmannite in the studied tailings suggest that for geochemical modeling of processes affecting sulfide mine waste it is crucial to incorporate schwertmannite into the data-bases of geochemical codes (e.g. Puura and Neretnieks, 2000). Further it illustrates how necessary are comprehensive studies on the primary mineralogy (e.g. sulfide/carbonate ratios, availability of certain key-elements) to predict the secondary ferric mineralogy for ABA and environmental assessment, as the different ferric phases produce different amounts of acidity and some are able to store acidity and release it later (e.g. jarosite).

In Piuquenes (Andina) and Cauquenes (El Teniente) tailings no cemented layers or 'hardpans' are recognized at the oxidation front or below, as they are observed in other tailings (Blowes et al., 1991; Jambor, 1994; Dold, 1999), and which could stop the downwards migration of ferric iron. This is seen as a result of the low sulfide and carbonate contents of these tailings.

Microbial acitivity tests indicate that high Mo contents may suppress microbiological oxidation activity (El Salvador No.1), due to poisoning of sulfide oxidizing bacteria (e.g. *T. ferrooxidans*), and limit the formation of important amounts of secondary ferric minerals. At El Salvador No. 1 tailings, with pyrite contents around 6.2 wt%, all but one sample yield Fe values $<0.77\%$ in the Fe(III) oxyhydroxide leach. In contrast, in the oxidation zone of the younger tailings of Piuquenes (Andina) the original pyrite (1.7 w% in average) has been almost completely oxidized to schwertmannite and jarosite (sh/jt ratio = 1.0). In Piuquenes the Fe(III) oxyhydroxide leaches yield Fe values in the range 0.5–1.5% Fe (mainly from schwertmannite), and the Fe(III) oxide leaches in the range of the 1–2.3% Fe (mainly from secondary jarosite). Similar results were obtained in the Cauquenes (El Teniente) tailings (1.0 wt% original pyrite) where jarosite is the dominant secondary phase with Fe content in the Fe(III) oxide leach up to 1% (average sh/jt ratio = 0.5 except in one layer with 1.58).

Elements which are stable as oxyanions ($HMoO_4^-$, $H_2AsO_4^-$) under acid oxidizing conditions are less mobile and adsorbed to the secondary ferric minerals formed in the oxidation zone under acidic conditions (schwertmannite and jarosite). In precipitation-controlled climates the liberated elements stable as bivalent cations under acid conditions (e.g. Cu^{2+}, Zn^{2+}, and Mn^{2+}) are leached out of the oxidation zone (Piuquenes and Cauquenes). Cu is enriched in the neutralization zone below the ground-water level as replacement of chalcopyrite by covellite. This replacement seems to be pH controlled. Below pH 6 this replacement can occur due to the mobility of Cu^{2+}, at higher pH adsorption of Cu^{2+} inhibits replacement. Mo shows also enrichment in the neutralization zone.

At El Salvador and in part at Cauquenes (El Teniente), where evaporation exceeds precipitation, the water-flow direction may change to upwards migration via capillary forces. As a result, the

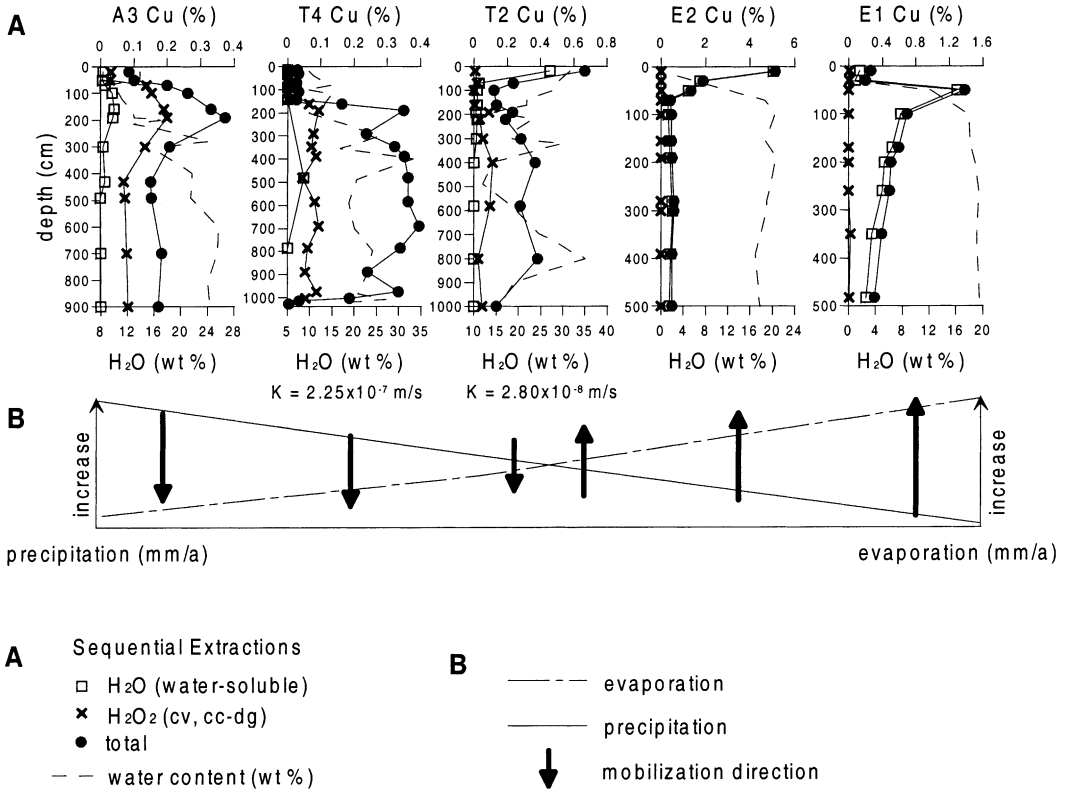

Fig. 14. The results for Cu of five drill cores from the three studied tailings demonstrate the influence of climate, grain size, and water-content to the mobilization direction. In precipitation-dominated climates as Piuquenes (Andina; A3) Cu is leached out from the oxidation zone and enriched below the water level mainly as secondary covellite. In the Mediterranean climate of Cauquenes (El Teniente; T4 and T2) the effect of grain size to capillary force is displayed. Coarser grain sizes (T4) lead to leaching out from the oxidation zone as in Piuquenes, whereas finer grain size (T2) allows a higher capillary force and consequently lead to a higher water content at the top the oxidation zone, resulting in Cu enrichment in the water-soluble fraction (e.g. as chalcanthite) in summer. In extremely arid climates (El Salvador) moisture contents as low as 3 wt% (E2) are enough for enrichment of the water-soluble Cu–sulfates at the surface of the tailings. However, complete dryness in the evaporite zone of E1 (moisture = 0.002 wt%) limits the capillary upwards migration.

mobilized elements are transferred to oxidizing conditions at the top of the tailings. Supersaturation controls the precipitation of mainly water-soluble secondary sulfates (e.g. bonattite, chalcanthite) and leads to partly strong enrichment at the top of the tailings. In the low-pH oxidation zone, due to their high ionic activity, certain mobile elements, are found to substitute into secondary minerals. Examples are Al-substitution for Fe in jarosite, and substitution of Cu and Zn for K in biotite, resulting to a peak shift to lower *d*-values of the resulting vermiculite-type mixed-layer mineral.

Geochemical data from sequential extractions of Cu (Fig. 14) illustrate best the different migration direction, resulting from climatic conditions and grain size distribution in the tailings impoundments.

5.2. Schematic model of element cycling in sulfidic mine tailings

The present study illustrates how climate has a direct influence in addition to the primary mineralogy (e.g. sulfide/carbonate contents, alterations) on the composition of secondary minerals and so on the availability of certain metals for remobilization. The main results are summarized in two schematic models of element cycling in porphyry copper tailings (Fig. 15). These models concern only the general

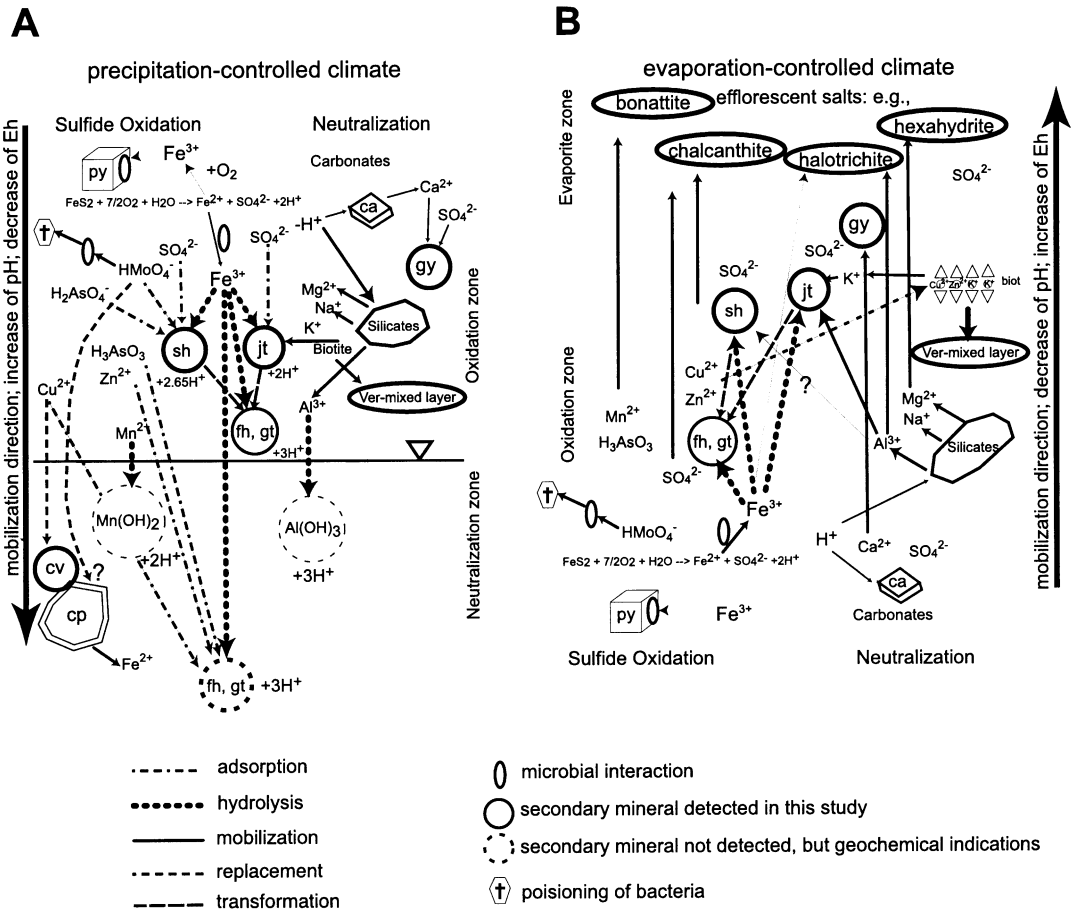

Fig. 15. The proposed schematic model for element cycling in precipitation-dominated climates is shown in A and applies for the Piuquenes tailings (La Andina) and the drill core T4 from Cauquenes (El Teniente). In B the model for evaporation-controlled climate is presented (El Salvador). For explanation see text.

trends observed in this study and cannot cover all possible secondary mineralogical and geochemical effects. The first model (Fig. 15A) deals with the case of precipitation-dominated tailings and the second one (Fig. 15B) that of evaporation-controlled tailings.

(A) The model for precipitation-dominated climates (Fig. 15A) applies for the Piuquenes tailings (La Andina) and the drill core T4 from Cauquenes (El Teniente) as examples. Sulfide oxidation (e.g. Eqs. (1)–(3)) leads to the liberation of bivalent cations as for example Fe^{2+}, Cu^{2+}, Zn^{2+}, Mn^{2+}, oxyanions as $HMoO_4^-$, $H_2AsO_4^-$, and SO_4^{2-}, as well as protons (H^+)

$$FeS_2 + 7/2O_2 + H_2O \rightarrow Fe^{2+} + 2SO_4^{2-} + 2H^+ \quad (1)$$

$$Fe^{2+} + 1/4O_2 + H^+ \Leftrightarrow Fe^3 + 1/2H_2O \quad (2)$$

(much faster if in presence of certain bacteria, e.g. *T. ferrooxidans*)

$$FeS_2 + 14Fe^{3+} + 8H_2O \rightarrow 15Fe^{2+} + 2SO_4^{2-} + 16H^+ \quad (3)$$

Oxidation of molybdenite, a common mineral in porphyry coppers, is lethal for *T. ferrooxidans* and may limit the kinetics of reaction (2). After Fe^{3+} is produced following reaction (2), it may take over the role of the principle sulfide oxidant (Eq. (3)) or may hydrolyze to secondary phases as jarosite, schwertmannite, ferrihydrite (Eqs. (4)–(6)), goethite or others Fe(III) hydroxides, depending on pH-Eh

conditions and activity of for example Fe, SO_4, Cl, Al, Na and K. Jarosite, which forms generally at oxidizing low-pH conditions (pH < 3), seems to be the first phase precipitating subsequently to pyrite oxidation in low-sulfide porphyry copper tailings depending on the availability of K and Na deriving from aluminosilicate alteration (e.g. biotite and feldspar). Jarosite forms mainly at the source of the monovalent cations as K (feldspar and biotite) in a more acidic microenvironment (Barker et al., 1998), and therefore is disseminated in the oxidation zone. Despite the low pyrite content of Cauquenes (El Teniente), very low rainfall during 7–9 months of the year may be a reason to the formation of very acid conditions (pH 1.7) in the oxidation zone and favors the jarosite formation as dominant secondary mineral in combination with the high availability of K. Additionally, the acid conditions favors the silicate dissolution and upwards migration of Cu and Zn may increase the alteration kinetics of biotite to release the necessary K for jarosite formation (Farquhar et al., 1997). The ferric iron, which could not find a partner to form jarosite is mobile under the prevailing acid condition and migrates with the water-flow system. Together with sulfate it may hydrolyze to schwertmannite when slightly higher pH (2.8–3.5, Bigham et al., 1996) conditions are encountered. This might occur due to dilution by rainfall or neutralization reactions, resulting in the accumulation of schwertmannite in streaks, dots, and grain size interfaces (Piuquenes and Cauquenes), i.e. a different distribution than jarosite. In this step, sulfate is the limiting factor and the ferric iron may reach the neutralization zone if not enough sulfate (low-sulfide tailings) is available, where it may hydrolyze to ferrihydrite and/or goethite. In case of high-sulfide tailings and/or in combination with carbonates saturation for goethite may be reached rapidly and lead to direct precipitation of goethite in form of coating or in cemented layers (Blowes et al., 1991; Jambor, 1994; Dold, 1999). Eqs. (4)–(6) show that the hydrolysis is the main proton-producing process resulting in 3 mole protons per mole hydrolyzed Fe^{3+} for ferrihydrite or goethite, 2.625 for schwertmannite and 2 for jarosite. It has to be mentioned, as the ferric hydroxide sulfates jarosite and schwertmannite are metastable in respect to goethite, this transformation is a source for future proton liberation (Eqs. (7)–(9)), indicating the importance of an accurate prediction of the secondary ferric mineralogy for ARD assessment.

Hydrolysis:

ferrihydrite :

$$10Fe^{3+} + 60H_2O \Leftrightarrow 5Fe_2O_3{\cdot}9H_2O + 30H^+ \quad (4)$$

schwertmannite :

$$16Fe^{3+} + 3SO_4^{2-} + 26H_2O \Leftrightarrow Fe_{16}O_{16}(OH)_{10}(SO_4)_3 + 42H^+ \quad (5)$$

jarosite :

$$3Fe^{3+} + K^+ + 2SO_4^{2-} + 6H_2O \Leftrightarrow KFe_3(SO_4)_2(OH)_6 + 6H^+ \quad (6)$$

Transformation:

jarosite ⇒ goethite :

$$KFe_3(SO_4)_2(OH)_6 \Rightarrow 3FeO(OH) + K^+ + 2SO_4^{2-} + 3H^+ \quad (7)$$

schwertmannite ⇒ goethite :

$$Fe_{16}O_{16}(OH)_{10}(SO_4)_3 + 6H_2O \Rightarrow 16FeO(OH) + 3SO_4^{2-} + 6H^+ \quad (8)$$

schwertmannite ⇒ goethite :

$$Fe_8O_8(OH)_6(SO_4) + 2H_2O \Rightarrow 8FeO(OH) + SO_4^{2-} + 2H^+ \quad (9)$$

The protons produced by reactions (1)–(9) may react with neutralizing minerals as carbonates and silicates. These neutralization reactions control pH, the liberation of cations as for example Ca^{2+}, Mg^{2+}, Al^{3+}, K^+, Na^+, and the formation of secondary minerals as jarosite, gypsum, and vermiculite-type

minerals. As an example, the neutralization reaction of biotite resulting in the formation of vermiculite is shown in Eq. (10)

$$3K_2(Mg_3Fe_3)Al_2Si_6O_{20})(OH)_4 + 5H_2O + 12H_2CO_3 + 6H^+ + 3/2O_2 \rightarrow 2[(Mg_3Fe_3)Al_3Si_5O_{20}(OH)_4{\cdot}8H_2O] + 6K^+ + 3Mg^{2+} + 3Fe^{2+} + 8SiO_2 + 12HCO_3^- \quad (10)$$

The liberated cations play a limiting role in the formation of secondary minerals as for example K in jarosite. Fe^{2+} released during biotite alteration may be oxidized to Fe^{3+} and liberate additional protons during hydrolysis. Al^{3+} and Mn^{2+} also may hydrolyze with concomitant liberation of protons as in the formation of gibbsite ($Al(OH)_3$). Bivalent cations are very mobile under acid conditions and are leached out of the oxidation zone. Below, with increasing pH, change in solubility of the mobilized element and sorption processes fix these elements. Below the water table, with increasingly reducing conditions, replacement processes, as the replacement of chalcopyrite by covellite take place.

Oxyanions are mainly adsorbed to the secondary ferric minerals under the low-pH conditions of the oxidation zone. Nevertheless, less oxidizing conditions and different oxidation states of the elements may increase their mobility and may lead to enrichments in the neutralization zone as it is typical for As. For example, arsenate is adsorbed to ferric hydroxides or substitutes for SO_4^{2-} in jarosite under low-pH conditions, whereas arsenite is more mobile even under neutral pH, explaining the phenomena that neutral mine effluents have often an arsenic problem.

As long as the underlying tailings have enough neutralization potential to control the pH distribution, the metals leached from the oxidation zone are retained and effluents of the tailings have acceptable water quality. Once the neutralization potential is consumed or was originally not available due to the primary mineralogical composition or treatment (e.g. flotation process), the underlying material is no longer able of scavenging the mobilized elements and acid mine drainage (AMD) develops.

(B) The model for evaporation-controlled climates (Fig. 15B) applies to El Salvador No.1 impoundment and, with restrictions, to the central part of the Cauquenes tailing at El Teniente (T1, T2, and T3). With increasing evaporation and decreasing grain size the water-flow direction changes to upwards migration via capillary forces. The mobilized elements are transferred to the top of the tailings with oxidizing conditions. Supersaturation controls the precipitation of the mainly water-soluble secondary salts as for example bonattite ($CuSO_4{\cdot}3H_2O$), chalcanthite ($CuSO_4{\cdot}5H_2O$), pickeringite ($MgAl_2(SO_4)_4{\cdot}22H_2O$), magnesioaubertite ($(Mg,Cu)Al(SO_4)_2Cl{\cdot}14H_2O$), halotrichite ($FeAl_2(SO_4)_4{\cdot}22H_2O$), hexahydrite ($MgSO_4{\cdot}6H_2O$), and gypsum. Sulfide enrichment processes are less important. Due to their high activity in the low-pH oxidation zone, these mobile elements may substitute into secondary phases as Al in jarosite, or K replacement by Cu and Zn in biotite.

The availability of the mobilized metals as water-soluble phases under arid conditions makes it necessary to prevent the flush-out during seasonally strong rainfalls even in very arid conditions. The hazardous potential of such impoundment, especially if they are constructed near rivers or with connection to the groundwater, therefore should not be underestimated. However, the availability of metals in water-soluble form at the top of the tailings can lead to very economic metal recovering methods for low ore-grade material in evaporation-controlled climates.

5.3. Implications from the ore mineralogy for the ABA of porphyry copper deposits

1. Calc-alkaline rock types (andesite and dacite as extrusions and quartzdiorite, monzodiorite and granodiorite as intrusives) contain normally certain amounts of plagioglase, but due to intense K- and Na-alteration alkali-feldspars dominate (albite and K–feldspar). The latter are characterized by low neutralizing reactivity (Jambor and Blowes, 1998).
2. Due to the low reactivity of the silicate assemblage, the carbonate content is the main acid neutralizer, but generally, this deposit type has a very low carbonate content.
3. Supergene enrichment (El Salvador) and alteration additionally may decrease the neutralization reactivity of the host rock assemblage. This has to be

taken in account for waste dumps from leached cap material, which may have very low residual sulfide contents in combination with supergene ferric sulfates (e.g. jarosite) and low or near zero neutralization potential. Thus, this material may produce AMD although standard ABA tests do not consider this type of acid potential.

4. Low pyrite contents decrease the possibility that Fe(III) oxyhydroxide coatings develop, which could prevent the sulfides from further oxidation. Low concentrations of ferric iron in combination with the low carbonate content do not favor the formation of a cemented layer (hardpan), which could limit oxygen flux into the tailings.
5. The clay mineral assemblage can make it necessary to use an acid flotation circuit (El Teniente) for higher recovery, resulting in a NP zero owing the dissolution of carbonates in the flotation process.
6. High molybdenite contents may lower or suppress microbial oxidation activity as suggested by the case of El Salvador No. 1. This in combination with zero carbonate neutralization potential and primary ferric sulfate minerals (e.g. jarosite) may lead also to low-pH values and strong element mobilization, although the sulfide content is low and the sulfides are not strongly oxidized.

Summarizing, it can be pointed out that flotation tailings from porphyry copper deposits have, despite their low sulfide contents, and because of very low NP, a high potential for acid production.

Acknowledgements

We thank John Jambor and Steven Banwart for the challenging review and helpful corrections. We also would like to thank U. Schwertmann, H. Stanjek, J. Friedl, University of Munich, for supplying the synthetic schwertmannite sample, analytical support, and helpful comments. H.-R. Pfeifer, P. Thélin, and L. Dufresne from the University of Lausanne are thanked for their analytical support and helpful discussions. Special thanks are due to the management and the geologists and all staff involved in this project from CODELCO for their interest, the access to the properties, their logistic support and their collaboration, especially A. Puig (Exploration Division, CODELCO), L. Serrano, R. Vargas, C. Aguila, C. Castillo, and M. Bustos (Division Andina, CODELCO), P. Zúñiga, F. Celhay, and A. Morales (Division El Teniente, CODELCO), J. Blondel, and R. Novajas (Division Salvador, CODELCO). For their support in Chile in the field work, sampling, sample preparation, and analytical approaches we also would like thank to G. Cáceres and K. Eppinger (IDICTEC — University of Atacama), S. Elqueta (Geological Department, University of Chile, Santiago), B. Escobar, J. Wiertz, and J. Casas (Chemical Department, Biometallurgy, University of Chile, Santiago), R. Troncoso, A. Hauser, C. Reuschmann, C. Espejo, E. Fonseca, I. Aguirre, W. Vivallo (Servicio Nacional de Geología y Minería SERNAGEOMIN), W. Eberle, and H.W. Müller (Bundesanstalt für Geowissenschaften und Rohstoffe BGR). The project is supported by the German Academic Exchange Service (DAAD) and the Swiss National Science Foundation project No. 21-50778.97.

Appendix A

See Table A1
See Table A2.
See Table A3

Table A1
Sequential extractions of drill core A2 from Piuquenes/Andina (Abbreviations: BDL = below detection limit; – = leach interference, NH_4-OAc = Ammonium acetate leach; NH_4-OxD = Ammonium oxalate 1 h dark; NH_4-OxH = Ammonium oxalate 2 h hot; sulfide = $KClO_3$; HCl, HNO_3 leach; residual = $HClO_4$, HF, HNO_3, HCl leach)

Sample	Depth	H_2O	NH_4-OAc	NH_4-OxD	NH_4-OxH	H_2O_2	Sulfide	Residual	Total	Bulk
Fe (%)										
A2/020	20	BDL	0.06	1.71	1.16	BDL	0.39	1.06	4.38	5.78
A2/050	50	BDL	0.06	1.68	1.82	0.03	1.03	1.68	6.3	7.87
A2/100	100	BDL	0.06	0.84	1.4	0.05	2.2	2.17	6.72	8.15
A2/150	150	BDL	0.1	0.92	1.22	0.05	0.96	1.57	4.82	6.21

Table A1 (*continued*)

Sample	Depth	H_2O	NH_4-OAc	NH_4-OxD	NH_4-OxH	H_2O_2	Sulfide	Residual	Total	Bulk
A2/200	200	BDL	0.09	1.18	0.99	0.03	0.93	0.86	4.08	4.95
A2/295	295	BDL	0.09	1.2	1.18	0.03	1.68	1.51	5.69	7.3
A2/400	400	BDL	0.08	1.1	1.18	0.02	1.57	1.52	5.47	7.5
A2/500	500	BDL	0.14	1.08	1.07	0.02	1.15	0.75	4.21	5.41
A2/700	700	0.01	0.09	1.4	1.56	0.02	1.83	1.46	6.37	7.58
A2/900	900	0.01	0.1	1.64	1.75	0.07	1.61	1.36	6.54	7.42
Al (%)										
A2/020	20	BDL	0.03	0.05	0.09	0.03	0.28	5.81	6.29	8.03
A2/050	50	BDL	0.04	0.09	0.13	0.05	0.66	5.77	6.74	8.27
A2/100	100	BDL	0.07	0.1	0.09	BDL	0.42	5.68	6.36	8.09
A2/150	150	BDL	0.1	0.15	0.11	BDL	0.43	6.03	6.82	8.33
A2/200	200	BDL	0.05	0.11	0.07	BDL	0.46	5.97	6.66	8.25
A2/295	295	BDL	0.05	0.11	0.07	BDL	0.46	5.9	6.59	8.55
A2/400	400	BDL	0.04	0.08	0.07	BDL	0.43	5.21	5.83	8.58
A2/500	500	BDL	0.04	0.08	0.07	BDL	0.52	5.47	6.18	8.18
A2/700	700	BDL	0.04	0.08	0.08	BDL	0.53	6.05	6.78	8.55
A2/900	900	0.01	0.05	0.12	0.11	BDL	0.69	6.12	7.1	8.24
K (%)										
A2/020	20	0.02	BDL	0.24	0.03	BDL	–	3.83	4.12	5.57
A2/050	50	0.02	BDL	0.19	0.08	0.02	–	3.09	3.4	4.67
A2/100	100	0.03	BDL	0.01	0.02	BDL	–	3.2	3.26	4.59
A2/150	150	0.05	0.01	0.02	0.05	BDL	–	3.16	3.29	4.55
A2/200	200	0.03	0.01	0.02	0.01	BDL	–	3.28	3.35	4.63
A2/295	295	0.04	0.02	0.02	0.01	BDL	–	2.91	3	4.52
A2/400	400	0.03	0.02	0.02	0.01	BDL	–	3.02	3.1	4.75
A2/500	500	0.03	0.02	0.02	0.01	BDL	–	3.19	3.27	4.89
A2/700	700	0.03	0.02	0.02	0.02	BDL	–	3.35	3.44	5.01
A2/900	900	0.03	0.02	0.03	0.02	BDL	–	3.38	3.48	4.79
Mg (%)										
A2/020	20	BDL	BDL	BDL	0.05	BDL	0.22	0.31	0.58	0.7
A2/050	50	0.02	BDL	0.01	0.07	0.01	0.52	0.35	0.98	1.14
A2/100	100	0.02	BDL	BDL	0.02	BDL	0.32	0.4	0.76	0.89
A2/150	150	0.03	BDL	BDL	0.03	BDL	0.32	0.31	0.69	0.81
A2/200	200	0.03	0.01	0.01	0.02	BDL	0.36	0.24	0.67	0.75
A2/295	295	0.02	BDL	0.02	0.03	BDL	0.36	0.33	0.76	0.93
A2/400	400	0.02	0.01	0.02	0.03	0.01	0.35	0.28	0.72	0.94
A2/500	500	BDL	0.02	0.03	0.03	BDL	0.41	0.2	0.69	0.8
A2/700	700	BDL	BDL	0.03	0.03	0.01	0.4	0.29	0.76	0.89
A2/900	900	BDL	0.01	0.03	0.04	BDL	0.53	0.31	0.92	0.99
Na (%)										
A2/020	20	BDL	BDL	BDL	BDL	BDL	BDL	0.56	0.56	0.72
A2/050	50	BDL	BDL	BDL	BDL	BDL	BDL	0.63	0.63	0.81
A2/100	100	BDL	BDL	BDL	BDL	BDL	BDL	0.48	0.48	0.6
A2/150	150	BDL	BDL	BDL	BDL	BDL	BDL	0.79	0.79	1
A2/200	200	BDL	BDL	BDL	BDL	BDL	BDL	0.99	0.99	1.23
A2/295	295	BDL	BDL	BDL	BDL	BDL	BDL	0.67	0.67	0.86
A2/400	400	BDL	BDL	BDL	BDL	BDL	BDL	0.66	0.66	0.89
A2/500	500	BDL	BDL	BDL	BDL	BDL	BDL	0.89	0.89	1.16
A2/700	700	BDL	BDL	BDL	BDL	BDL	BDL	0.69	0.69	0.9
A2/900	900	BDL	BDL	BDL	BDL	BDL	BDL	0.72	0.72	0.86

Table A1 (*continued*)

Sample	Depth	H_2O	NH_4-OAc	NH_4-OxD	NH_4-OxH	H_2O_2	Sulfide	Residual	Total	Bulk
Ca (%)										
A2/020	20	0.02	BDL	0.01	BDL	BDL	0.06	0.09	0.18	0.22
A2/050	50	0.01	BDL	0.01	BDL	0.02	0.07	0.17	0.28	0.37
A2/100	100	0.06	BDL	0.01	BDL	0.04	0.07	0.08	0.26	0.29
A2/150	150	0.13	0.01	BDL	BDL	0.04	0.05	0.1	0.33	0.38
A2/200	200	0.13	0.03	BDL	0.01	0.05	0.06	0.09	0.37	0.41
A2/295	295	0.12	0.03	BDL	BDL	0.06	0.06	0.12	0.39	0.46
A2/400	400	0.05	0.04	BDL	BDL	0.06	0.06	0.09	0.3	0.39
A2/500	500	0.07	0.08	BDL	BDL	0.06	0.07	0.1	0.38	0.47
A2/700	700	0.04	0.05	BDL	BDL	0.08	0.07	0.08	0.32	0.37
A2/900	900	0.06	0.08	BDL	BDL	0.08	0.06	0.09	0.37	0.41
Ti (%)										
A2/020	20	BDL	BDL	BDL	0.01	BDL	0.02	0.13	0.16	0.21
A2/050	50	BDL	BDL	BDL	0.01	BDL	0.05	0.19	0.25	0.31
A2/100	100	BDL	BDL	BDL	0.01	BDL	0.03	0.18	0.22	0.27
A2/150	150	BDL	BDL	BDL	BDL	BDL	0.03	0.15	0.18	0.23
A2/200	200	BDL	BDL	BDL	0.01	BDL	0.04	0.12	0.17	0.2
A2/295	295	BDL	BDL	BDL	0.02	BDL	0.03	0.16	0.21	0.28
A2/400	400	BDL	BDL	BDL	0.01	BDL	0.03	0.17	0.21	0.29
A2/500	500	BDL	BDL	BDL	0.01	BDL	0.04	0.13	0.18	0.24
A2/700	700	BDL	BDL	BDL	0.02	BDL	0.04	0.17	0.23	0.3
A2/900	900	BDL	BDL	BDL	0.02	BDL	0.06	0.19	0.27	0.31
Ba (ppm)										
A2/020	20	BDL	BDL	53	20	BDL	12	617	702	994
A2/050	50	BDL	BDL	20	34	2	22	420	498	719
A2/100	100	1	4	11	26	BDL	16	364	422	625
A2/150	150	BDL	6	10	30	BDL	22	386	454	649
A2/200	200	1	15	13	21	1	20	405	476	679
A2/295	295	BDL	15	10	16	BDL	17	367	425	633
A2/400	400	BDL	16	7	13	BDL	15	368	419	668
A2/500	500	BDL	20	8	14	BDL	19	420	481	737
A2/700	700	1	30	8	26	1	24	446	536	777
A2/900	900	BDL	22	12	14	BDL	24	458	530	732
Cu (ppm)										
A2/020	20	21.1	17.3	113	9.4	42.7	221	11.2	436	442
A2/050	50	73.3	54.2	169	24.6	260	775	13.6	1370	1360
A2/100	100	472	217	308	95.6	1550	435	103	3181	3140
A2/150	150	359	213	343	69.2	1050	217	13.1	2264	2160
A2/200	200	128	334	314	44.2	1190	382	11.5	2404	2370
A2/295	295	14.6	406	173	55.6	2440	714	60.6	3864	3850
A2/400	400	8.5	327	191	52.3	2230	1070	27.5	3906	4110
A2/500	500	5.6	206	83.3	22.5	1050	350	12.1	1730	1760
A2/700	700	18.6	368	199	59.4	1840	1030	25.6	3541	3710
A2/900	900	18.6	500	264	37.2	1090	407	12.8	2330	2250
Zn (ppm)										
A2/020	20	1.2	BDL	2.7	5	BDL	12.1	11.9	32.9	43.8
A2/050	50	2.3	0.9	3.3	6.1	2.5	25	16.1	56.2	60.3
A2/100	100	7.1	0.7	10.8	7.6	11.3	20.7	18.2	76.4	68.2
A2/150	150	14	2.1	8.1	14.8	9.2	14.1	18.8	81.1	82.5
A2/200	200	70	28.5	97.1	40.7	38.1	23.5	27.3	325.2	321

Table A1 (*continued*)

Sample	Depth	H_2O	NH_4-OAc	NH_4-OxD	NH_4-OxH	H_2O_2	Sulfide	Residual	Total	Bulk
A2/295	295	19.1	36.5	99.5	36.5	45	30.7	17.7	285	299
A2/400	400	1.1	23.7	77.9	35.1	76.7	44.5	18	277	308
A2/500	500	1.4	29.8	94.2	43.1	54.8	29.1	22	274.4	288
A2/700	700	2.4	25.8	109	48.8	66.5	40.4	18.9	311.8	333
A2/900	900	2	25.5	118	59.2	37.1	27.3	29.6	298.7	286
Mn (ppm)										
A2/020	20	4	BDL	9	19	BDL	52	34	118	141
A2/050	50	8	2	12	24	5	104	50	205	241
A2/100	100	8	BDL	7	16	3	59	36	129	148
A2/150	150	28	3	13	21	3	44	26	138	148
A2/200	200	257	68	254	214	52	59	19	923	909
A2/295	295	111	44	207	135	77	92	30	696	750
A2/400	400	36	156	257	164	109	112	28	862	975
A2/500	500	5	128	333	211	94	82	20	873	953
A2/700	700	7	60	299	198	124	109	27	824	931
A2/900	900	5	60	275	196	70	87	28	721	727
Cr (ppm)										
A2/020	20	BDL	BDL	3	5	BDL	6	3	17	8
A2/050	50	BDL	BDL	3	8	BDL	13	6	30	23
A2/100	100	BDL	BDL	3	6	BDL	8	8	25	16
A2/150	150	BDL	BDL	3	3	BDL	13	6	25	13
A2/200	200	BDL	BDL	3	3	BDL	10	3	19	8
A2/295	295	BDL	BDL	4	4	BDL	9	5	22	13
A2/400	400	BDL	BDL	4	4	BDL	8	5	21	14
A2/500	500	BDL	BDL	4	5	BDL	13	3	25	12
A2/700	700	BDL	BDL	4	7	BDL	10	6	27	21
A2/900	900	BDL	BDL	6	8	BDL	8	5	27	16
Pb (ppm)										
A2/020	20	BDL	BDL	9	6	BDL	5	BDL	20	21
A2/050	50	BDL	BDL	12	BDL	BDL	3	BDL	15	25
A2/100	100	BDL	BDL	6	5	BDL	9	BDL	20	28
A2/150	150	BDL	BDL	BDL	10	BDL	8	BDL	18	33
A2/200	200	BDL	2	14	3	BDL	10	BDL	29	33
A2/295	295	BDL	3	16	5	BDL	21	BDL	45	44
A2/400	400	BDL	5	12	5	BDL	17	BDL	39	40
A2/500	500	BDL	6	8	3	BDL	9	BDL	26	34
A2/700	700	BDL	6	10	9	2	22	BDL	49	61
A2/900	900	BDL	4	17	9	BDL	26	BDL	56	50
Mo (ppm)										
A2/020	20	BDL	BDL	37	3	27	6	3	76	80
A2/050	50	BDL	BDL	15	BDL	13	7	BDL	35	35
A2/100	100	BDL	BDL	1	BDL	BDL	32	5	38	35
A2/150	150	BDL	BDL	5	BDL	BDL	49	4	58	59
A2/200	200	BDL	BDL	4	BDL	BDL	69	7	80	58
A2/295	295	BDL	BDL	3	BDL	BDL	51	6	60	61
A2/400	400	BDL	BDL	2	BDL	BDL	64	9	75	64
A2/500	500	BDL	BDL	1	BDL	BDL	41	3	45	44
A2/700	700	BDL	BDL	1	BDL	BDL	49	7	57	62
A2/900	900	BDL	BDL	4	BDL	BDL	28	3	35	32

Table A1 (*continued*)

Sample	Depth	H_2O	NH_4-OAc	NH_4-OxD	NH_4-OxH	H_2O_2	Sulfide	Residual	Total	Bulk
V (ppm)										
A2/020	20	BDL	BDL	8	14	BDL	7	52	81	99
A2/050	50	BDL	BDL	11	19	BDL	19	70	119	149
A2/100	100	BDL	BDL	6	15	BDL	16	78	115	137
A2/150	150	BDL	BDL	6	9	BDL	13	61	89	113
A2/200	200	BDL	BDL	5	10	BDL	16	50	81	97
A2/295	295	BDL	BDL	9	14	BDL	13	68	104	133
A2/400	400	BDL	BDL	9	14	BDL	13	68	104	138
A2/500	500	BDL	BDL	9	15	BDL	17	47	88	109
A2/700	700	BDL	BDL	11	23	BDL	17	67	118	139
A2/900	900	BDL	BDL	14	24	BDL	21	66	125	141
As (ppm)										
A2/020	20	BDL	BDL	13	BDL	BDL	BDL	BDL	13	38
A2/050	50	BDL	BDL	25	BDL	BDL	5	BDL	30	BDL
A2/100	100	BDL	BDL	15	BDL	BDL	25	BDL	40	33
A2/150	150	BDL	BDL	41	5	BDL	26	BDL	72	BDL
A2/200	200	BDL	BDL	53	BDL	BDL	51	BDL	104	105
A2/295	295	BDL	BDL	46	4	BDL	59	BDL	109	42
A2/400	400	BDL	4	33	3	BDL	89	BDL	129	44
A2/500	500	BDL	BDL	21	BDL	BDL	52	BDL	73	38
A2/700	700	BDL	5	36	4	BDL	83	BDL	128	119
A2/900	900	BDL	7	64	BDL	BDL	52	BDL	123	77

Table A2
Sequential extractions of drill core T1 from Cauquenes/Teniente (Abbreviations as in Table A1)

Sample	Depth	H_2O	NH_4-OAc	NH_4-OxD	NH_4-OxH	H_2O_2	Sulfide	Residual	Total	Bulk
Fe (%)										
T1/010	10	BDL	0.25	0.46	0.96	0.03	1.09	0.91	3.7	4.3
T1/040	40	0.01	0.11	0.42	1.41	0.01	1.03	1.01	4	5.4
T1/100	100	BDL	0.04	0.31	0.67	BDL	1.61	0.93	3.56	5.03
T1/105	105	BDL	0.13	0.5	1.46	0.04	1.14	0.84	4.11	5.72
T1/200	200	BDL	0.05	0.31	0.51	BDL	1.93	0.93	3.73	5.5
T1/290	290	BDL	0.05	0.4	0.55	BDL	1.98	0.9	3.88	5.57
T1/400	400	BDL	0.09	0.51	0.52	BDL	1.75	1.01	3.88	5.42
T1/580	580	BDL	0.07	0.49	0.39	BDL	1.71	0.84	3.5	4.87
T1/800	800	BDL	0.1	0.42	0.5	BDL	1.79	0.85	3.66	5.18
T1/890	890	BDL	0.07	0.36	0.49	BDL	1.83	0.91	3.66	5.06
Al (%)										
T1/010	10	BDL	0.32	0.37	0.34	0.03	1.2	6.44	8.7	8.31
T1/040	40	0.01	0.13	0.23	0.33	0.07	1.13	6.43	8.33	10.3
T1/100	100	0.01	0.09	0.19	0.21	BDL	1.25	5.62	7.37	9.85
T1/105	105	BDL	0.09	0.17	0.24	0.02	1.16	5.2	6.88	9.73
T1/200	200	BDL	0.07	0.16	0.19	BDL	1.28	5.49	7.19	10.2
T1/290	290	BDL	0.07	0.15	0.18	BDL	1.18	5.56	7.14	9.76
T1/400	400	BDL	0.09	0.21	0.23	BDL	1.27	5.6	7.4	10.1
T1/580	580	BDL	0.07	0.18	0.2	BDL	1.19	5.43	7.07	9.61
T1/800	800	BDL	0.09	0.28	0.31	BDL	1.54	5.15	7.37	10.2
T1/890	890	BDL	0.08	0.21	0.24	BDL	1.31	5.52	7.36	9.85

Table A2 (*continued*)

Sample	Depth	H_2O	NH_4-OAc	NH_4-OxD	NH_4-OxH	H_2O_2	Sulfide	Residual	Total	Bulk
K (%)										
T1/010	10	0.15	0.05	0.04	0.13	BDL	–	2.31	2.68	2.26
T1/040	40	0.05	0.01	0.05	0.17	0.02	–	2.23	2.53	3.73
T1/100	100	0.03	BDL	0.01	0.03	BDL	–	1.83	1.9	3.42
T1/105	105	0.06	0.02	0.06	0.18	BDL	–	1.81	2.13	3.6
T1/200	200	0.04	BDL	0.01	0.02	BDL	–	1.83	1.9	3.62
T1/290	290	0.03	BDL	BDL	0.02	BDL	–	1.84	1.89	3.48
T1/400	400	0.05	0.01	0.01	0.02	BDL	–	1.96	2.05	3.57
T1/580	580	0.03	0.02	BDL	0.01	BDL	–	1.86	1.92	3.47
T1/800	800	0.04	0.02	BDL	0.02	BDL	–	1.83	1.91	3.82
T1/890	890	0.04	0.02	0.01	0.02	BDL	–	1.86	1.95	3.51
Mg (%)										
T1/010	10	0.15	0.04	0.05	0.13	0.02	0.94	0.61	1.94	2.4
T1/040	40	0.06	0.01	0.02	0.13	BDL	0.9	0.7	1.82	2.25
T1/100	100	0.04	BDL	0.02	0.09	BDL	0.96	0.69	1.8	2.24
T1/105	105	0.05	0.01	0.03	0.11	0.02	0.9	0.59	1.71	2.17
T1/200	200	0.03	BDL	0.02	0.08	BDL	0.99	0.65	1.77	2.3
T1/290	290	0.04	BDL	0.01	0.07	BDL	0.91	0.63	1.66	2.1
T1/400	400	0.04	0.02	0.02	0.09	0.01	0.98	0.71	1.87	2.38
T1/580	580	0.01	0.02	0.02	0.07	BDL	0.94	0.58	1.64	2
T1/800	800	0.01	0.02	0.03	0.11	0.01	1.22	0.64	2.04	2.55
T1/890	890	0.02	0.02	0.02	0.09	BDL	1.08	0.69	1.92	2.34
Na (%)										
T1/010	10	0.01	BDL	BDL	0.02	BDL	0.03	0.86	0.92	0.96
T1/040	40	BDL	BDL	BDL	0.01	BDL	0.03	0.87	0.91	1.11
T1/100	100	BDL	BDL	BDL	0.01	BDL	0.03	0.83	0.87	1.2
T1/105	105	BDL	BDL	BDL	BDL	BDL	0.03	0.78	0.81	1.13
T1/200	200	BDL	BDL	BDL	BDL	BDL	0.03	0.85	0.88	1.28
T1/290	290	BDL	BDL	BDL	BDL	BDL	0.03	0.8	0.83	1.22
T1/400	400	BDL	BDL	BDL	BDL	BDL	0.03	0.8	0.83	1.15
T1/580	580	BDL	BDL	BDL	BDL	BDL	0.02	0.93	0.95	1.3
T1/800	800	BDL	BDL	BDL	BDL	BDL	0.03	0.72	0.75	1.13
T1/890	890	BDL	BDL	BDL	BDL	BDL	0.03	0.86	0.89	1.19
Ca (%)										
T1/010	10	0.25	0.02	0.01	0.02	0.02	0.12	0.43	0.87	1.04
T1/040	40	0.21	0.01	0.01	0.02	BDL	0.15	0.47	0.87	1.09
T1/100	100	0.11	BDL	0.01	0.02	0.07	0.14	0.48	0.83	1.11
T1/105	105	0.11	0.01	BDL	0.01	0.04	0.13	0.46	0.76	1.08
T1/200	200	0.05	BDL	0.02	0.01	0.05	0.14	0.52	0.79	1.12
T1/290	290	0.07	BDL	BDL	0.01	0.05	0.13	0.47	0.73	1.05
T1/400	400	0.13	0.01	BDL	BDL	0.08	0.14	0.45	0.81	1.1
T1/580	580	0.12	0.04	BDL	BDL	0.06	0.11	0.46	0.79	1.08
T1/800	800	0.14	0.05	BDL	0.01	0.09	0.14	0.4	0.83	1.13
T1/890	890	0.12	0.02	BDL	0.01	0.06	0.12	0.44	0.77	1.01
Ti (%)										
T1/010	10	BDL	BDL	BDL	BDL	BDL	0.07	0.2	0.27	0.36
T1/040	40	BDL	BDL	BDL	BDL	BDL	0.07	0.19	0.26	0.34
T1/100	100	BDL	BDL	BDL	BDL	BDL	0.08	0.14	0.22	0.31
T1/105	105	BDL	BDL	BDL	BDL	BDL	0.07	0.16	0.23	0.33
T1/200	200	BDL	BDL	BDL	BDL	BDL	0.08	0.14	0.22	0.32
T1/290	290	BDL	BDL	BDL	BDL	BDL	0.07	0.13	0.2	0.3

Table A2 (*continued*)

Sample	Depth	H_2O	NH_4-OAc	NH_4-OxD	NH_4-OxH	H_2O_2	Sulfide	Residual	Total	Bulk
T1/400	400	BDL	BDL	BDL	BDL	BDL	0.08	0.16	0.24	0.32
T1/580	580	BDL	BDL	BDL	BDL	BDL	0.09	0.13	0.22	0.31
T1/800	800	BDL	BDL	BDL	BDL	BDL	0.11	0.15	0.26	0.34
T1/890	890	BDL	BDL	BDL	BDL	BDL	0.08	0.15	0.23	0.3
Ba (ppm)										
T1/010	10	BDL	1	7	37	1	39	263	348	503
T1/040	40	BDL	BDL	2	44	2	35	256	339	465
T1/100	100	BDL	2	13	19	1	40	226	301	454
T1/105	105	BDL	BDL	9	36	2	39	205	291	437
T1/200	200	BDL	3	18	11	1	39	223	295	477
T1/290	290	BDL	2	16	13	1	35	225	292	470
T1/400	400	1	8	10	13	1	41	251	325	502
T1/580	580	BDL	11	8	11	1	42	241	314	472
T1/800	800	BDL	12	8	10	1	51	226	308	517
T1/890	890	BDL	8	8	8	1	36	208	269	406
Cu (ppm)										
T1/010	10	298	939	510	377	212	214	14.2	2564	2330
T1/040	40	593	309	332	370	14.5	155	16.3	1790	1930
T1/100	100	847	265	260	96.1	870	175	13.8	2527	2570
T1/105	105	128	198	251	218	266	172	16	1249	1340
T1/200	200	505	463	483	189	2100	1930	62.1	5732	5970
T1/290	290	1230	414	481	145	1740	1080	40.1	5130	5240
T1/400	400	114	1300	508	99.7	778	345	16.4	3161	3260
T1/580	580	6.2	692	348	105	835	183	18.4	2188	2250
T1/800	800	3.7	882	605	123	532	378	19	2543	2650
T1/890	890	6.2	443	430	108	1060	764	27.2	2838	2830
Zn (ppm)										
T1/010	10	31.9	28.8	7.7	8.7	1	20.7	16.2	115	104
T1/040	40	15.2	2.7	3.1	8.2	BDL	21.3	16.2	66.7	82.4
T1/100	100	25	4.2	2.2	5.7	2.1	22.3	15.8	77.3	94.6
T1/105	105	13.9	14.3	5.8	6	1.6	20.9	14.7	77.2	95.7
T1/200	200	14.6	3.2	2.9	5.3	4.5	26.9	16.3	73.7	82.5
T1/290	290	22.3	3.2	2.5	5	3.5	23.2	15.8	75.5	82.8
T1/400	400	19.5	28.5	12.6	7.8	3	24.5	18.6	114.5	139
T1/580	580	BDL	16.3	6.9	5.7	1.8	23.1	18.4	72.2	87.5
T1/800	800	BDL	23.8	6.9	7.5	1.8	25.4	17.6	83	86.7
T1/890	890	1.2	18.9	5.5	5.9	2	23.1	16	72.6	74.2
Mn (ppm)										
T1/010	10	51	9	10	22	3	108	65	268	344
T1/040	40	27	3	6	26	BDL	111	77	250	313
T1/100	100	22	BDL	5	18	4	127	76	252	316
T1/105	105	14	3	7	21	6	115	63	229	302
T1/200	200	19	2	5	16	3	131	74	250	326
T1/290	290	31	BDL	4	16	3	127	71	252	326
T1/400	400	95	19	18	25	6	140	80	383	473
T1/580	580	6	17	18	19	3	126	66	255	318
T1/800	800	4	16	14	24	5	135	63	261	333
T1/890	890	10	7	8	19	3	123	70	240	294

Table A2 (*continued*)

Sample	Depth	H_2O	NH_4-OAc	NH_4-OxD	NH_4-OxH	H_2O_2	Sulfide	Residual	Total	Bulk
Cr (ppm)										
T1/010	10	BDL	3	1	11	BDL	20	8	43	28
T1/040	40	BDL	2	4	13	BDL	21	7	47	34
T1/100	100	BDL	1	4	10	BDL	22	7	44	26
T1/105	105	BDL	1	3	15	BDL	30	6	55	38
T1/200	200	BDL	BDL	6	7	BDL	25	8	46	29
T1/290	290	BDL	BDL	2	7	BDL	21	5	35	30
T1/400	400	BDL	1	5	7	BDL	20	7	40	30
T1/580	580	BDL	1	4	6	BDL	21	5	37	25
T1/800	800	BDL	2	3	7	BDL	28	5	45	29
T1/890	890	BDL	1	5	8	BDL	27	7	48	25
Pb (ppm)										
T1/010	10	BDL	BDL	BDL	7	BDL	9	BDL	16	29
T1/040	40	BDL	BDL	BDL	11	BDL	4	BDL	15	27
T1/100	100	BDL	BDL	4	11	BDL	5	BDL	20	22
T1/105	105	BDL	BDL	3	5	BDL	3	BDL	11	20
T1/200	200	BDL	BDL	19	BDL	BDL	6	BDL	25	12
T1/290	290	BDL	BDL	BDL	BDL	BDL	4	BDL	4	19
T1/400	400	BDL	BDL	BDL	2	BDL	5	BDL	7	20
T1/580	580	BDL	BDL	BDL	7	BDL	6	BDL	13	14
T1/800	800	BDL	2	BDL	5	BDL	5	BDL	12	24
T1/890	890	BDL	BDL	3	3	BDL	4	BDL	10	13
Mo (ppm)										
T1/010	10	BDL	2	37	37	27	2	BDL	105	92
T1/040	40	BDL	2	33	53	29	6	BDL	123	139
T1/100	100	BDL	BDL	17	12	BDL	48	BDL	77	87
T1/105	105	BDL	2	32	35	49	32	1	151	155
T1/200	200	BDL	1	20	6	BDL	82	10	119	143
T1/290	290	BDL	1	21	5	BDL	74	9	110	122
T1/400	400	BDL	1	22	2	BDL	32	4	61	67
T1/580	580	3	BDL	17	2	BDL	32	4	58	85
T1/800	800	8	2	42	7	BDL	20	BDL	79	84
T1/890	890	2	1	23	7	BDL	61	5	99	111
V (ppm)										
T1/010	10	BDL	4	13	18	BDL	48	105	188	184
T1/040	40	BDL	BDL	7	21	BDL	46	107	181	222
T1/100	100	BDL	BDL	6	19	BDL	54	88	167	209
T1/105	105	BDL	BDL	7	25	BDL	47	89	168	221
T1/200	200	BDL	BDL	10	13	BDL	57	90	170	221
T1/290	290	BDL	BDL	4	13	BDL	50	83	150	204
T1/400	400	BDL	BDL	8	12	BDL	54	92	166	216
T1/580	580	BDL	BDL	7	11	BDL	54	76	148	190
T1/800	800	BDL	BDL	4	13	BDL	66	80	163	211
T1/890	890	BDL	BDL	7	13	BDL	58	88	166	211
As (ppm)										
T1/010	10	BDL	6	37	25	BDL	BDL	BDL	68	72
T1/040	40	BDL	7	44	38	BDL	BDL	BDL	89	134
T1/100	100	BDL	7	52	17	BDL	BDL	BDL	76	96
T1/105	105	BDL	BDL	26	28	BDL	BDL	BDL	54	112
T1/200	200	BDL	4	41	4	BDL	8	BDL	57	83
T1/290	290	BDL	4	20	4	BDL	7	BDL	35	43

Table A2 (*continued*)

Sample	Depth	H_2O	NH_4-OAc	NH_4-OxD	NH_4-OxH	H_2O_2	Sulfide	Residual	Total	Bulk
T1/400	400	BDL	4	36	5	BDL	BDL	BDL	45	59
T1/580	580	BDL	6	40	10	BDL	BDL	BDL	56	25
T1/800	800	BDL	19	134	22	BDL	BDL	BDL	175	202
T1/890	890	BDL	8	61	12	BDL	BDL	BDL	81	103

Table A3
Sequential extractions of drill core E2 from El Salvador (Abbreviations as in Table A1)

Sample	Depth	H_2O	NH_4-OAc	NH_4-OxD	NH_4-OxH	H_2O_2	Sulfide	Residual	Total	Bulk
Fe (%)										
E2/010	10	0.17	0.06	0.34	0.88	0.73	0.23	0.07	2.48	2.89
E2/030	30	0.03	0.01	0.29	2.16	1.63	1.44	0.22	5.78	6.72
E2/050	50	0.05	0.02	0.26	2.44	1.58	1.49	0.28	6.12	6.93
E2/070	70	0.03	0.04	0.2	2.73	1.43	1.89	0.34	6.66	7.8
E2/100	100	0.04	0.06	0.2	2.45	1.46	1.58	0.35	6.14	7.23
E2/155	155	0.04	0.05	0.26	2.45	1.48	1.06	0.34	5.68	6.81
E2/190	190	0.03	0.04	1.88	1.47	1.1	1.41	0.37	6.3	7.49
E2/280	280	0.04	0.03	0.16	3.94	1.26	0.96	0.36	6.75	8.03
E2/300	300	0.05	0.05	0.18	3.96	1.13	1.07	0.39	6.83	8.36
E2/390	390	0.06	0.03	0.21	2.89	1.69	1.09	0.4	6.37	8.33
E2/500	500	0.03	0.06	0.25	1.89	1.18	2.43	0.57	6.41	8.24
Al (%)										
E2/010	10	3.09	0.06	0.04	0.12	BDL	0.03	1.44	4.78	5.27
E2/030	30	1.1	0.09	0.18	0.41	0.02	0.12	4.39	6.31	7.17
E2/050	50	0.88	0.06	0.12	0.38	0.01	0.09	5.22	6.76	7.55
E2/070	70	0.25	0.06	0.1	0.33	0.01	0.11	6.36	7.22	8.9
E2/100	100	0.28	0.1	0.14	0.29	0.02	0.14	6.58	7.55	8.77
E2/155	155	0.32	0.07	0.1	0.21	0.01	0.12	6.66	7.49	8.67
E2/190	190	0.33	0.09	0.13	0.24	0.02	0.15	6.69	7.65	8.63
E2/280	280	0.39	0.13	0.19	0.34	0.03	0.18	6.21	7.47	8.68
E2/300	300	0.41	0.1	0.13	0.2	0.03	0.15	6.17	7.19	8.01
E2/390	390	0.5	0.07	0.1	0.2	0.02	0.13	6.18	7.2	8.33
E2/500	500	0.2	0.09	0.16	0.33	0.02	0.31	6.79	7.9	9.46
K (%)										
E2/010	10	BDL	BDL	0.01	0.04	BDL	–	0.4	0.45	0.55
E2/030	30	BDL	BDL	0.02	0.13	BDL	–	1.32	1.47	1.83
E2/050	50	BDL	BDL	0.02	0.15	BDL	–	1.58	1.75	2.11
E2/070	70	BDL	BDL	0.01	0.19	BDL	–	2.02	2.22	2.84
E2/100	100	BDL	BDL	0.02	0.18	BDL	–	1.95	2.15	2.68
E2/155	155	BDL	BDL	0.02	0.19	BDL	–	1.83	2.04	2.48
E2/190	190	BDL	BDL	0.17	0.12	BDL	–	1.73	2.02	2.35
E2/280	280	BDL	BDL	0.02	0.44	BDL	–	1.48	1.94	2.35
E2/300	300	BDL	BDL	0.02	0.42	BDL	–	1.42	1.86	2.2
E2/390	390	BDL	BDL	0.02	0.27	BDL	–	1.56	1.85	2.28
E2/500	500	BDL	BDL	0.02	0.21	BDL	–	1.67	1.9	2.47
Mg (%)										
E2/010	10	1.45	0.02	BDL	BDL	BDL	BDL	0.04	1.51	1.63
E2/030	30	0.57	0.02	BDL	BDL	BDL	BDL	0.11	0.7	0.79

Table A3 (*continued*)

Sample	Depth	H_2O	NH_4-OAc	NH_4-OxD	NH_4-OxH	H_2O_2	Sulfide	Residual	Total	Bulk
E2/050	50	0.47	0.01	BDL	BDL	BDL	BDL	0.14	0.62	0.63
E2/070	70	0.14	BDL	BDL	BDL	BDL	0.01	0.18	0.33	0.45
E2/100	100	0.16	BDL	BDL	BDL	BDL	0.02	0.18	0.36	0.47
E2/155	155	0.18	BDL	BDL	BDL	BDL	0.02	0.17	0.37	0.46
E2/190	190	0.2	0.01	BDL	BDL	BDL	0.02	0.18	0.41	0.47
E2/280	280	0.24	BDL	BDL	0.01	BDL	0.02	0.16	0.43	0.5
E2/300	300	0.23	BDL	BDL	BDL	BDL	0.01	0.15	0.39	0.43
E2/390	390	0.24	BDL	BDL	BDL	BDL	0.02	0.15	0.41	0.5
E2/500	500	0.17	BDL	BDL	0.07	BDL	0.17	0.2	0.61	0.71
Na (%)										
E2/010	10	BDL	BDL	0.02	0.09	BDL	BDL	0.17	0.28	0.32
E2/030	30	0.25	0.01	0.03	0.25	BDL	0.01	0.53	1.08	1.37
E2/050	50	0.11	BDL	0.03	0.27	BDL	BDL	0.6	1.01	1.22
E2/070	70	0.01	BDL	0.01	0.27	BDL	BDL	0.69	0.98	1.4
E2/100	100	0.01	BDL	BDL	0.22	BDL	BDL	0.63	0.86	1.24
E2/155	155	0.01	BDL	0.01	0.19	BDL	BDL	0.54	0.75	0.98
E2/190	190	0.01	BDL	0.13	0.09	BDL	BDL	0.55	0.78	0.89
E2/280	280	0.01	BDL	BDL	0.12	BDL	BDL	0.54	0.67	0.82
E2/300	300	BDL	BDL	BDL	0.09	BDL	BDL	0.54	0.63	0.8
E2/390	390	BDL	BDL	0.02	0.14	BDL	BDL	0.55	0.71	0.94
E2/500	500	BDL	BDL	BDL	0.06	BDL	BDL	0.63	0.69	0.93
Ca (%)										
E2/010	10	0.18	BDL	BDL	BDL	BDL	BDL	0.02	0.2	0.24
E2/030	30	0.93	0.03	BDL	0.02	BDL	BDL	0.06	1.04	1.1
E2/050	50	0.59	0.01	BDL	0.01	BDL	BDL	0.07	0.68	0.66
E2/070	70	0.49	0.02	BDL	0.01	BDL	BDL	0.09	0.61	0.71
E2/100	100	0.77	0.03	BDL	0.01	BDL	BDL	0.09	0.9	0.93
E2/155	155	0.91	0.04	BDL	BDL	BDL	BDL	0.09	1.04	1.09
E2/190	190	0.53	0.03	0.01	BDL	BDL	BDL	0.09	0.66	0.68
E2/280	280	0.46	0.02	BDL	0.01	BDL	BDL	0.09	0.58	0.61
E2/300	300	0.37	0.01	BDL	BDL	BDL	BDL	0.09	0.47	0.5
E2/390	390	0.53	0.02	BDL	0.01	BDL	BDL	0.1	0.66	0.78
E2/500	500	0.39	0.02	0.01	0.01	BDL	BDL	0.1	0.53	0.63
Ti (%)										
E2/010	10	BDL	BDL	BDL	BDL	BDL	BDL	0.04	0.04	0.05
E2/030	30	BDL	BDL	BDL	BDL	BDL	BDL	0.13	0.13	0.12
E2/050	50	BDL	BDL	BDL	BDL	BDL	BDL	0.15	0.15	0.14
E2/070	70	BDL	BDL	BDL	BDL	BDL	BDL	0.19	0.19	0.17
E2/100	100	BDL	BDL	BDL	BDL	BDL	BDL	0.2	0.2	0.18
E2/155	155	BDL	BDL	BDL	BDL	BDL	BDL	0.18	0.18	0.18
E2/190	190	BDL	BDL	BDL	BDL	BDL	BDL	0.2	0.2	0.19
E2/280	280	BDL	BDL	BDL	BDL	BDL	BDL	0.2	0.2	0.2
E2/300	300	BDL	BDL	BDL	BDL	BDL	BDL	0.22	0.22	0.2
E2/390	390	BDL	BDL	BDL	BDL	BDL	BDL	0.2	0.2	0.21
E2/500	500	BDL	BDL	BDL	BDL	BDL	0.01	0.25	0.26	0.28
Ba (ppm)										
E2/010	10	BDL	BDL	BDL	8	BDL	2	51	61	95
E2/030	30	BDL	BDL	BDL	18	BDL	9	162	189	359
E2/050	50	BDL	BDL	BDL	22	BDL	8	187	217	383
E2/070	70	BDL	BDL	BDL	24	BDL	10	226	260	569
E2/100	100	BDL	BDL	BDL	21	BDL	10	213	244	526

Table A3 (*continued*)

Sample	Depth	H_2O	NH_4-OAc	NH_4-OxD	NH_4-OxH	H_2O_2	Sulfide	Residual	Total	Bulk
E2/155	155	BDL	BDL	2	21	BDL	9	202	234	432
E2/190	190	BDL	BDL	5	21	BDL	10	199	235	353
E2/280	280	BDL	BDL	BDL	27	BDL	16	182	225	341
E2/300	300	BDL	BDL	BDL	25	BDL	26	183	234	360
E2/390	390	BDL	BDL	5	22	BDL	14	190	231	382
E2/500	500	BDL	BDL	1	17	BDL	10	216	244	383
Cu (ppm)										
E2/010	10	50386	592	40.9	138	8.5	5.5	12.7	51184	48918
E2/030	30	17430	617	125	554	26	42.3	34.5	18829	20120
E2/050	50	12330	347	95.8	605	27.3	24.9	32.5	13463	12140
E2/070	70	2900	160	138	738	42	35.1	38.6	4052	3980
E2/100	100	3420	291	194	710	48.2	49.1	43.2	4756	4540
E2/155	155	3780	225	70.1	459	22.1	38.2	44.1	4639	4740
E2/190	190	4030	306	113	406	71.9	48.1	46.2	5021	5230
E2/280	280	5040	294	81	421	23.3	42.3	53.3	5955	6250
E2/300	300	5220	245	76.1	266	28.8	48.4	57.6	5942	5690
E2/390	390	4380	164	61.1	347	22.8	38.3	51.5	5065	5160
E2/500	500	3870	283	175	346	117	101	64.7	4957	5140
Zn (ppm)										
E2/010	10	112	1.2	BDL	0.8	BDL	0.8	3.5	118.3	101
E2/030	30	41.1	1.1	BDL	1.6	BDL	2.1	9.2	55.1	51.5
E2/050	50	32.6	0.7	BDL	1.2	0.8	2.2	12.2	49.7	39.5
E2/070	70	10.1	BDL	BDL	1.3	BDL	2.2	14.4	28	26.2
E2/100	100	11.7	BDL	BDL	1.2	BDL	2.4	12.8	28.1	30.5
E2/155	155	12.3	BDL	BDL	0.8	BDL	3.7	14	30.8	27.9
E2/190	190	13.6	0.7	BDL	1.6	0.5	3.2	16	35.6	43.6
E2/280	280	17.2	0.5	BDL	2.1	BDL	4.2	16.7	40.7	52.1
E2/300	300	15.5	BDL	BDL	1.5	BDL	4	18.4	39.4	39.3
E2/390	390	15.5	BDL	0.5	1.8	0.5	4.5	19.4	42.2	44.6
E2/500	500	13.3	0.5	0.6	5	0.9	8.6	37.4	66.3	79.2
Mn (ppm)										
E2/010	10	539	6	BDL	2	BDL	BDL	BDL	547	620
E2/030	30	161	4	BDL	7	BDL	BDL	4	176	189
E2/050	50	127	3	BDL	7	BDL	BDL	5	142	128
E2/070	70	39	BDL	BDL	4	BDL	2	7	52	52
E2/100	100	45	BDL	BDL	3	BDL	3	7	58	57
E2/155	155	50	BDL	BDL	2	BDL	3	6	61	62
E2/190	190	53	3	5	3	BDL	3	7	74	71
E2/280	280	62	BDL	BDL	4	BDL	2	7	75	73
E2/300	300	55	BDL	BDL	3	BDL	BDL	7	65	60
E2/390	390	59	BDL	BDL	2	BDL	2	7	70	73
E2/500	500	42	BDL	BDL	9	BDL	19	13	83	90
Cr (ppm)										
E2/010	10	23	3	6	5	BDL	BDL	BDL	37	42
E2/030	30	5	BDL	BDL	7	BDL	1	BDL	13	6
E2/050	50	4	BDL	2	5	BDL	BDL	BDL	11	5
E2/070	70	1	1	BDL	6	BDL	BDL	BDL	8	7
E2/100	100	1	1	1	5	BDL	BDL	1	9	8
E2/155	155	BDL	1	1	4	BDL	BDL	BDL	6	6
E2/190	190	1	1	4	3	BDL	BDL	2	11	10
E2/280	280	1	1	BDL	8	BDL	BDL	2	12	11

Table A3 (*continued*)

Sample	Depth	H_2O	NH_4-OAc	NH_4-OxD	NH_4-OxH	H_2O_2	Sulfide	Residual	Total	Bulk
E2/300	300	2	BDL	BDL	3	BDL	BDL	BDL	5	7
E2/390	390	2	1	3	5	BDL	1	BDL	12	9
E2/500	500	BDL	1	1	BDL	BDL	4	2	8	10
Pb (ppm)										
E2/010	10	BDL	BDL	3	BDL	BDL	BDL	BDL	3	BDL
E2/030	30	BDL	BDL	2	BDL	BDL	3	5	10	8
E2/050	50	BDL	BDL	BDL	BDL	BDL	3	3	6	10
E2/070	70	BDL	BDL	BDL	BDL	BDL	4	6	10	30
E2/100	100	BDL	BDL	5	4	BDL	3	4	16	24
E2/155	155	BDL	BDL	9	BDL	BDL	4	4	17	16
E2/190	190	BDL	BDL	4	3	BDL	BDL	2	9	16
E2/280	280	BDL	BDL	3	BDL	BDL	BDL	BDL	3	21
E2/300	300	BDL	BDL	4	BDL	BDL	3	3	10	25
E2/390	390	BDL	BDL	26	2	BDL	3	6	37	21
E2/500	500	BDL	BDL	7	BDL	BDL	4	3	14	27
Mo (ppm)										
E2/010	10	BDL	BDL	1	5	129	40	6	181	178
E2/030	30	3	1	10	24	268	176	28	510	502
E2/050	50	BDL	BDL	8	26	239	230	36	539	505
E2/070	70	BDL	BDL	2	33	59	108	28	230	232
E2/100	100	BDL	BDL	6	38	94	127	25	290	274
E2/155	155	BDL	BDL	4	28	63	92	11	198	197
E2/190	190	BDL	BDL	19	28	96	165	13	321	311
E2/280	280	BDL	BDL	4	33	77	88	7	209	206
E2/300	300	BDL	BDL	5	27	81	117	9	239	228
E2/390	390	BDL	BDL	6	22	89	105	8	230	229
E2/500	500	BDL	BDL	4	15	46	112	19	196	200
V (ppm)										
E2/010	10	9	15	13	8	BDL	BDL	18	63	68
E2/030	30	3	BDL	7	17	BDL	BDL	57	84	102
E2/050	50	BDL	BDL	8	12	BDL	BDL	66	86	107
E2/070	70	BDL	BDL	2	11	BDL	2	80	95	124
E2/100	100	BDL	BDL	5	12	BDL	3	85	105	134
E2/155	155	BDL	BDL	6	12	BDL	3	88	109	141
E2/190	190	BDL	BDL	15	10	BDL	3	91	119	144
E2/280	280	BDL	BDL	7	15	BDL	3	84	109	140
E2/300	300	BDL	BDL	8	9	BDL	3	84	104	132
E2/390	390	BDL	BDL	11	13	BDL	3	86	113	138
E2/500	500	BDL	BDL	7	10	BDL	12	99	128	166
As (ppm)										
E2/010	10	BDL	14	25	15	BDL	BDL	BDL	54	35
E2/030	30	BDL	BDL	14	37	BDL	3	BDL	54	57
E2/050	50	BDL	BDL	17	56	BDL	4	BDL	77	74
E2/070	70	BDL	7	40	131	BDL	5	BDL	183	204
E2/100	100	BDL	17	68	151	BDL	11	4	251	223
E2/155	155	BDL	10	59	127	BDL	9	5	210	229
E2/190	190	BDL	4	54	37	BDL	5	BDL	100	112
E2/280	280	BDL	BDL	23	36	BDL	5	BDL	64	51
E2/300	300	BDL	BDL	16	20	BDL	4	BDL	40	77
E2/390	390	BDL	BDL	40	44	BDL	4	BDL	88	129
E2/500	500	BDL	BDL	18	14	BDL	BDL	BDL	32	65

References

Acker, J.G., Bricker, O.P., 1992. The influence of pH on biotite dissolution and alteration kinetics at low temperature. Geochimica et Cosmochimica Acta 56, 3073–3092.

Ahonen, L., Tuovinen, O.L., 1994. Solid-phase alteration and iron transformation in column bioleaching of a complex sulfide ore. In: Alpers, C.N., Blowes, D.W. (Eds.), Environmental Geochemistry of Sulfide Oxidation. ACS Symposium Series, Washington, DC, vol. 550. pp. 79–89.

Alpers, C.N., Brimhall, G.H., 1989. Paleohydrologic evolution and geochemical dynamics of cumulative supergene metal enrichment at La Escondida, Atacama Desert, northern Chile. Economic Geology 84, 229–255.

Alpers, C.N., Nordstrom, D.K., Ball, J.W., 1989. Solubility of jarosite solid solutions precipitated from acid mine waters, Iron Mountain, California, USA. Science Geological Bulletin Strasbourg 42 (4), 281–298.

Alpers, C.N., Nordstrom, D.K., Thompson, J.M., 1994a. Seasonal variations of Zn/Cu ratios in acid mine water from Iron mountain, California. In: Alpers, C.N., Blowes, D.W. (Eds.), Environmental Geochemistry of Sulfide Oxidation. ACS Symposium Series, Washington, DC, vol. 550. pp. 324–344.

Alpers, C.N., Blowes, D.W., Nordstrom, D.K., Jambor, J.L., 1994b. Secondary minerals and acid mine-water chemistry. In: Jambor, J.L., Blowes, D.W. (Eds.), Short Course Handbook on Environmental Geochemistry of Sulfide Mine Waste. Mineralogical Association of Canada, Nepean, vol. 22. pp. 247–270.

Barker, W.W., Welch, S.A., Chu, S., Banfield, J.F., 1998. Experimental observations of the effects of bacteria on aluminosilicate weathering. American Mineralogist 83, 1551–1563.

Bigham, J.M., Schwertmann, U., Carlson, L., Murad, E., 1990. A poorly crystallized oxyhydroxysulfate of iron formed by bacterial oxidation of Fe(II) in acid mine waters. Geochimica et Cosmochimica Acta 54, 2743–2758.

Bigham, J.M., Carlson, L., Murad, E., 1994. Schwertmannite, a new iron oxyhydroxy-sulphate from Pyhäsalmi, Finland, and other localities. Mineralogical Magazine 58, 641–648.

Bigham, J.M., Schwertmann, U., Traina, S.J., Winland, R.L., Wolf, M., 1996. Schwertmannite and the chemical modeling of iron in acid sulfate waters. Geochimica et Cosmochimica Acta 60 (2), 185–195.

Blowes, D.W., Jambor, J.L., 1990. The pore-water geochemistry and the mineralogy of the vadose zone of sulfide tailings, Waite Amulet, Quebec, Canada. Applied Geochemistry 5, 327–346.

Blowes, D.W., Reardon, E.J., Jambor, J.L., Cherry, J.A., 1991. The formation and potential importance of cemented layers in inactive sulfide mine tailings. Geochimica et Cosmochimica Acta 55, 965–978.

Boorman, R.S., Watson, D.W., 1976. Chemical processes in abandoned sulphide tailings dumps and environmental implication for Northeastern New Brunswick. CIM Bulletin 69, 86–96.

Brady, K.S., Bigham, J.M., Jaynes, W.F., Logan, T.J., 1986. Influence of sulfate on Fe-oxide formation: comparisons with a stream receiving acid mine drainage. Clays and Clay Minerals 34 (3), 266–274.

Brindley, G.W., Brown, G., 1980. Crystal Structures of Clay Minerals and other X-ray Identification. Mineralogical Society, London.

Brookins, D.G., 1988. Eh-pH Diagrams for Geochemistry. Springer, Berlin.

Camus, F., 1975. Geology of the El Teniente orebody with emphasis on wall-rock alteration. Economic Geology 70, 1341–1372.

Cardoso Fonseca, E., Martin, H., 1986. The selective extraction of Pb and Zn in selected mineral and soil samples, application in geochemical exploration (Portugal). Journal of Geochemical Exploration 26, 231–248.

Carlson, L., Schwertmann, U., 1990. The effect of CO_2 and oxidation rate on the formation of goethite versus lepidocrocite from an Fe(II) system at pH 6 and 7. Clay Minerals 25, 65–71.

Chao, T.T., Sanzolone, R.F., 1977. Chemical dissolution of sulfide minerals. Journal of Research US Geological Survey 5, 409–412.

Childs, C.W., Inoue, K., Mizota, C., 1998. Natural and anthropogenetic schwertmannites from Towada-Hachimantai National Park, Honshu, Japan. Chemical Geology 144, 81–86.

Cornell, R.M., Schwertmann, U., 1996. The Iron Oxides. VCH Verlagsgesellschaft mbH, Weinheim, 573 p.

Davis, B.S., 1997. Geomicrobiology of the oxic zone of sulfidic mine tailings. In: McIntosh, J.M., Groat, L.A. (Eds.), Short Course Handbook on Biological and Mineralogical Interactions. Mineralogical Association of Canada, Nepean, vol. 25. pp. 93–112.

Dold, B., 1999. Mineralogical and geochemical changes of copper flotation tailings in relation to their original composition and climatic setting — implications for acid mine drainage and element mobility. PhD thesis, Terre et Environment, Université de Genève, vol. 18, 230 p.

Dold, B., Fontboté, L., Wildi, W., 1997. Mobilization and secondary enrichment processes in the sulfide porphyry copper tailings of Cauquenes (El Teniente) and Piuquenes (La Andina), Chile. VIII Congreso Geologico Chileno Actas, vol. 2. pp. 940–944.

Dutrizac, J.E., Jambor, J.L., 2000. Jarosites and their application in hydrometallurgy. In: Alpers, C.N., Jambor, J.L., Nordstrom, D.K. (Eds.), Sulfate Minerals: Crystallography, Geochemistry, and Environmetnal Significance. Reviews in Mineralogy and Geochemistry, vol. 40.

Dzombak, D.A., Morel, F.M.M., 1990. Surface Complexation Modeling — Hydrous Ferric Oxides. Wiley, New York.

Ehrlich, H.L., 1996. Geomicrobiology. Dekker, New York.

Fanfani, L., Zuddas, P., Chessa, A., 1997. Heavy metals speciation analysis as a tool for studying mine tailings weathering. Journal of Geochemical Exploration 58, 241–248.

Farquhar, M.L., Vaughan, D.J., Hughes, C.R., Charnock, J.M., England, K.E.R., 1997. Experimental studies of the interaction of aqueous metal cations with mineral substrates: lead, cadmium, and copper with perthitic feldspar, muscovite, and biotite. Geochimica et Cosmochimica Acta 61, 3051–3064.

Gatehouse, S., Roussel, D.W., Van Moort, J.C., 1977. Sequential soil analysis in exploration analysis. Journal of Geochemical Exploration 8, 483–494.

Gustafson, L.B., Hunt, J.P., 1975. The porphyry copper deposit at El Salvador, Chile. Economic Geology 70, 857–912.

Gustafson, L.B., Quiroga, J., 1995. Patterns of mineralization and alteration below the porphyry copper orebody at El Salvador, Chile. Economic Geology 90, 2–16.

Hall, G.E.M., Vaive, J.E., Beer, R., Hoashi, M., 1996. Selective leaches revisited, with emphasis on the amorphous Fe oxyhydroxide phase extraction. Journal of Geochemical Exploration 56, 59–78.

Holmström, H., Ljungberg, J., Ekström, M., Öhlander, B., 1999. Secondary copper enrichment in tailings at the Laver mine, northern Sweden. Environmental Geology 38 (4), 327–342.

Hölting, B., 1989. Hydrogeologie. Enke, Stuttgart.

Ingeneria y Geotecnia LTDA, 1990a. Tranques de relaves Planta Division Andina. Levantamiento catastral de los tranques de relaves en Chile, pp. 8–20.

Ingeneria y Geotecnia LTDA, 1990b. Tranques de relaves Division El Teniente de CODELCO Chile. Levantamiento catastral de los tranques de relaves en Chile, pp. 10–52.

Jambor, J.L., 1994. Mineralogy of sulfide-rich tailings and their oxidation products. In: Jambor, J.L., Blowes, D.W. (Eds.), Short Course Handbook on Environmental Geochemistry of Sulfide Mine Waste. Mineralogical Association of Canada, Nepean, vol. 22. pp. 59–102.

Jambor, J.L., Blowes, D.W., 1998. Theory and applications of mineralogy in environmental studies of sulfide-baring mine waste. In: Cabri, L.J., Vaughan, D.J. (Eds.), Short Course Handbook on Ore and Environmental Mineralogy. Mineralogical Association of Canada, Nepean, vol. 27. pp. 367–401.

Jambor, J.L., Groat, L.A., Shaw, S.C., Blowes, D.W., Hanton-Fong, C.J., 1999. Mineralogical reactions in lysimeters containing tailings with different sulfide contents. Global Symposium on Recycling, Waste Treatment and Clean Technology, vol. 2. TMS, Warrendale, PA, pp. 1381–1390.

Jamieson, H.E., Shaw, S.C., Clark, A.H., 1995. Mineralogical factors controlling metal release from tailings at Geco, Manitouwadge, Ontario. In: Hynes, T.P., Blanchette, M.C. (Eds.), Proceedings Sudbury '95 — Mining and the Environment, CANMET, Ottawa, vol. 1. pp. 405–413.

Jang, H.J., Wadsworth, M.E., 1994. Kinetics of hydrothermal enrichment of chalcopyrite. In: Alpers, C.N., Blowes, D.W. (Eds.), Environmental Geochemistry of Sulfide Oxidation. ACS Symposium Series, Washington, DC, vol. 550. pp. 45–58.

Lin, Z., 1996. Leachate chemistry and precipitates mineralogy of Rudolfsgruvan mine waste rock dump in Central Sweden. Water Science Technology 33 (6), 163–171.

Lin, Z., Qvarfort, U., 1996. A study of the Lilla Bredsjön tailings impoundment in mid-Sweden — a comparison of observations with RATAP model simulations. Applied Geochemistry 11, 293–298.

Lowell, J.D., Guilbert, J.M., 1970. Lateral and vertical alteration mineralization zoning in porphyry ore deposits. Economic Geology 65, 373–408.

LRC, 1999. Determination of schwertmannite in hydrometallurgical leach residues. Leslie Research and Consulting, contract report 028SQ.2344-7-1012. Natural Resources Canada, Ottawa.

Malmström, M., Banwart, S., 1997. Biotite dissolution at 25°C the pH dependence of dissolution rate and stoichometry. Geochimica et Cosmochimica Acta 61, 2779–2799.

McCarty, D.K., Moore, J.N., Marcus, W.A., 1998. Mineralogy and trace element association in an acid mine drainage iron oxide precipitate; comparison of selective extractions. Applied Geochemistry 13, 165–176.

MEND, Mine Environment Neutral Drainage Program, 1991. Acid rock drainage prediction manual, Report 1.16.1b. CANMET, Deptartment of Natural Resources Canada, Ottawa.

Moore, D.M., Reynolds, R.C., 1997. X-ray Diffraction and the Identification and Analysis of Clay Minerals. 2nd ed. Oxford University Press, Oxford.

Murad, E., Schwertmann, U., Bigham, J.M., Carlson, L., 1994. Mineralogical characteristics of poorly crystallized precipiates formed by oxidation of Fe^{2+} in acid sulfate waters. In: Alpers, C.N., Blowes, D.W. (Eds.), Environmental Geochemistry of Sulfide Oxidation. ACS Symposium Series, Washington, DC, vol. 550. pp. 190–200.

Parkhurst, D.L., 1995. User's guide to PHREEQC — a computer program for speciation, reaction-path, advective-transport, and inverse geochemical calculations. USGS Water Resources Investigations Report 95-4227, Lakewood, Colorado.

Puura, E., Neretnieks, I., 2000. Atmospheric oxidation of the pyritic waste rock in Maardu, Estonia, 2: an assessment of aluminosilicate buffering potential. Environmental Geology 39 (6), 560–566.

Raven, K.P., Jain, A., Loeppert, R.H., 1998. Arsenite and arsenate adsorption on ferrihydrite: Kinetics, equilibrium, and adsorption envelopes. Environmental Science and Technology 32, 344–349.

Ribet, I., Ptacek, C.J., Blowes, D.W., Jambor, J.L., 1995. The potential for metal release by reductive dissolution of weathered mine tailings. Journal of Contaminant Hydrology 17 (3), 239–273.

Schulze, D.G., 1981. Identification of soil iron oxide minerals by differential X-ray diffraction. Soil Science Society of American Journal 45, 437–440.

Schulze, D.G., 1994. Differential X-ray Diffraction Analysis of Soil Material. Quantitative Methods in Soil Mineralogy. SSSA Miscellaneous Publication pp. 412–429.

Schwertmann, U., 1964. Differenzierung der Eisenoxide des Bodens durch Extraktion mit Ammoniumoxalat Lösung. Zeitschrift für Pflanzenernährung und Bodenkunde 105, 194–202.

Schwertmann, U., Bigham, J.M., Murad, E., 1995. The first occurrence of schwertmannite in a natural stream environment. European Journal of Mineralogy 7, 547–552.

Schwertmann, U., Friedl, J., Stanjek, H., 1999. From Fe(III) ions to ferrihydrite and then to hematite. Journal of Colloid and Interface Science 209, 215–223.

Serrano, L., Vargas, R., Stambuk, V., 1996. The late Miocene to early Pliocene Rio Blanco-Los Bronces copper deposit, Central Chilean Andes. Andean Copper Deposits: New Discoveries, Mineralization, Styles and Metallogeny, Camus, F., Sillitoe, R.H., Petersen, R. (Eds.), Society of Economic Geology Special Publication vol. 5, 119–130.

Shaw, S.C., Groat, L.A., Jambor, J.L., Blowes, D.W., Hanton-Fong,

C.J., Stuparyk, R.A., 1998. Mineralogical study of base metal tailings with various sulfide contents, oxidized in laboratory columns and field lysimeters. Environmental Geology 33, 209–217.

Singer, P.C., Stumm, W., 1970. Acid mine drainage: the rate-determining step. Science 167, 1121–1123.

Sondag, F., 1981. Selective extraction procedures applied to geochemical prospecting in an area contaminated by old mine workings. Journal of Geochemical Exploration 15, 645–652.

Stambuk, V., Blondel, L., Serrano, L., 1982. Geológia del yacimiento Río Blanco. Congreso Geologico Chileno, 3rd ed., Conception, Actas, vol. 2, pp. E419–E442.

Stichbury, M.L.K., Bain, J.G., Blowes, D.W., Gould, W.D., 2000. Microbially-mediated reductive dissolution of arsenic.bearing minerals in a gold mine tailings impoundment. Proceedings from the Fifth International Conference on Acid Rock Drainage, SME, Littleton. vol. 1, pp. 97–106.

Stoffregen, R.E., Alpers, C.N., 1992. Observation on the unit-cell dimensions, H_2O contents, and δD values of natural and synthetic alunite. American Mineralogist 77, 1092–1098.

Stone, A.T., 1987. Microbial metabolites and the reductive dissolution of manganese oxides: Oxalate and pyruvate. Geochimica et Cosmochimica Acta 51, 919–925.

Stumm, W., Morgan, J.J., 1996. Aquatic Chemistry. 3rd ed. Wiley, New York, 1022 p.

Stumm, W., Sulzberger, B., 1992. The cycling of iron in natural environments: considerations based on laboratory studies of heterogeneous redox processes. Geochimica et Cosmochimica Acta 56, 3233–30257.

Tuovinen, O.H., Kelley, B.C., 1973. Studies of the growth of *Thiobacillus ferrooxidans*. Archiv of Mikrobiologie 88, 285–298.

Tuovinen, O.H., Niemelae, S.I., Gyllenberg, H.G., 1971. Tolerance of *Thiobacillus ferrooxidans* to some metals. Antonie van Leeuwenhoek 37, 489–496.

Waychunas, G.A., Ning, Xu, Fuller, C.C., Davis, J.A., Bigham, J.M., 1995. XAS study of AsO_4^{3-} and SeO_4^{2-} substituted schwertmannites. Physica B 208 and 209, 481–483.

Webster, J.G., Swedlund, P.J., Webster, K.S., 1998. Trace metal adsorption onto an acid mine drainage iron(III)oxyhydry sulfate. Environmental Science and Technology 32 (10), 1362–1368.

Yu, J.-Y., Heo, B., Chang, H.-W., 1998. Stability of schwertmannite and ferrihydrite in stream waters of Imgok and Osheep Creek polluted by acid mine drainage. Mineral Magazine 62A, 1675–1677.

Yu, J.-Y., Heo, B., Choi, I.-K., Cho, J.-P., Chang, H.-W., 1999. Apparent solubilities of schwertmannite and ferrihydrite in natural stream waters polluted by mine drainage. Geochimica et Cosmochimica Acta 63, 3407–3416.